DETERMINATION OF ROCK MATERIAL PROPERTIES TO DESIGN ROBUST SUPPORT AT UNKI MINE

Ereck Mponya

A research report submitted to the Faculty of Engineering and the Built Environment, University of the Witwatersrand, Johannesburg, in partial fulfilment of the requirements for the degree of Master of Science in Engineering.

Johannesburg, 2016

DECLARATION

I declare that this research report is my own, unaided work. It is being submitted for the Degree of Master of Science in Engineering to the University of the Witwatersrand, Johannesburg. It has not been submitted before for any degree or examination in any other University.

……..
(Signature of Candidate)

…….. day of …….., ……
(day) *(month)* *(year)*

ABSTRACT

Since mining platinum started at Unki Mine in 2005, large and small geologically controlled falls of ground (FOG) have been problematic especially in 2011 where a FOG caused a fatality. This study is about determining the rock properties at Unki Mine and then using the results to design and recommend robust support to reduce the FOG problems that are continuously happening.

The study analysed all the FOG data from the mine database from 2010 to 2015 using statistical methods. Rock properties of the hangingwall, ore zone and footwall were determined from the laboratory tests. The geological structures were also mapped carefully. The results were then used as input data to the numerical modelling softwares Phase^2 and J-Block.

The J-Block program was used to determine the number of keyblocks that were stable, unstable and failed with support in designated and specified bords. A probabilistic approach was used to evaluate the stable span with special reference from small to large hangingwall instabilities for different mining scenarios. It was found out using Phase^2 that large spans at Unki Mine are possible provided appropriate and robust support system is adopted. To fully address the issue of FOG problem at Unki Mine, a probabilistic approach is recommended as this is considered to be more appropriate than a deterministic approach that has been the traditional design approach so far.

For the one I ever dreamed of and only one for me…

Together, forever, I long to be.

ACKNOWLEDGEMENTS

In prelude I would like to express my profound gratitude to my supervisor Dr. Halil Yilmaz from the School of Mining Engineering at the University of the Witwatersrand for his advice, guidance and patience throughout the study and all members of staff in the department. Also many thanks go to University of Zimbabwe Laboratory staff for affording me the opportunity to carry out the laboratory tests and their support.

My appreciation is extended to the management of AngloAmerican Unki Mines for granting me the permission and the opportunity to explore, learn and experience more in the field of mining and rock engineering.

My heartfelt and deepest gratitude also goes to Unki Mine Rock Engineering Department in gathering data and samples in particular the Chief Rock Engineer Mr. Omberai Mandingaisa.

My entire gratitude also goes to the management within the mining department and all the subordinates who were willing to corporate and work with me in the whole study process. I really appreciate the encouragement, patience and understanding from my parents Simon Mponya and Fostin Mponya. To God be the glory.

TABLE OF CONTENTS

CONTENTS **PAGE**

LIST OF FIGURES

LIST OF TABLES

LIST OF ACRONYMS

PGE	Platinum Group Elements
FOG	Fall of Ground
UCS	Uniaxial Compressive Strength
TCS	Triaxial Compressive Strength
POF	Probability of Failure
FOS	Factor Of Safety
PDF	Probability Density Function
FDM	Finite Difference Method
FWF	Footwall Fault
HWF	Hanging Wall Fault
VH	Ventilation Holing
CD	Conveyor Decline
MD	Material Decline
LDs	Ledging Declines
GCDs	Ground Control Districts
ABS-P	Angloamerican rock classification system
MSZ	Main Sulphide Zone
BMSZ	Base of the Base Metal Sub Zone
ISRM	International Society for Rock Mechanics
LHD	Load Haul Dump
MPa	Mega Pascal
kN	Kilo Newton

LIST OF SYMBOLS

σ_v	Virgin (Vertical) stress
ρ	Rock density
g	Gravitational acceleration
A	Total area
σ_t	Maximum tensile stress of beam
γ	Unit weight of beam
t	Thickness of beam
L	Length of unsupported span
η	Maximum deflection of beam
E	Young's modulus
τ	Maximum shear stress
φ	Internal friction angle
c	Cohesion
v	Poisson's ratio
σ_n	Normal stress
w	Wide
h	High
s	Spacing
l	Long
m	Meter
mm	Millimeter
m^2	Square meters
m^3	Cubic meters

1. INTRODUCTION

In Zimbabwe extensive hard rock tabular mining is done along the Great Dyke. Mining of these tabular bodies is done from near surface (Shallow Mining Environment) which is typically less than 1 000 m in depth. The focus of this study is Unki Mine and falls within this shallow mining environment (Ryder and Jager, 2002). The economic minerals associated with these tabular bodies include nickel, copper, Platinum Group Elements (PGEs) and chromitite. The extraction of these minerals from underground excavations uses a wide variety of support systems and mining methods. The support systems include pillars, packs, welded mesh, wire mesh, Osro straps, rock bolts, cable anchors, steel arches, shotcrete and thin sprayed liners (Van der Merwe and Madden, 2000). The aim of this research project is to determine the mechanical properties of the rocks at Unki Mine and then use these properties in the design of robust support of the underground excavations. This follows from the falls of ground (FOGs) that have been occurring ranging from small rock falls of size 0.01 m^3 to large hangingwall failures of size 107 m^3 in the bords. Therefore there is need to re-evaluate and redesign the support in order to control the FOG.

1.1. Location and description of Unki Mine

Unki Mine is one of the AngloAmerican platinum mines operating in Zimbabwe. The mine is located on the southern Great Dyke of Zimbabwe in Shurugwi Town, about 60 km south west of the city of Gweru in Midlands Province.

The township of Shurugwi was established in 1897 when gold mining was the mainstay of the district. Although a few gold mines are still operating currently, chrome and platinum mining has become the most important industry in the district. Apart from mining, Shurugwi Township has long been an area of active farming operations endowed with rich arable land (Stowe, 1968). The area lies between 1 450 m and 1 500 m above sea-level. Figure 1.1 shows the map of Zimbabwe with Shurugwi Township and Unki Mine's position. Unki Mine area is approximately 1 300 square kilometres (Maps, 2013).

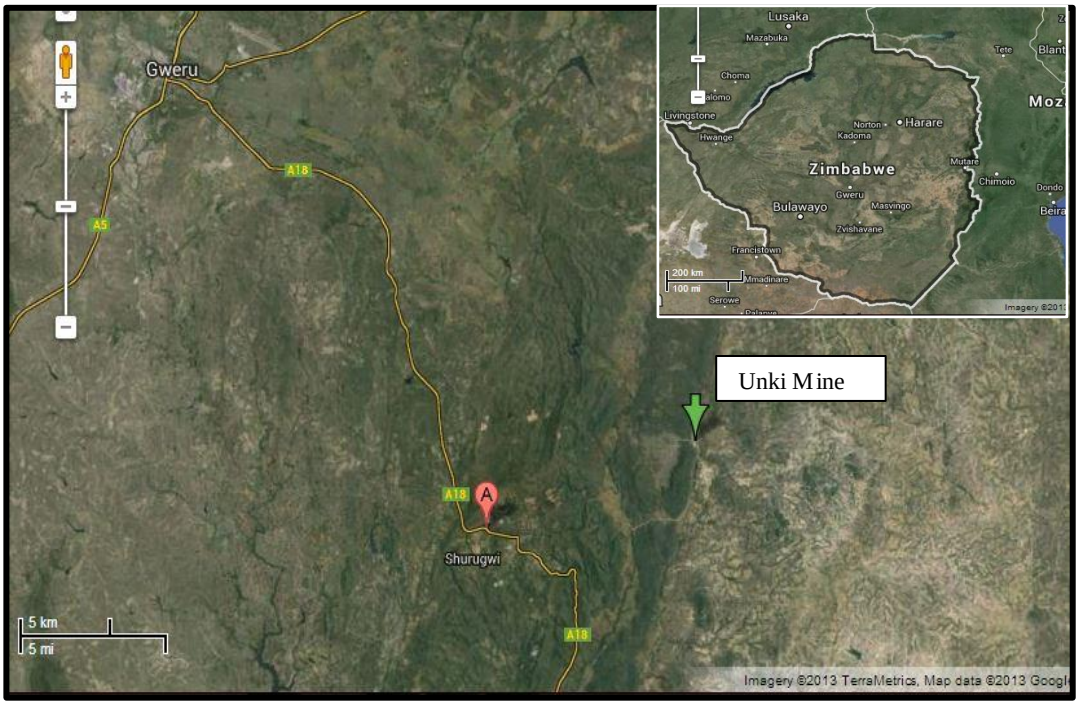

Figure 1.1 Map of Zimbabwe locating Shurugwi and Unki Mine (Maps, 2013)

Mining at Unki started in the early 20th century when the platinum reserves were discovered. Access to the ore body was through a vertical shaft and at that time railbound mining system was employed. Mining at the site was abandoned after failure to fully extract the ore body due to inferior technology and prevailing low metal prices (Brown and Mwatahwa, 2005). Full exploration of the ore body was done in 1996 and development of the twin declines commenced in 2002 after agreement with the government and the local community (Brown and Mwatahwa, 2005). The mine is designed to produce 120 000 tons of ore per month from the decline shaft system (Chunnett and Mwatawha, 2008).

1.2. Mining method at Unki Mine

Unki Mine practices on-reef mining using trackless machinery for drilling, loading, hauling and transportation with full face slicing as shown in Figure 1.2. The orebody is 2.1 m thick and dips at 14° and shallows to 0° at an inflection point as the orebody starts going up again on the western side of the Great Dyke. Access to the orebody is through on-reef twin declines that dip at 14° which are the conveyor decline (CD) and material decline (MD). Two ledging declines (LDs) are established from the twin declines and from those LDs production bords are established. The two declines are connected at every 60 m by lateral breakaways

and they maintain 15 m wide pillars along the declines. The MD is 5 m wide (w) × 2.5 m high (h) and houses the service pipes and serves as a downcast shaft for fresh air.

The CD is 6 m (w) × 2.5 m (h) and serves in the transportation of ore through the use of the conveyor belt and also downcast fresh air. The up-cast is through two vertical ventilation shafts and exhausts mechanically through the top most level for every production unit.

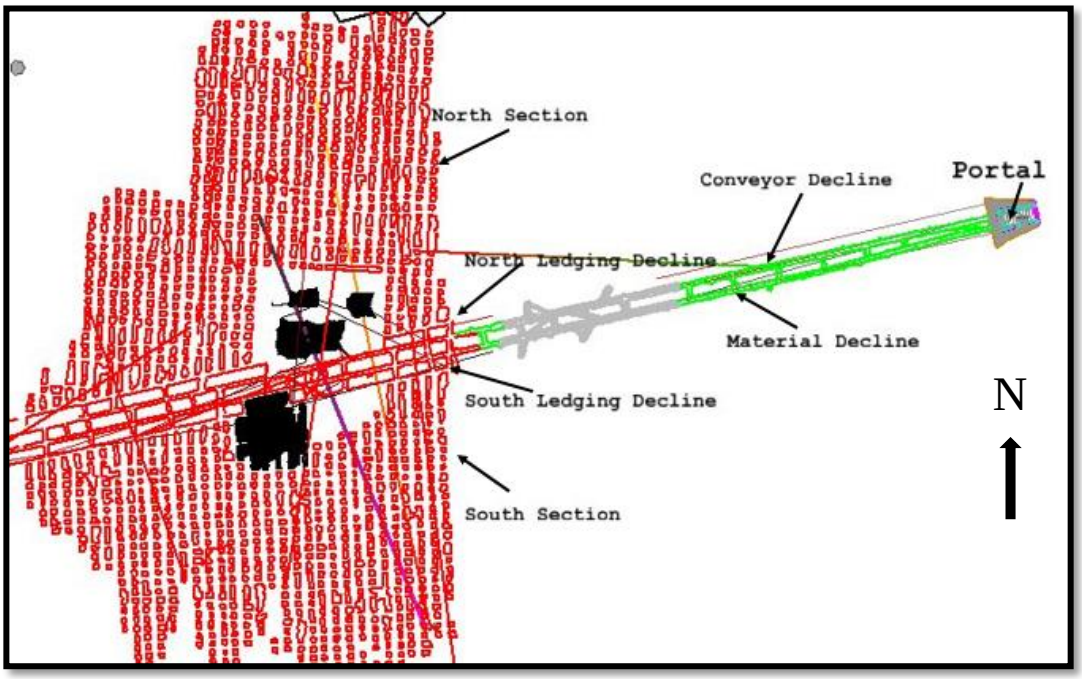

Figure 1.2 Mine layout-plan view illustrating the bord and pillar mining method (Chikuni, 2012)

The LDs are mined parallel to the CD and MD in the dimensions of 6 m (w) × 2.1 m (h). Secondary Development involves mining six production bords that are 12 m (w) × 2.1 m (h) and one strike conveyor bord that is 8 m (w) × 3.5 m (h) at the take-off. The height of the strike conveyor is reduced to 2.1 m after 74 m from take-off on the LD. Production section highlights the mining method as bords are blasted out leaving pillars for support hence the term "bord and pillar mining method". Each production section comprises of 7 bords (Figure 1.3).

The production bords are of the dimensions which measure 12 m (w) x 2.1 m (h). These bords are serving as the main production panels. In the production panels, the support consists of rows of pillars that are 5 m (w) on dip x 6 m (w) on strike

separated by 6 m (w) ventilation holings (VH) and these pillars are aligned along strike 12 m apart (skin to skin), except the strike conveyor bord. Regional pillars are left between the MD and the CD (Figure 1.4). These pillars are 15 m (w) separated by 4.3 m (w) VH. Pillars of 15 m (w) are also left between declines and their respective LDs. The design of pillars is such that the width to height ratio is above 3.

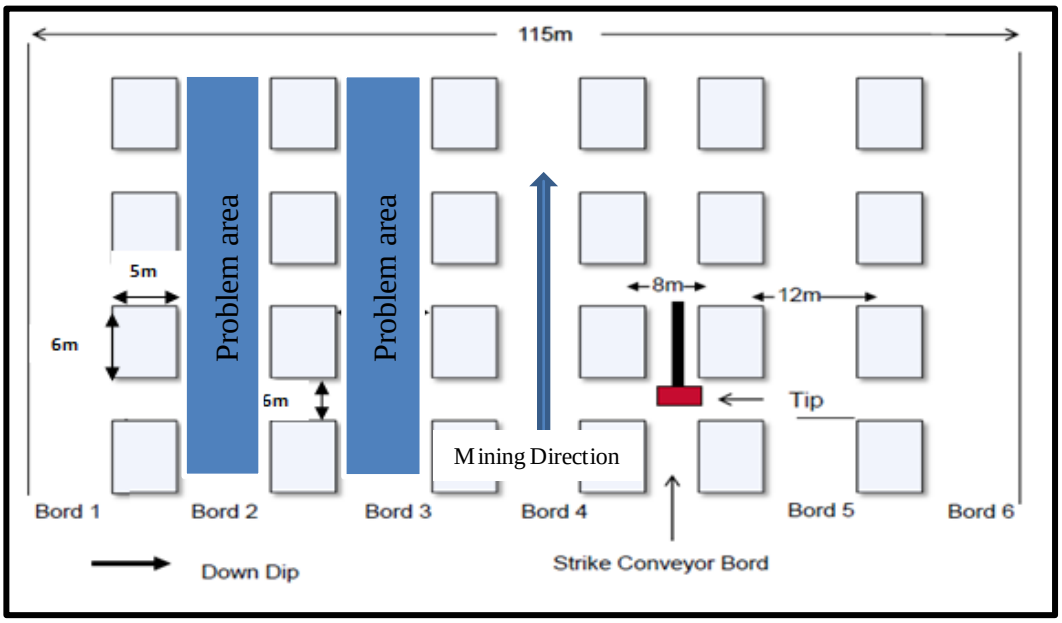

Figure 1.3 Pillar layout at Unki Mine (Mathemera, 2010)

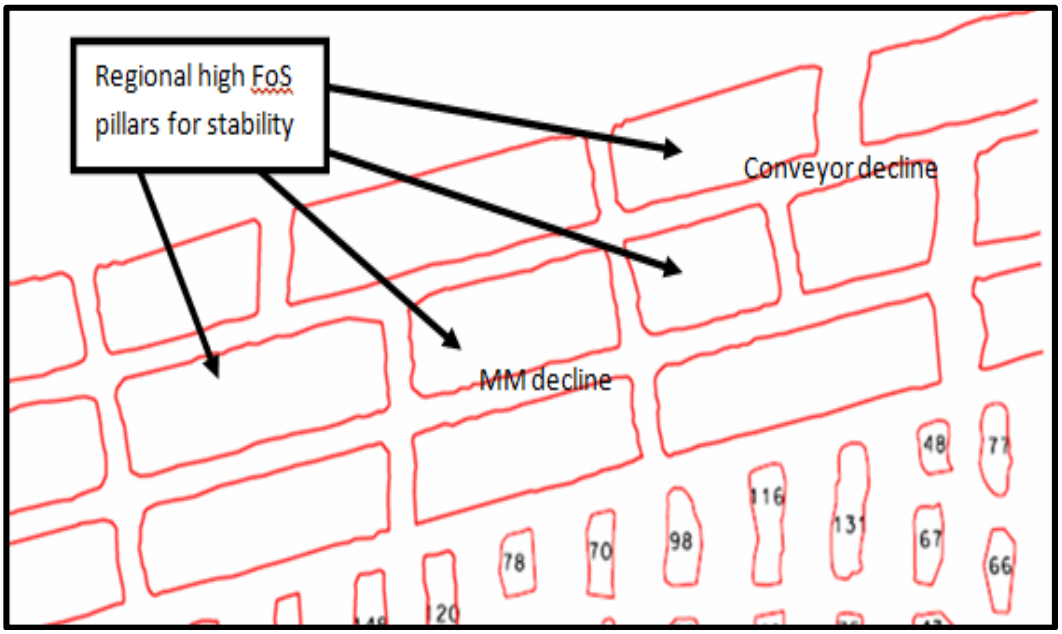

Figure 1.4 The regional pillars in access ways (Mugwadi, 2012)

1.3. Existing support strategy at Unki Mine

Unki Mine currently uses the Fletcher mechanical bolter for dry drilling and bolting. Prior to supporting, the bord is classified according to ABS-P classification system. If the ground is in A-Class it means good ground condition, then normal support of 1.5 m long (l) bolt is used at 1.5 m x 1.5 m spacing (s). If the ground is in B-Class it means bad ground condition, then 2.2 m (l) rock bolt is used at 1 m x 1 m (s). If the ground is in S-Class very poor ground condition, then Osro straps are used with 2.2 m (l) rock bolt at 1 m x 1 m (s).

The bolts used are high profile deformed resin bars having 20 mm diameter, 150 kN yield strength and 45° cut end. The bolt has spherical nut with tension indicator and 125 mm square domed bearing plate (King, 2006).

1.4. Project background

Since production started at Unki Mine, large and small FOGs have occurred both in the northern and southern production sections in ground control districts (GCDs) 1 and 3. The delineation of the GCDs at Unki Mine is be based on presence or absence of footwall fault (FWF), position of FWF relative to the mining cut, presence or absence of hangingwall fault (HWF), joints, dykes and presence or absence of slimes dam loading.

At Unki Mine FOGs are categorised the major risk in terms of safety. There are quite a number of recorded incidents of these FOGs in the mine data base (Table 1.1). They range from span failure to failure of blocks larger than the current support span of 1.5 m x 1.5 m grid in GCD1 and GCD3. Production is likely to be affected as a direct result of FOGs due to the span failure causing:

- Unsafe mining conditions to employees and machinery.
- Loss of production bords.
- Loss of roadways and walkways.
- Unnecessary reconditioning of bords, roadways and walkways.

This FOG database is required to analyse critical fall dimensions for support design purposes to cater for 95% of the FOG thickness.

Table 1.1 Fall of ground summary sheet (Mahove, 2014)

Date	Working Place	Width (m)	Length (m)	Thick (m)	Size	Damage	Injury	Comments
01-Feb-10	LDN	0.17	0.35	0.12	L	N	Y	MTC involving Lazarus Nyika while removing barricade
04-May-10	1SB1	0.1	0.25	0.1	S	N	Y	MTC involving Bland Zulu, Head and hand injury
25-Nov-10	1NB4	1.1	2.3	0.45	L	Y	N	LHD Mud guard damaged during lashing
01-Feb-11	3NB2	0.25	0.65	0.5	L	N	N	No Injuries or damage to property
08-Mar-11	2NS	1.4	2.16	0.98	L	N	N	FOG after blast
07-Apr-11	4NB1	0.52	0.77	0.15	L	N	Y	Fatality Involving Tainos Shumba while barring down
03-May-11	2SB6	0.66	1.1	0.24	L	Y	N	Autorock damaged
23-Oct-11	5NB1	0.41	0.08	0.06	L	N	Y	MTC involving Kundai Burayayi, Head and Shoulder injury
16-Nov-11	3NB5	4.5	2.5	0.6	L	N	N	FOG after blast
16-Dec-11	1NS	4.2	3.2	8	L	N	N	FOG after blast
20-Mar-12	3NB3	0.38	0.225	0.12	L	N	N	Near miss involving Lawrence Mzizi
04-Apr-12	2SB1	0.54	0.39	0.11	L	Y	N	MTC involving Prosper Masuku's right hand
15-May-12	6NB6	0.92	3.6	0.33	L	Y	N	Damage to property LHD work light housing
16-Oct-12	7SB1	0.1	0.05	0.03	S	Y	N	Josiah Mawarire sustained soft tissue injury
17-Jan-13	2NB4	0.5	3.2	0.79	L	N	N	FOG occurred at face during rig drilling
01-Feb-13	4SB5	0.35	0.5	0.15	L	N	N	FOG occurred at face during face marking for rig drilling
14-Feb-13	1NB2	1.26	0.39	0.36	L	N	Y	Significant Incident involving K. Hwacha
15-Oct-13	1NB3	MSZ	1.64	1.97	0.82	N	N	
08-Jun-14	5SB5 V/H49	MSZ	6.00	7.00	0.85	N	N	FOG occurred during or after blast
06-Aug-14	4SB2	MSZ	1.26	0.39	0.36	N	Y	Significant Incident involving Prince Dindi
08-Sep-14	1SB2	MSZ	0.12	0.21	0.0525	N	Y	Significant Incident involving Alfred Manda
26-Feb-15	3NB2	MSZ	7	20	2.5	N	N	High Potential Incident
10-Apr-15	7NB1 V/H21	MSZ	0.5	1.4	0.3	N	Y	Significant Incident involving Zuze Nzerere
06-Nov-15	5NB3	MSZ	7	7.2	2.3	N	N	High Potential Incident

Figure 1.5 shows bar graph for the FOG recorded incidents from 2010 to 2015 as recorded in the database. There has been a sharp FOG decrease from 2011 to 2014. FOG incidents were constant from 2014 to 2015. The mine set a target of only one or no FOG incident per year as compared to three FOG incidents in 2015. This means more efforts has to be done to meet the target set. Out of a total of 24 FOG

incidents reported in Table 1.1, 8 (~33%) caused personal injury and 5 (~21%) caused equipment damage. The frequency distribution of fall thickness is discussed in Chapter 4 in Figure 4.1 and Figure 4.2.

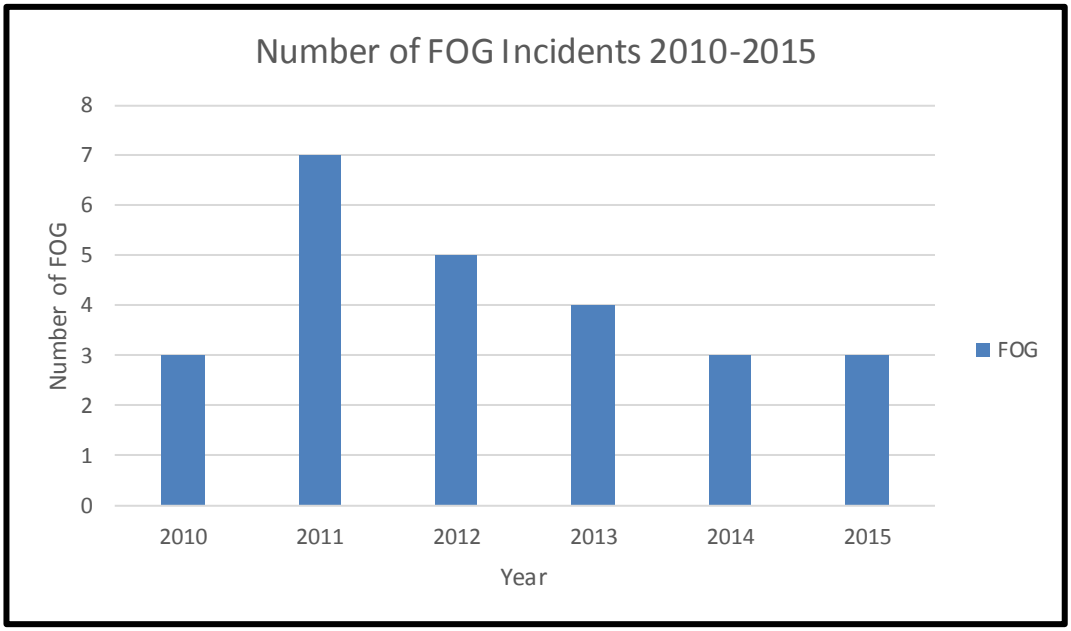

Figure 1.5 Bar graph showing number of FOG incidents yearly

1.5. Problem statement

The current Unki Mine support strategy appears to have been successful in controlling large hangingwall instabilities with a general downward trend in the number of occurrences as shown in Figure 1.5. However large and small hangingwall instabilities still occur occasionally. These problems highlight the inadequacy with the current panel support and inter-pillar span design. There are also concerns that some bords are either over-supported or under supported. The problem can be summarised as follows:

The current design parameter for the 12 m panel span was determined from the stability graph method from a Q value of 7. This method was developed by Potvin (1988) after taking cognisance of specific geological and rock mass conditions using Barton's Q-System (Mandingaisa, 2014). The calculation yielded a maximum stable span of 14 m. Therefore a supported span of 12 m was chosen to provide a reasonable factor of safety (FOS).

The current design does not consider the proper method which best models the bord and pillar mining methods thus either over-estimates or under-estimates the support requirement to the detriment of safety and production as evidenced by the FOG incidents still occurring in Figure 1.5. The stability graph method is mainly used in the design of other mining methods such as the sub-level open stoping and caving method as illustrated by Potvin (1988). Large and small hangingwall instabilities pose a threat to both safety and productivity. There is therefore need to review and redesign current support at Unki Mine.

The aim of this research report is to determine the rock properties at Unki Mine and to determine the factors governing the stability of spans in order to design a robust support system that will minimize rock fall risk. It is hoped that by reviewing the current support design and defining geotechnical parameters at Unki Mine, the current design can be optimised with benefits in terms of safety, productivity and increased profitability.

1.6. Project objectives

This section will cover the project objectives. It should be understood however that pillar stability is not part of the objectives therefore will not be discussed. The core objectives of this research project are:

- To analyze the mine FOG statistics and accident data.
- To determine the rock properties or geotechnical parameters at Unki Mine.
- To investigate the factors influencing the instability of spans in the production sections.
- To identify the different geological features contributing to instability.
- To review and elaborate the current inter-pillar span design.
- To design robust span and support by using numerical modelling programs.

It is anticipated that FOG incidents will reduce after the span and support re-design is done. The benefits that are to be achieved from this research are as follows:

- Improved safety of employees.
- Improved productivity.
- Secured jobs of employees.

- Increased profit margins by reducing the damage to properties and injuries due to FOG.
- Longer life of mine by avoiding loss of production bords, roadways and walkways due to FOG.

1.7. Research methodology and data collection

A brief overview of the research methodology is outlined in this section. The methodology is done in order to achieve the objectives of the project.

1.7.1. Research context

This research will analyse the FOG statistics at the mine and the accidents related to the ground stability. The structures that contribute to the ground instabilities will be investigated as well. The critical factors will then be used as input to the design of stable spans for safe mining environment (Swart and Handley, 2004). The determination of the rock properties will be done through laboratory testing. The results will be used to design robust support at Unki mine using analytical and numerical models.

1.7.2. Research approach

The research approach to be adopted is outlined in this section. Literature review is carried out from the onset of the project on the design of stable spans, factors governing span failures, testing of mechanical properties of rocks and numerical modelling. The data for this research project is collected for the various aspects that improve understanding of the inter-pillar span stability as follows:

- Mine FOG statistics,
- Geotechnical parameters from the mine and data from the laboratory tests,
- Pillar dimensions,
- Span physical measurements.

The review of the current support design will be done to identify possible short comings, limitations and to determine potential improvements. The results for the study will be discussed, recommendations arising from the study will be provided and the conclusions will be made.

1.8. Project resources

This section will discuss where the project resources will be sourced. The information required for the smooth progression of this project report is available at the following resources:

- Unki Mine database,
- Wits University libraries,
- The internet (journals and publications),
- Institute of Mining Research at University of Zimbabwe.

1.9. Chapter summary

This chapter provided a brief description of Unki Mine with special reference to location, mining method and the existing support strategy. The research methodology and project resources has been described.

2. LITERATURE REVIEW

This chapter will review the literature pertaining to the bord and pillar stable span designs, different failure modes, the effects of geological features and horizontal stress on span stability. Originally the span and support methods were obtained through experience, trial and error methods.

2.1. Methods to assess span stability

There are several methods to assess span stability that can be used. According to Swart et al (2000), the design methods available for assessing the stability of stopes can be categorised as:

- Analytical methods;
- Observational methods.

Analytical methods involve the application of conceptual models with the aim of reproducing the same behaviour and response. Closed form solutions, numerical methods and structural analysis are examples of analytical methods (Swart and Handley, 2005). These methods are useful for making comparisons and assessing sensitivity for varying input parameters. Observational methods rely on the monitoring of the rock mass deformation and FOG statistics during mining to detect instabilities. This approach is data driven and should start early in the implementation of a design, to allow sufficient data to be generated over time (Swart et al., 2000).

There are quite a number of recorded incidents resulting from FOGs. The incidents range from span failure to failure of blocks smaller than the support span (Swart and Handley, 2004). Span failure is when the hangingwall collapse with more than support spacing due to support failing to provide adequate clamping effect leading to beam collapsing. This may be caused by the existence of parting planes in the hangingwall such as sub-horizontal jointing and chromitite stringers. According to Ryder and Jager (2002), the presence of an extended tensile zone in the hangingwall due to dead weight promotes bed separation and the potential for massive collapses.

The stability of the span between pillars is a function of the pillar spacing and the ability of the in-panel support to control or prevent large-scale panel collapses

(Haile and Jager, 1995). Stable inter-pillar spans can be defined as the spacing between pillars at which large hangingwall instabilities are not likely to occur. Swart and Handley (2005), emphasized to control panel span as the most effective means of controlling roof without any artificial means.

To reduce the risk of FOG, combinations of different support systems are used such as cable anchors, rock bolts and thin sprayed liners just to mention a few. Pillars are also used as primary in-stope support. Currently very few mines design the stope panels according to a systematic design methodology (Swart and Handley, 2004). A lot of rock engineering elements are neglected in the design process such as rock mass characterisation, estimation of rock mass properties, identification of potential failure modes and appropriate stability analyses. Swart and Handley (2004) went further to explain that instead, span or stope lengths and heights are dictated by the equipment in use and by superimposing methods or previous experiences from other mines with similar conditions. The design of a support system is normally based on experience and past practices. The design of safe spans must take into account the variability in the immediate beam thickness, rock strength, horizontal stresses, keyblock failure, block dimensions and the intensity orientation and alteration of hangingwall jointing (Swart and Handley, 2005). There are several common approaches to the design of stable spans as outlined in the next sections. The rock mass classification and the tributary area theory will not be used in this study as they are not relevant to bord stability analysis and therefore they will not be discussed in the literature review.

2.2. Analytical methods

The analytical methods include beam analysis and keyblock analysis. Roof stability is affected by quite a number of different mechanisms. To make sure the roof is stable, it is good to identify and understand the mechanisms. In mining environment, roof stability varies as the geology varies resulting in different effects in different areas. The critical parameters are the thickness of lithological units in the roof and the existence of discontinuities such as joints, faults and dykes (Swart and Handley, 2005).

The mine roof behaviour can be approximated by beam behaviour if there is no structural weaknesses (Swart and Handley, 2005). The platinum mining environment is characterised by laminated geological units that can be simplified into beams. A beam is a structural element that is capable of withstanding load primarily by resisting bending. The length of a beam should at least be eight times its thickness (Van der Merwe and Madden, 2000). In stratified rock masses, the roof or hangingwall of an excavation will form a beam of rock. The beams normally exist in coal, manganese, chrome, gold and platinum mines where the depth is shallow (Yilmaz, 2011). The illustration and possible behaviour of such beams is shown in Figure 2.1. Separation and opening up may occur on the laminated planes.

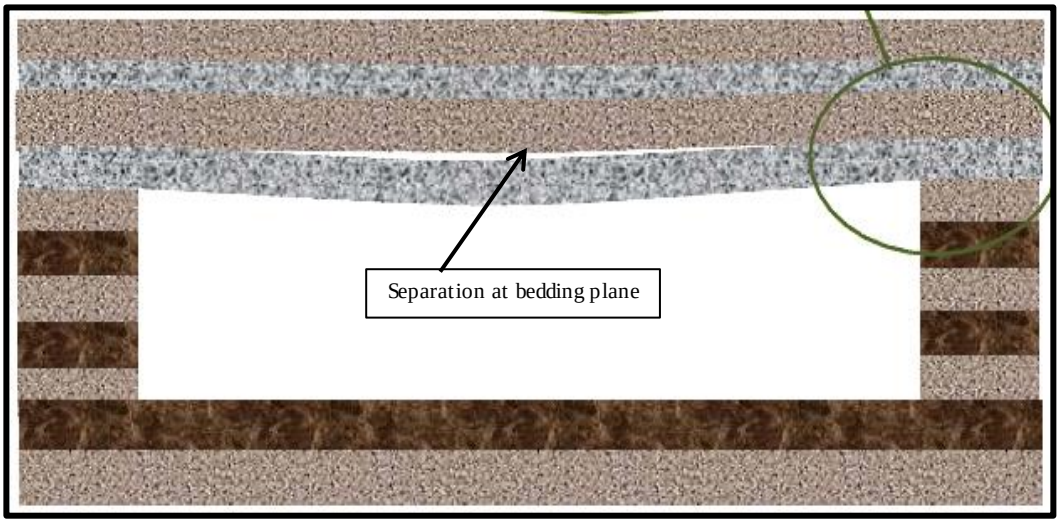

Figure 2.1 Separation occurring on the bedding plane (Van der Merwe, 2010)

The beam forming the roof of the excavation deflects as a result of the external loads, own weight, span and external reactions to these loads. At the haunches or corners of the excavation, shear displacement is highest and will cause fractures and opening up of joints as shown in Figure 2.2. If the strata in the hangingwall are competent enough to form beams, it may be possible to clamp a sufficient number of strata together to form a stable composite beam (Yilmaz, 2011).

There are several types of beams and in this section only the type of beams that have to be dealt with roof support will be discussed. There is a limitation in this study that the beams in the roof are assumed to be continuous, therefore Voussoir beam theory is excluded.

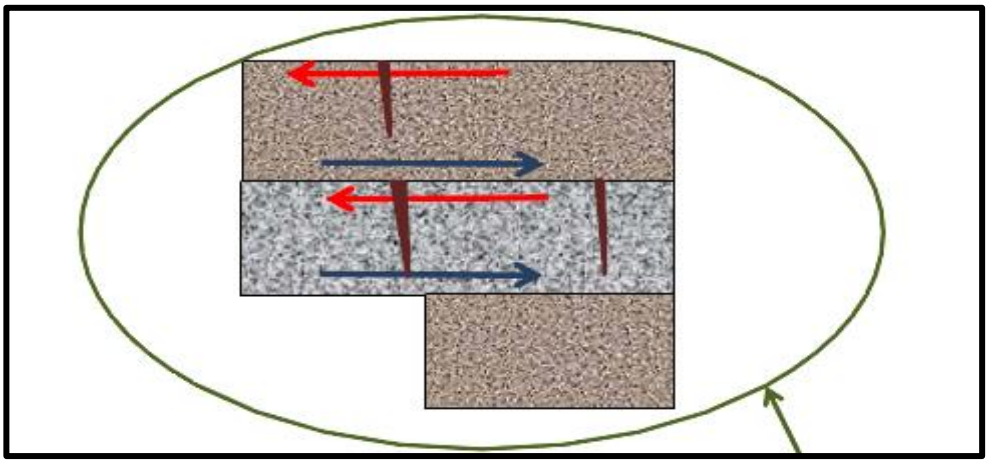

Figure 2.2 Cracks and joints opened by shear displacement (Van der Merwe, 2010)

2.2.1. Clamped beams

A clamped beam in its simplest form is as a result of unjointed roof layers clamped together in underground excavations (Swart and Handley, 2005). The important measurable parameter is its sag caused by its own weight and the in-situ stresses. The amount of sag is greatest at the center and approaches zero at the edges. A beam has unique stress distribution as seen in Figure 2.3. The beam will fail if the generated stresses exceed the strength of the rock material forming the beam (Van der Merwe and Madden, 2000).

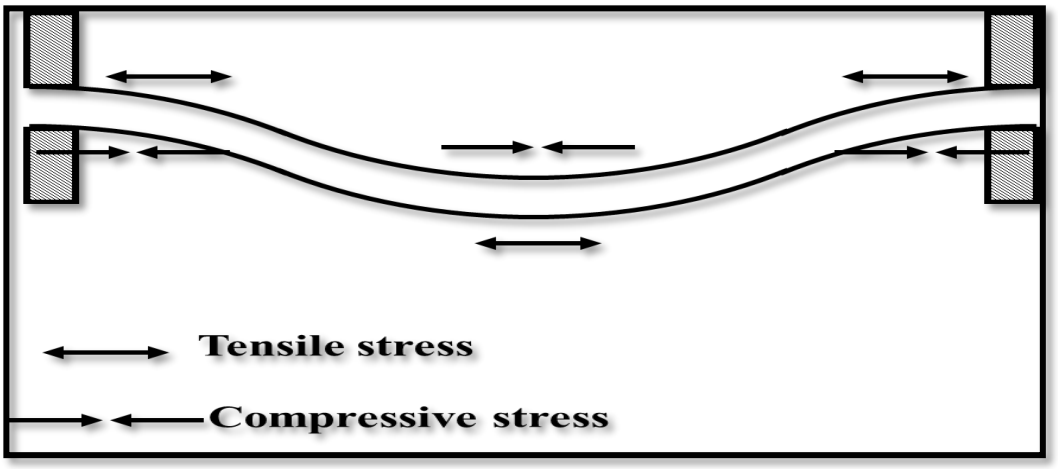

Figure 2.3 Clamped beam showing the positions of maximum stresses (Van der Merwe, 2010)

The maximum induced stresses in the beam occur at the edges and in the center. The stresses are compressive at the top of the beam and tensile at the bottom. Failure of rock is likely to begin at tensile stress locations following the concept that rock is weaker in tension than in compression (Van der Merwe and Madden, 2000). The magnitude of the maximum tensile stress is given by the following equation:

$$\sigma_t = \frac{\gamma L^2}{2t} \quad (1)$$

Where: γ is the unit weight of beam (N/m^3),

t is the thickness of beam (m),

L is the length of unsupported span (m).

The magnitude of the maximum deflection at the centre of the beam is given by the following equation:

$$\eta = \frac{\gamma L^4}{32Et^2} \quad (2)$$

Where: E is the Young's Modulus of material (MPa).

In both of these equations, the length of the unsupported span has the most important controllable contribution followed by the thickness. For instance the induced stress is directly proportional to the length squared and the sag is proportional to the fourth power of the span. Thus if the span doubles, the roof sag increase by a factor of sixteen (Van der Merwe and Madden, 2000). The deflection is greater for smaller thicknesses of strata implying that where thinner strata occurs above thicker strata, they will rest on and exert additional load on thicker strata. Separation between strata occurs when thinner strata occurs below thicker strata. At Unki Mine there is a layer in the hangingwall of pegmatoidal plagioclase that separates the ore zone and the hangingwall. This layer is weaker and is likely to cause hangingwall instability. The shear on the interfaces between the strata making up the composite beam must be prevented. If the shear of the interfaces is exceeded, then slip will occur between the strata. The maximum shear stress that will occur on an interface is given by the equation below. The slip is zero at the center of the span on the plan of symmetry (Van der Merwe and Madden, 2000).

$$\tau = \frac{3\gamma L}{4} \quad (3)$$

2.2.2. Cantilever beam

This is when the continuity of a clamped beam is broken by geological features such as joints, dykes and faults. The free end of the beam where the joint cuts across is now stress free (Figure 2.4). The magnitude of the maximum stress is given as follows:

$$\sigma_t = \frac{3\gamma L^2}{t} \quad (4)$$

It is evident that in a cantilever beam the magnitude of the tensile stress increases than that in a clamped beam. The practical implication of this is that the presence of a mere joint or fault in the roof results in increased tensile stress at the clamped abutment of the cantilever beam (Van der Merwe and Madden, 2000).

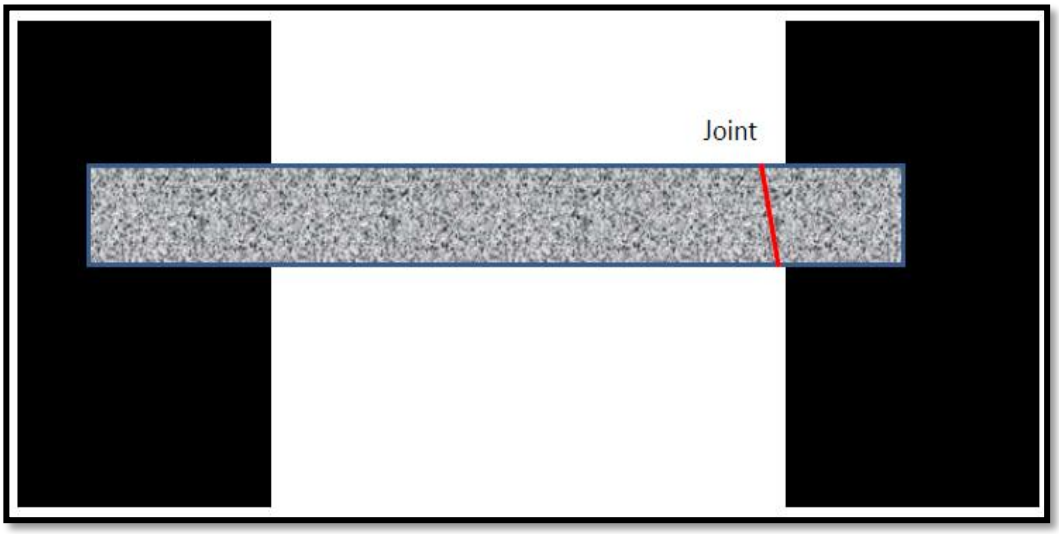

Figure 2.4 Cantilever cut by fault (Van der Merwe, 2010)

2.2.3. Keyblock Theory

Predicting span failure in bord and pillar platinum mining has been done for the last few decades using the deterministic methods such as the FOS but with limited success. The deterministic approach involves the calculation of input parameters assuming that they are accurate. For most rock engineering problems, the values of many input parameters are not very well known and they vary from place to place (Hoek, 1989). Surprisingly, due to increase of failed spans in mine data bases being updated, it is found out that spans are failing as well regardless of their so called stable design. This means that the deterministic method is not satisfactory in preventing span failure.

This section will consider variability in rock properties in order to calculate the stability of mining spans using the probabilistic approach using J-Block program. The method proves to be more reliable and produce meaningful results when designing and assessing span stability.

Owing to the short comings of the deterministic design method as mentioned above, rock engineers are focusing more on the probabilistic approach to assess span stability. The input parameters in rock engineering are variable and uncertain. This variation and uncertainty can be accounted for by probabilistic approach and subsequently evaluating the risk associated with support design.

The variation in each parameter is described by a statistical distribution. The parameters subjected to variation include different rock properties such as deformation and strength properties, cohesion and friction angles, joint spacing, joint length and ground water conditions (Stacey, 2012). The analysis results in a FOS distribution from which a probability of failure (POF) is calculated. The definition of POF is:

POF = Number of Failed Samples / Number of Total Samples (Hoek, 1989).

Stope hangingwall instabilities at Unki Mine are often controlled by the presence of geological discontinuities such as joints, dykes, faults and lava flow planes. The intersection of these discontinuities can result in the formation of wedges, which can fall or slide out from the hangingwall. This type of environment is suitable for the application of keyblock methods.

The application of keyblock methods is dependent on the correct interpretation of the structural geology and the identification of unstable wedges and blocks. With conventional deterministic keyblock analysis, the natural scatter is ignored and mean values are used (Goodman and Shi, 1985).

Probabilistic methods, as used in J-Block (Esterhuizen and Streuders, 1998), can be applied to overcome problems associated with the deterministic analysis. Esterhuizen and Streuders (1998) applied this approach in a mining environment that included both geological discontinuities and stress fractures. They were able to evaluate different support standards and determine whether keyblocks occur between support units or have potential to fail the support units. The procedure is repeated several thousand times to determine the probability of keyblock failure. It was concluded that this approach was suitable for the evaluation of support effectiveness in environments where large number of geological discontinuities and

stress fracturing are exposed. It was shown that as the keyblock size increases the probability of falling out between support units decreases but the probability of failing the support increases. This approach has subsequently been applied in the design of stable spans on various platinum mines using J-Block program (Esterhuizen and Streuders, 1998).

2.2.4. State of stress

Prior to making any excavations underground, the environment is subjected to vertical stresses caused by the weight of the overburden and the horizontal stress components. Toyra (2004) attributes these horizontal stresses to plate tectonics while others attribute to the intrusion of magma into faults forcing rock mass apart to create dykes. Some attribute to the crust being contracted and squeezed due to the cooling magma deep down the earth (Van der Merwe and Madden, 2000). Figure 2.5 shows the direction of the horizontal principal stresses at Unki Mine. The figure is not to scale.

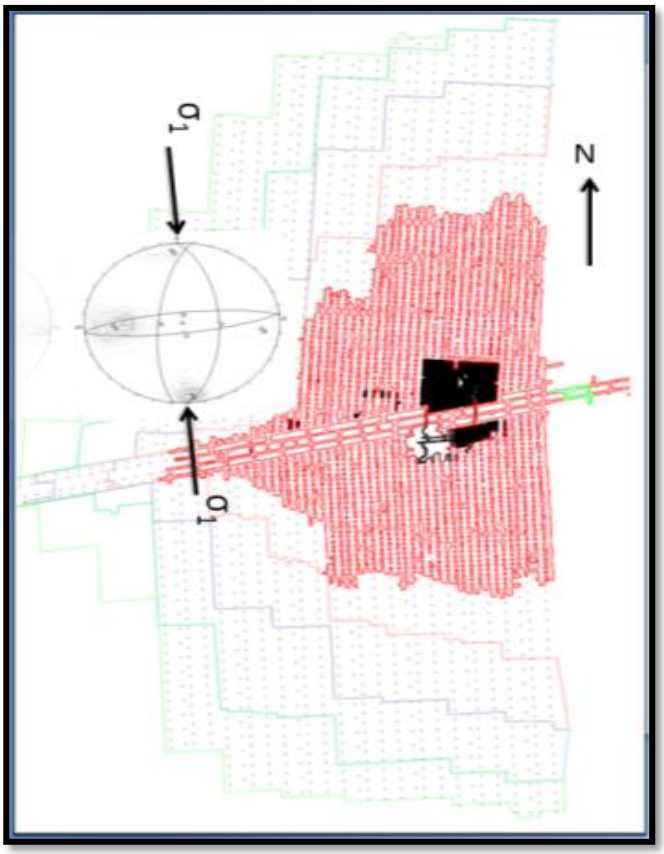

Figure 2.5 Schematic showing the direction of the horizontal principal stresses (Mandingaisa, 2014).

Unki is a shallow mine with a maximum depth of +/-300 m as determined from drilling carried out to date. This means that mining will be in a shallow low stress zone. The horizontal stress component is expressed as a multiple of the vertical stress known as the k-ratio. At shallow depth, the ratio is much higher ranging from 1 to 6, on average it is about 2 (Van der Merwe and Madden, 2000). The area under study Unki Mine has a measured k-ratio of 1.25.

2.3. Numerical models and constitutive behaviours

Numerical modelling is used to analyze and predict the behavior of rock mass, support response and the influence of geological structures on and around excavations. The analysis is done prior to, during or after mining has taken place.

To obtain comprehensive results from numerical modelling, a model is built using appropriate numerical modelling codes representing as close as possible the problem being faced by the rock engineer at a mine. Some appropriate or relevant geotechnical parameters are allocated for a specific area to be studied. The outcome of the model is then evaluated and analyzed through graphs, tables or through data output files. There are basically two types of models that can be used by the rock engineers and according to Lightfoot (2000) they are:

- Analytic models
- Numerical models.

Numerical models are used to analyze mostly situations when the geometry is too complex to be dealt with physically and analytically. The complex problems can go as far as determining accurately how stresses and strains are distributed in an irregular mining layout in both surface and underground mines (Lightfoot, 2000). This is made easier by the different computer programs available.

The aim of this project report is to use numerical modelling codes namely Phase^2 and J-Block to model and predict the extent of failure and the failure behavior that could be expected in highly stressed regions at Unki Mine. Phase^2 is applied to the analysis of underground layout and mining sequence problems as well as the

assessment of pillar designs and span stability. The modelling guidelines are outlined by (Lightfoot, 2000) as follows:

i. "*Know the reasons of building the model and the questions you want to answer using the model.*
ii. *Build a conceptual model as soon as possible to save on time, money and resources.*
iii. *Look at the mechanism of the problem such as deformations and failure modes.*
iv. *Come out with tests you need to perform on the model.*
v. *Design a simple model that will allow the important mechanism to occur.*
vi. *Implement the model and find the weaknesses associated with it.*
vii. *If the model is found to be weak, make a series of simulations to bracket the true case.*
viii. *Run more models to explore the neglected aspects which may affect your modelling*".

2.3.1. Discontinuum modelling

The discontinuum modelling technique is mostly appropriate for rock mass controlled by discontinuity behaviour. According to Eberhardt (2003), it has found applicability on rock mass with multiple joint sets that control the mechanism of failure. The joints are treated as interfaces between the blocks and are taken as boundary condition rather than an element in the model and can simulate large displacement due to slip and opening along discontinuities. This approach can formulate the influence of ground water pore pressures and seismic activity on blocks sliding and deformation (Eberhardt, 2003). The approach requires a rough idea of the governing failure mechanism for instance failure occurs when the shear strength of the discontinuities is exceeded. Also an assumption has to be made regarding the third dimension (Eberhardt, 2003). The discontinuum models used in this report are Phase^2 and J-Block.

2.4. Failure criteria commonly used

It is important to understand the failure criteria that are commonly used in numerical modelling with special reference to Phase[2]. There are basically two rock failure criteria which are the Mohr-Coulomb and the Hoek-Brown criteria that have been developed over the years in trying to understand the rock failure. They examine the limiting combinations of stress components and establish the inadmissible stress conditions. Inadmissible stress conditions are those that a rock mass cannot sustain because it will yield or fail before they are reached. Therefore it is necessary to understand the theory behind these rock failure criteria that are both used in this project.

2.4.1. Mohr-Coulomb Failure Criterion

This criterion states that failure will occur where the maximum shear stress reaches shear strength of the intact rock material. The criterion is represented by the following equation:

$$\tau = \sigma_n \tan\varphi + C \qquad (5)$$

Where: τ is the shear stress (MPa),

φ is the internal friction angle (^{O}),

σ_n is the normal stress (MPa),

C is the cohesion (MPa).

The cohesion and the friction angles can be determined from the plot of Mohr circles in the shear stress against normal stress graph. The failure line will be drawn tangent to the Mohr circles. The angle of friction is determined from the gradient of the failure line and the cohesion will be the vertical intercept of the failure line as illustrated in Figure 2.6. If the Mohr circle lies below the failure line as shown in Figure 2.7 then, according to Lightfoot (2000), the rock will remain intact. If the Mohr circle is tangent or touches the failure line as shown in Figure 2.8 then the rock will fail (Lightfoot, 2000). However, Lightfoot (2000) stated that the Mohr-Coulomb failure criterion has its own shortcomings as follows:

- "*It implies that a major shear fracture occurs at peak strength,*
- *It implies a direction of shear failure which often does not agree with observations, particularly in brittle rock,*

- *It is linear and peak strength envelopes determined experimentally are usually non-linear,*
- *The criterion is likely to give incorrect results if the failure mechanism is not shear*".

The Mohr-Coulomb failure criterion can however provide a good computation of residual strength conditions of fractured rock and excess shear strengths of geological discontinuities like faults and dykes. For these reasons highlighted, other criteria are preferred for intact rock (Lightfoot, 2000).

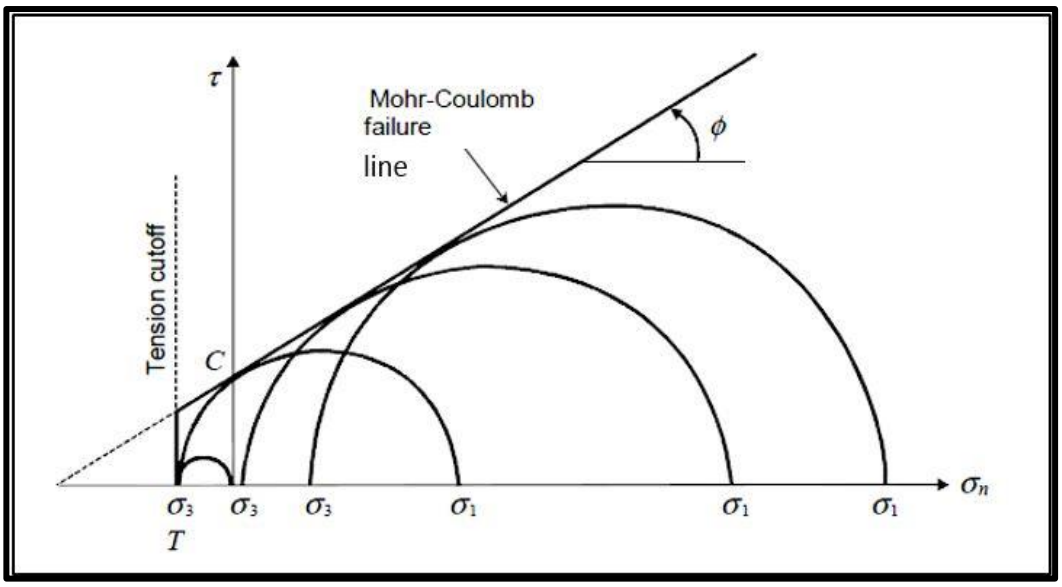

Figure 2.6 Mohr-Coulomb failure criterion (Lightfoot, 2000)

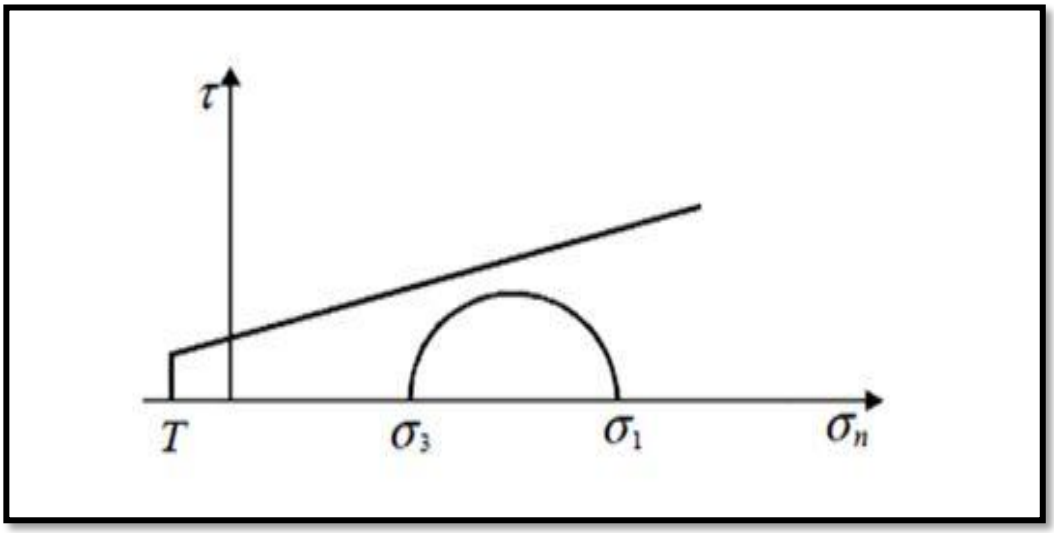

Figure 2.7 The Mohr-Coulomb failure criterion showing stable condition (Lightfoot, 2000)

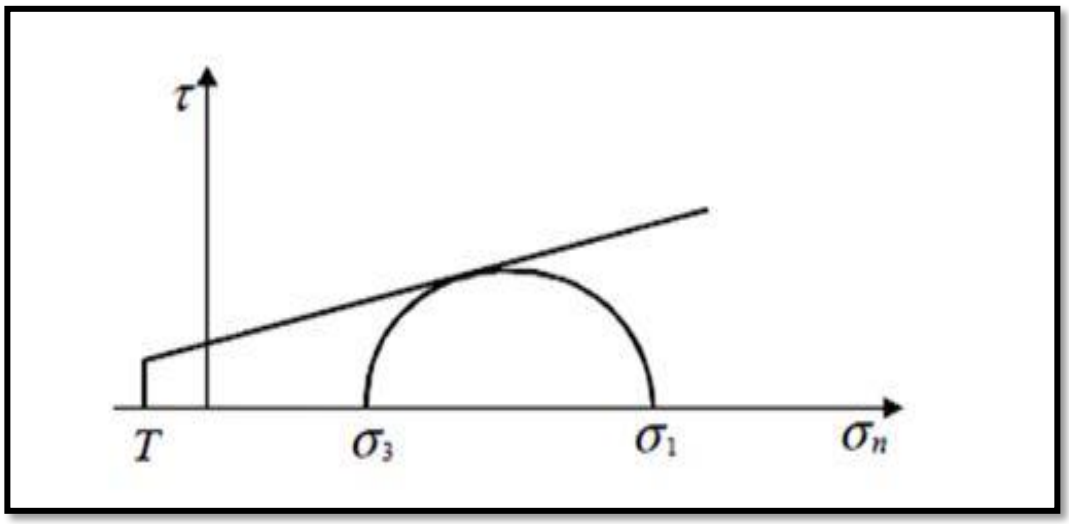

Figure 2.8 The Mohr-Coulomb failure criterion showing failure condition (Lightfoot, 2000)

2.4.2. Hoek-Brown Failure Criterion

This empirical criterion was developed by Hoek and Brown (1988) for rock and rock mass failure based on intact rock tests. The generalised form of the Hoek and Brown failure criterion is shown in the following equation:

$$\boldsymbol{\sigma_1 = \sigma_3 + \sigma_{ci}(\frac{m_b \cdot \sigma_3}{\sigma_{ci}} + s)^a} \quad (6)$$

Where: m_b is the Hoek-Brown constant for the rock mass,
s and a are constants which depend on the rock mass characteristics,
σ_{ci} is the UCS of the intact rock.

For brittle intact rock (Brady and Brown, 2005), the equation simplifies as follows:

$$\boldsymbol{\sigma_1 = \sigma_3 + \sqrt{(m_i \sigma_3 \sigma_{ci} + s\sigma_{ci}^2)}} \quad (7)$$

Where: m_i and σ_{ci} are determined from the laboratory triaxial tests.

The Hoek- Brown shortcomings are similar to the Mohr-Coulomb failure criterion (Stacey, 2012). This criterion applies to brittle intact rock and for rock mass with four or more joint sets with uniform strength (Brady and Brown, 2005).

2.5. Failure modes

In this section, the most common failure modes are described. This will be followed by their causes and quick remedies.

2.5.1. Keyblock or wedge failure

This is where three or more mutually intersecting joints are present in the hangingwall thereby creating an unstable block geometry (Haile and Jager, 1995). Figure 2.9 shows the image where a wedge dislodged at Unki Mine.

2.5.2. Open crack in centre of stope

These are visible cracks that tend to occur in the central areas of bords or stopes Figure 2.10. With special reference to Van der Merwe and Madden (2000), these cracks are an indication of excessive tension caused by:

- Excessive span length, resulting in higher induced tension in the bottom center of the roof beam.
- Excessive horizontal compression as a result of over-thrusting high up in the roof pushing the lower layers down.

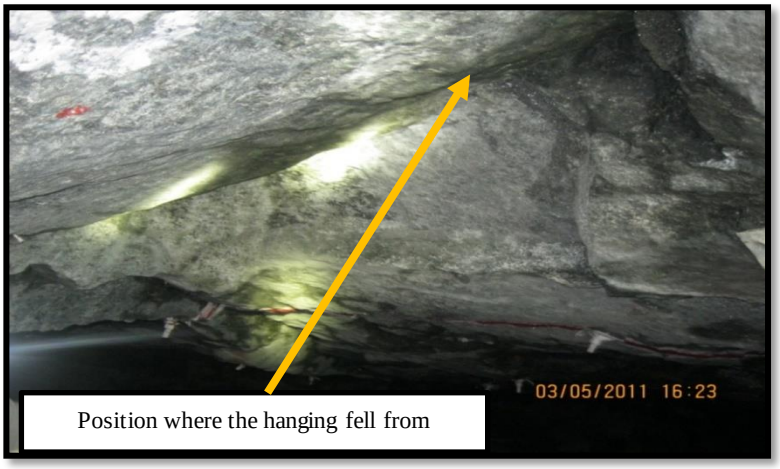

Figure 2.9 The image showing where a wedge dislodged

Figure 2.10 Tension crack in the roof

If this has been identified, the span should be reduced and augment support with cable anchors while the root cause is investigated (Van der Merwe and Madden, 2000).

2.5.3. Small thin falls between bolts

Small falls of ground between support bolts are caused by lack of areal coverage, aggravated by excessive bolt spacing as shown in Figure 2.11 and Figure 2.12. This is often seen where the mechanical anchor bolts are used. Lack of pretension is witnessed if there are no small sections of rock left between the washer plates and the intact roof. While relatively small falls of roof between bolts are generally not regarded with the same urgency as the more spectacular major roof falls, they cause the majority of injuries and fatalities (Van der Merwe and Madden, 2000). At Unki mine large FOGs occur in supported areas and smaller rocks fall in between support bolts.

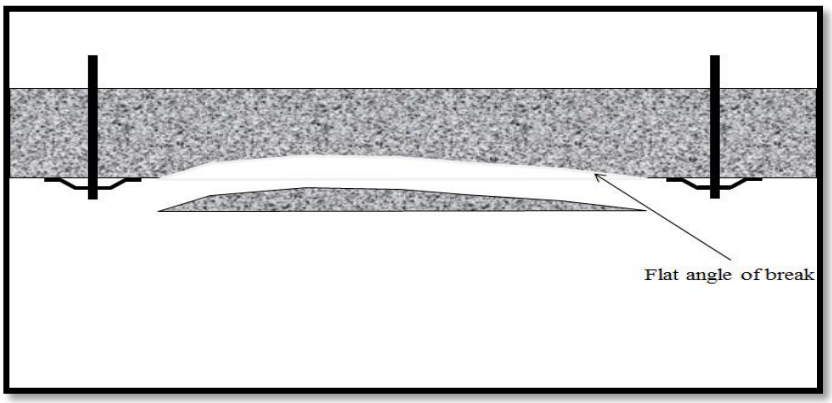

Figure 2.11 Falls between tendons – high horizontal stress (Van der Merwe, 2010)

Figure 2.12 Rock dimensions 0.25 m x 0.1 m x 0.1 m (Unki, 2014)

The best practice is to use areal coverage, reduce the bolt spacing and to check the bolt installations to ensure that proper pretension is applied (Van der Merwe & Madden, 2000).

2.5.4. Dome failure/ Roof falls higher than bolt length

When the FOG height is higher than the length of the bolts, it indicates that the bolts are too short or that the bolt density is insufficient to carry the overlying strata as shown in Figure 2.13. The roof bolts used to support this span was 1.5 m long and the fall out height was in excess of 2 m as depicted by the clinorule. The best practice is to increase the length of the bolts and the bolt density (Van der Merwe and Madden, 2000).

Figure 2.13 Roof fall out higher than the length of bolts (Unki, 2014)

2.6. Chapter summary

In this chapter, methods to assess the span stability were discussed in detail. The common rock failure criteria were also explained as well as the conditions they apply. Moreover, different failure modes were discussed followed by the causes and the remedies were also suggested. The following chapter will deal with the general geology of Unki Mine and the Great Dyke.

3. GENERAL GEOLOGY OF UNKI MINE AND THE GREAT DYKE

The Great Dyke is an elongate layered mafic to ultramafic intrusion similar in character to the Bushveld Complex of South Africa, and is second only to the Bushveld Complex in terms of size and PGE resources. The Great Dyke host major economic minerals in Zimbabwe.

The intrusion cuts across granite-greenstone terrain of the Zimbabwe Craton. The craton is bounded by the Zambezi metamorphic belt to the north, the Mozambique belt to the east, and the Limpopo belt to the south. The Great Dyke, aligned approximately NNE, is about 550 km long and between 4 km and 11 km wide. Parallel to it are a number of gabbro and quartz gabbro satellite dykes (Chunnett and Mwatawha, 2008). The Great Dyke is longitudinally subdivided into a series of narrow contiguous layered chambers and subchambers Figure 3.1. In transverse section the subchamber is synclinal in shape, with essentially the same lithological succession being exposed on both sides of the longitudinal axis Figure 3.2.

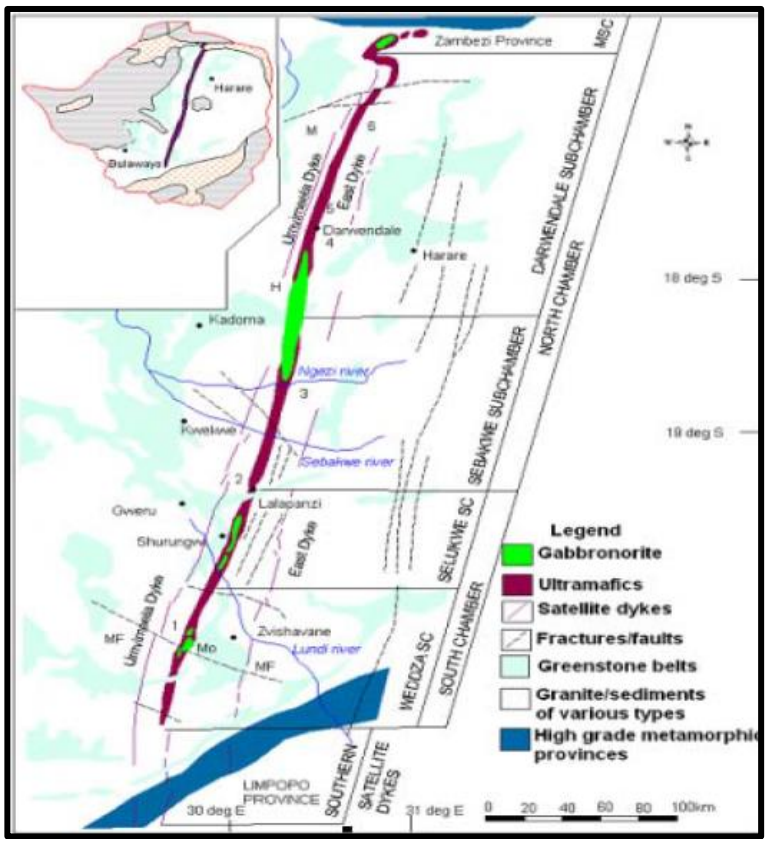

Figure 3.1 The Great Dyke of Zimbabwe (Chunnett and Mwatawha, 2008)

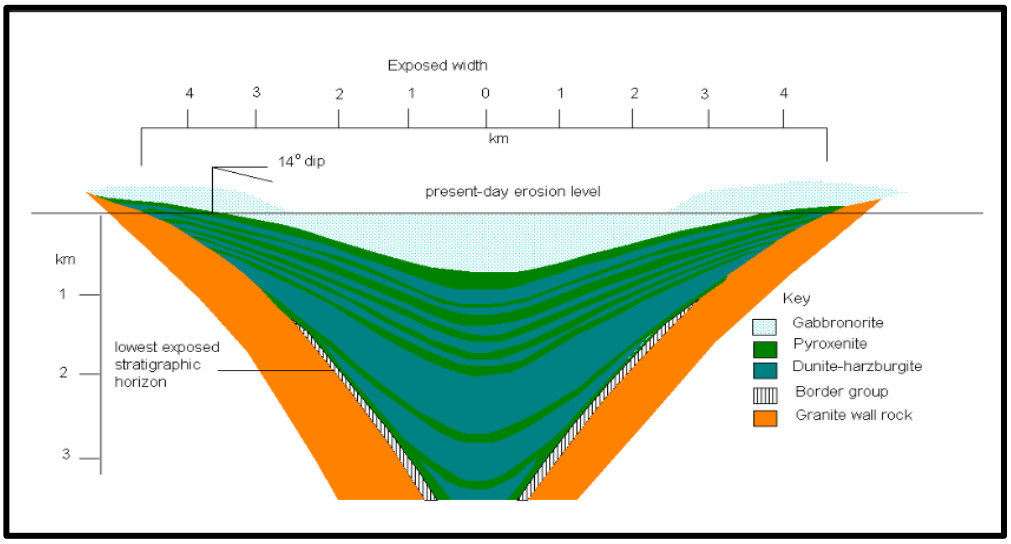

Figure 3.2 General transverse section across the Selukwe Sub-chamber (Chunnett and Mwatawha, 2008).

The PGEs are concentrated in the main sulphide zone (MSZ). The MSZ is located within the plagioclase pyroxenite of the P1 pyroxenite, close to the websterite-pyroxenite contact and extending from 2 m to 3 m beneath the websterite up into the base of the websterite Figure 3.3. The P1 pyroxenite is host to three sulphide zones known as S1, S2 and S3 respectively (Chunnett and Mwatawha, 2008).

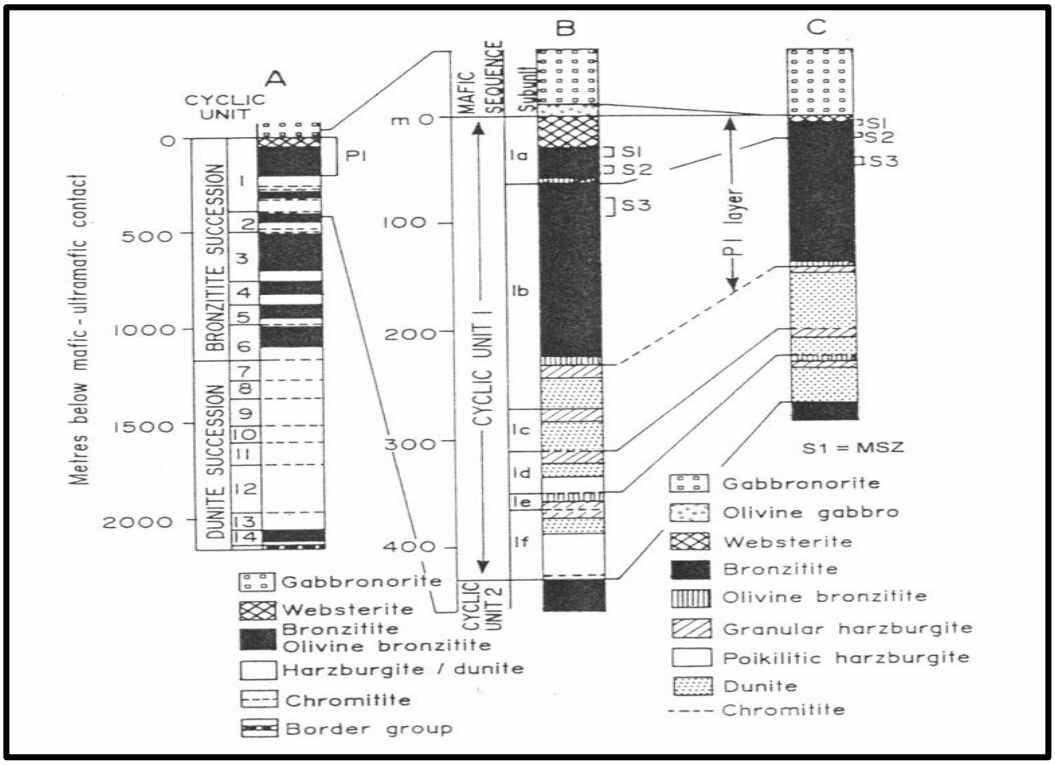

Figure 3.3 Great Dyke, showing the stratigraphic position of the S1, S2 and S3 sulphide zones (Chunnett and Mwatawha, 2008).

The local stratigraphy from the gabbronorite to P1 pyroxenite contact down to beneath the FWF is presented in Figure 3.4. The FWF is a layering parallel fault that occurs within the footwall of the MSZ. It is highly variable in thickness from 0.3 m to 0.6 m. The FWF only occurs at an average stratigraphic distance of 1.6 m below the base of the base metal sub zone (BMSZ) (Chunnett and Mwatawha, 2008). It consists of highly altered, mylonitised and brecciated plagioclase pyroxenite that does not swell in the presence of water. The ground conditions are expected to be poor due to the impact of the FWF (Chunnett and Mwatawha, 2008).

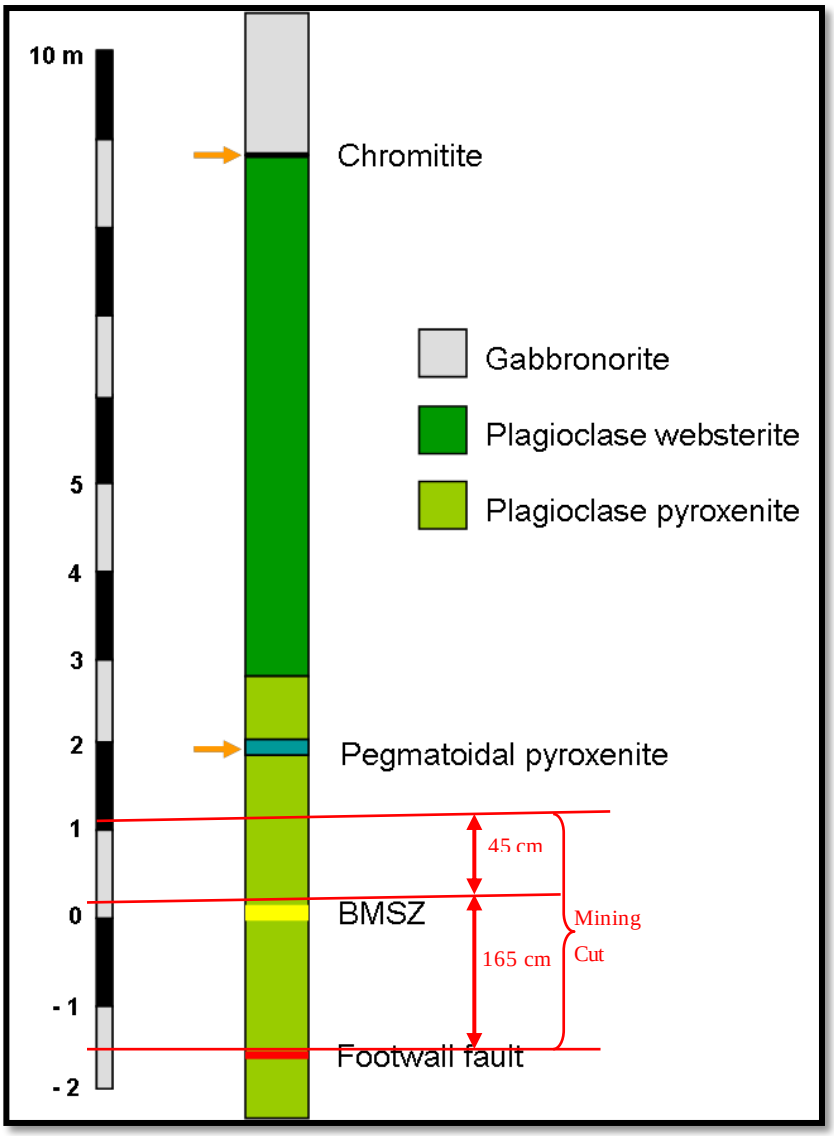

Figure 3.4 Average stratigraphic column for the Unki Mine area (Chunnett and Mwatawha, 2008)

A thin chromitite layer a few centimetres thick occurs at the gabbronorite-plagioclase websterite contact. According to Chunnett and Mwatawha (2008). The

chromitite layer causes a parting plane in the hangingwall. The websterite itself constitutes the uppermost ± 6 m of the P1 pyroxenite layer. It is underlain by plagioclase pyroxenite that makes up the remainder of 220 m thick P1 pyroxenite layer. The BMSZ lies at an average stratigraphic distance of 8.8 m below the gabbronorite-websterite contact, within the plagioclase pyroxenite and at an average of 2.8 m beneath the websterite basal contact and coincides with peak PGE values. A persistent pegmatoidal plagioclase pyroxenite layer occurs from 0.6 m to 2 m above the BMSZ. This could have some parting potential due to the larger grain-size perhaps allowing splitting along crystal cleavage planes. This also can cause a parting plane in the HW causing HW instability since it is very weak rock. The mining cut is 2.1 m as shown in Figure 3.4.

3.1. Regional geological features

The major regional geological structures around Unki Mine are best interpreted from LandSat, spot panchromatic and aeromagnetic datasets as shown in Figure 3.5 and Figure 3.6. Most of the lineaments interpreted from LandSat, spot and aeromagnetic data are major faults. These faults have vertical and horizontal displacements of up to ± 100 m.

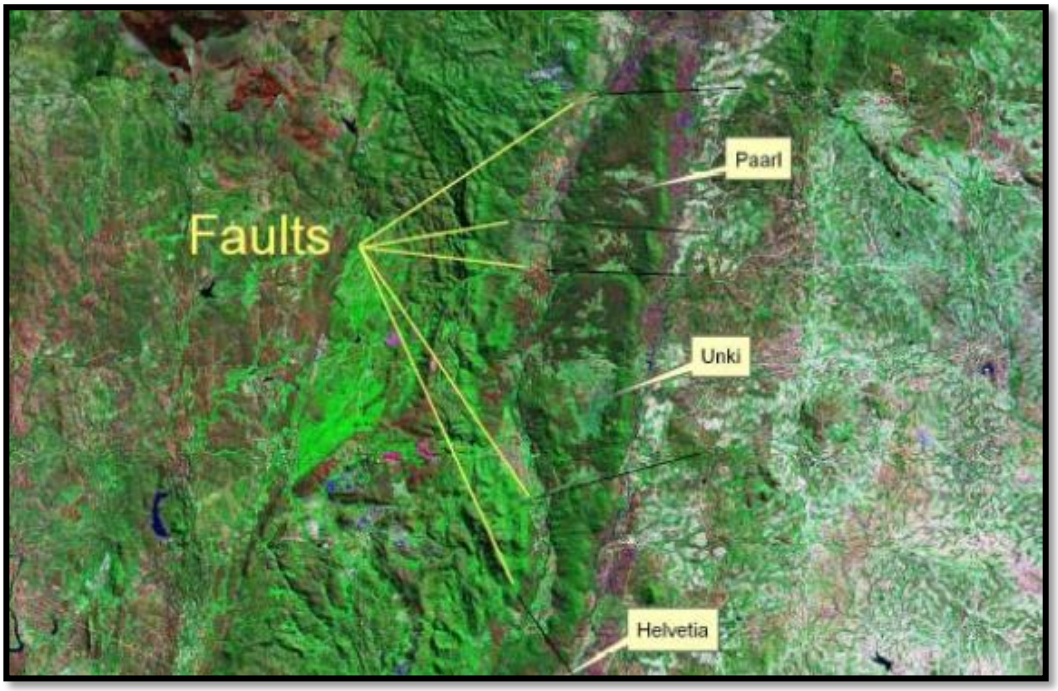

Figure 3.5 Landsat TM image showing transverse faults (Chunnett and Mwatawha, 2008)

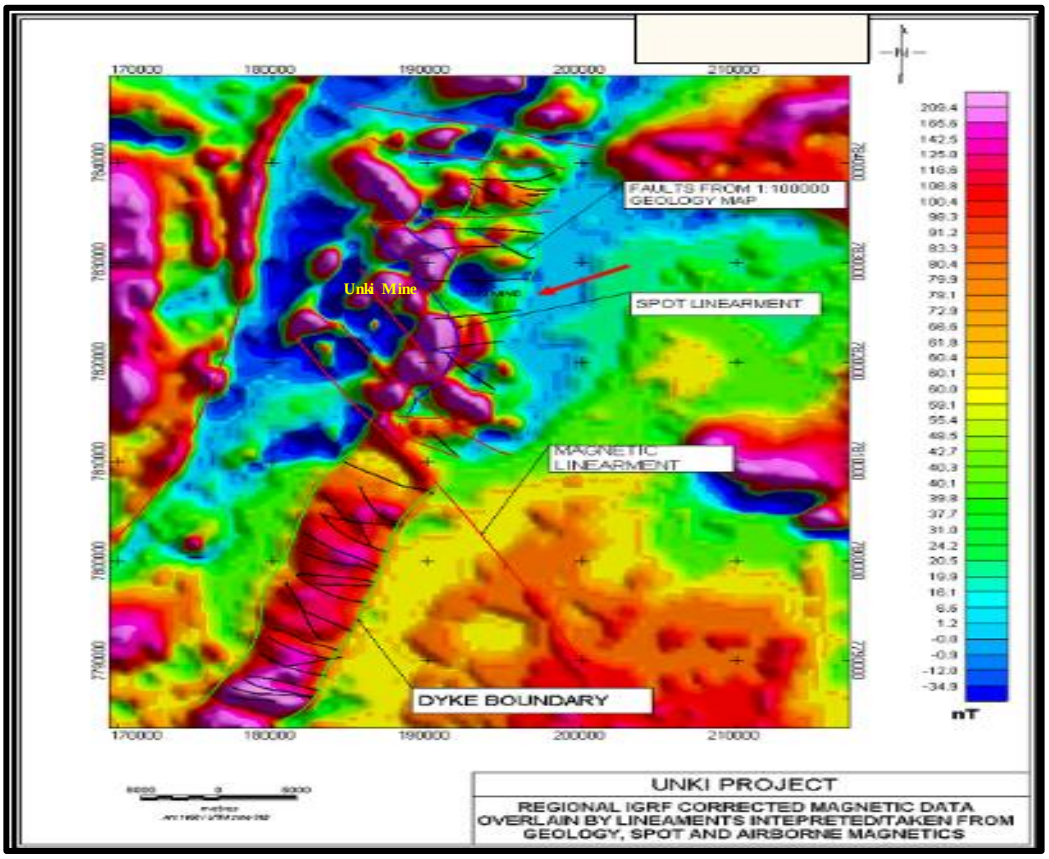

Figure 3.6 Aeromagnetic image showing faults around Unki Mine (Brown and Mwatahwa, 2005)

3.2. Local geological features

Understanding local geological structures in relation to the various mining methods used is essential for sustainable safety and productivity. There are a number of local geological features that need to be taken into account when designing support at Unki Mine. This section gives a brief explanation of some of the geological features as follows:

3.2.1. The footwall fault

The FWF is a layering parallel fault that occurs within the FW to the BMSZ, at an average distance of 1.6 m below the BMSZ. According to Chunnett and Mwatawha (2008), the FWF does not occur closer than 1 m below the BMSZ, and certainly does not cut through the BMSZ and occupy the HW as shown in Figure 3.7. It is a localized feature along which layering parallel movement has taken place and the extent is shown in Figure 3.8. This feature is filled with soft gouge material and occurs within the mining cut and parallel to the reef. The infill consists of highly altered, mylonitised and brecciated plagioclase pyroxenite.

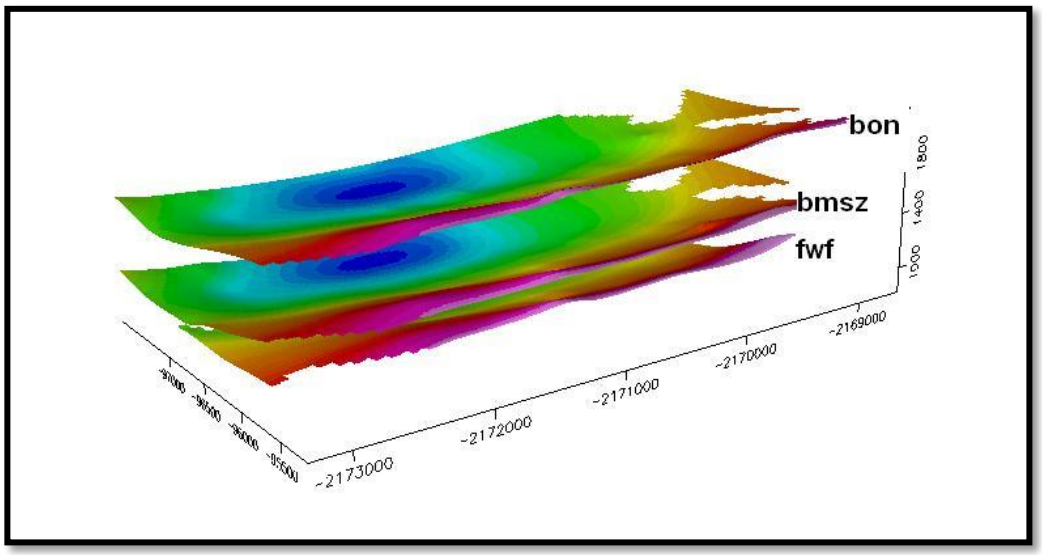

Figure 3.7 Location of the FWF and BMSZ looking from the south east (Brown and Mwatahwa, 2005)

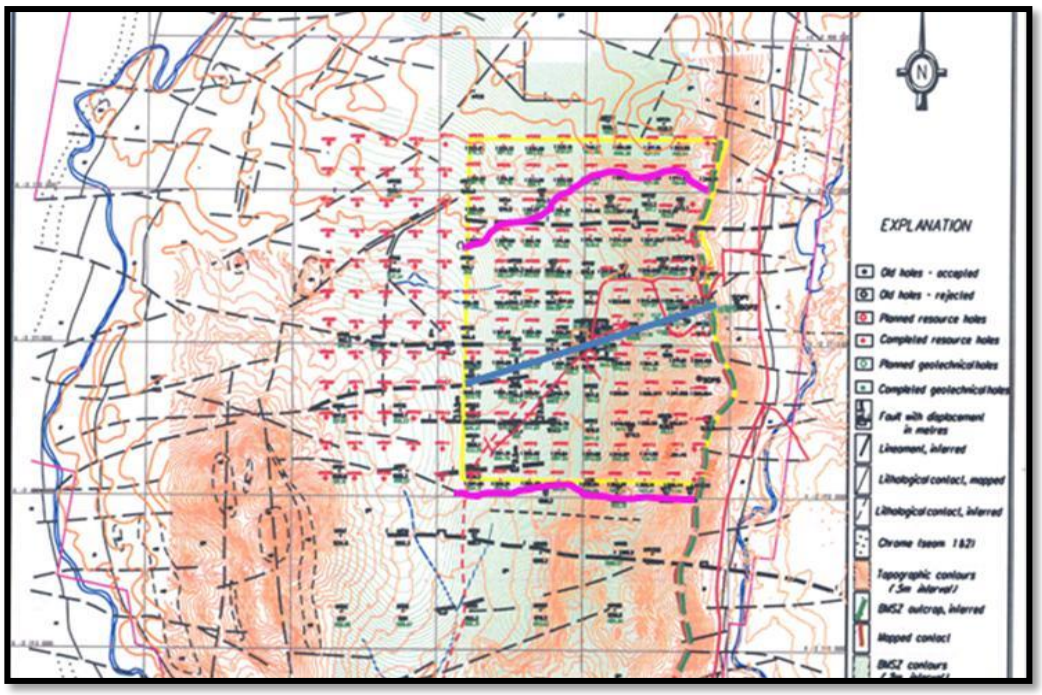

Figure 3.8 Extent of the FWF in Northern and Southern sections (bounded by solid pink lines (Brown and Mwatahwa, 2005)

The FWF is posing some negative effects on the stability of the excavations. Fortunately, the infill material is such that no swelling is anticipated in the presence of water. As the gouge material in the pillars is compressed, it deforms thereby failing the pillars in tension, effectively pulling the pillars apart. Once pillar failure has become extensive then HW failure initiates and differential movement of the HW becomes widespread (Roberts and Clark-Mostert, 2010).

3.2.2. Faults

Faults represent planes in the rock along which movement has occurred. Large displacement faults do exist in the mining area but are far fewer than small faults. The faults usually comprise relatively small throw and are generally reverse faults with displacements in the order of ± 1 m. These faults are intersected from time to time as mining progresses (Chunnett and Mwatawha, 2008).

3.2.3. Micro faults

Micro faulting of the BMSZ is relatively common especially within the mining cut. Micro faulting occur as one or more small-displacement layering oblique fault that occur in a bord that result in disruptions to the optimum cut and ground stability. To classify as a micro fault, the magnitude of displacement should be such that the reef layer (the BMSZ) must not be displaced outside the bord face (Chunnett and Mwatawha, 2008).

3.2.4. Joints

These are breaks or cracks in rock mass along which no movement has occurred. With reference to Chunnett and Mwatawha (2008), there are four dominant joint directions at Unki (Figure 3.9). Various portions of the GCD1 and GCD3 were examined and mapped for joints as shown in Figure 3.10.

The affected areas are in the upper sections from 1 North to 3 North sections on the northern side and 2 South to 3 South sections on the southern side. Mining 1 South section was abandoned due to poor ground conditions. It was found out that joints within the pyroxenite mining cut are typically altered mostly serpentinised, and even asbestos occurs within them. Joint density at Unki Mine however is relatively low. The joint frequency in the hangingwall is low and makes the hangingwall fairly competent.

The shallow dipping joints in the hangingwall may be a concern to hangingwall stability, particularly where they are highly altered and form wedges with the dominant joint sets. The jointing varies with intensity which can locally affect excavation stability and this can be measured by determining the rock mass rating

at a particular site (Roberts and Clark-Mostert, 2010). Table 3.1 shows the joint set parameters for dip, dip direction and spacing.

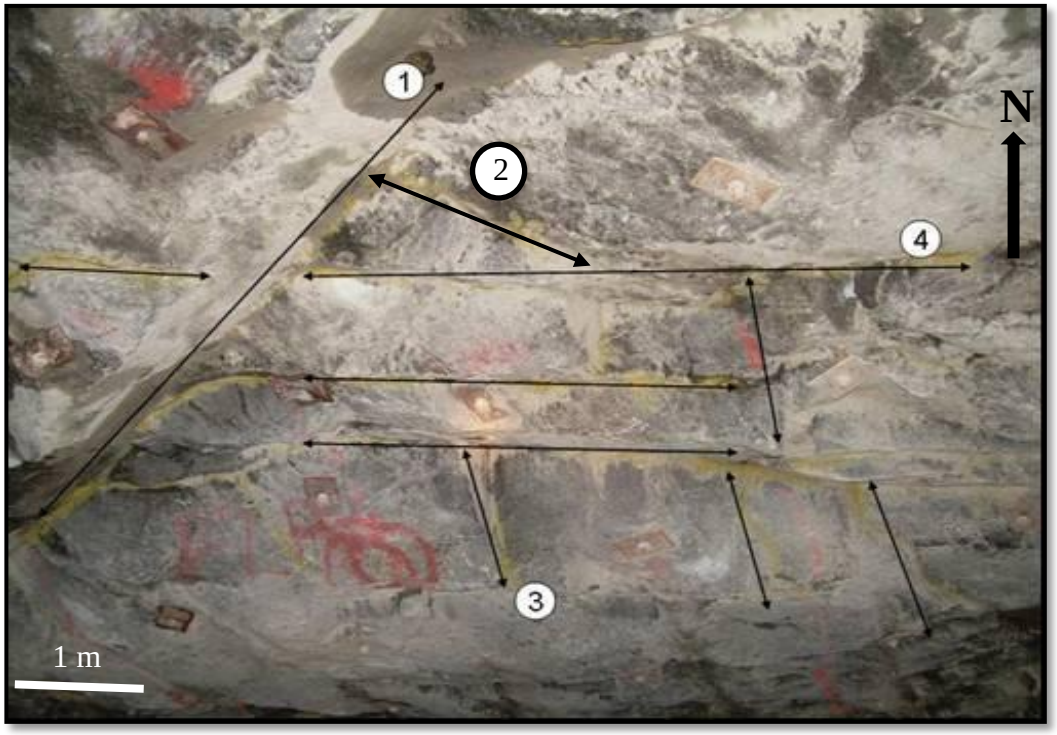

Figure 3.9 Unki Mine major joint sets (Chunnett and Mwatawha, 2008)

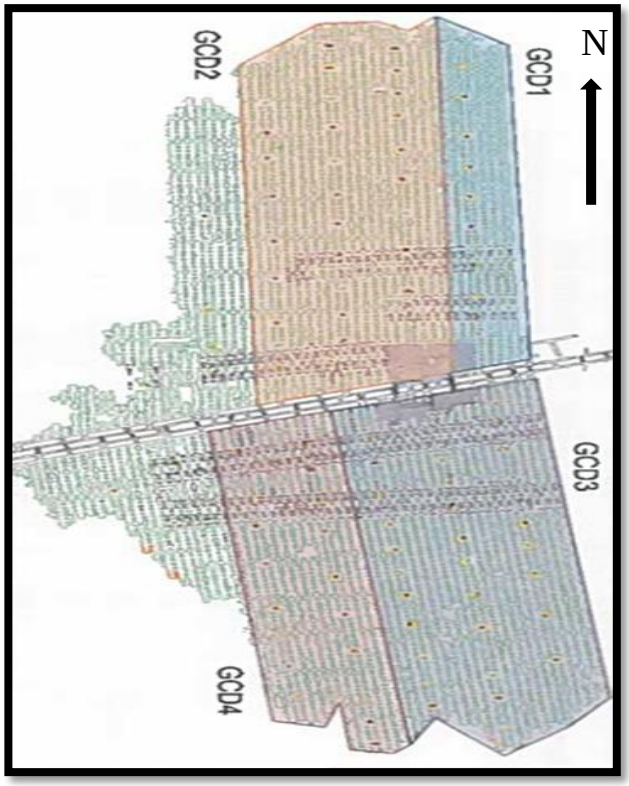

Figure 3.10 The four GCDs at Unki Mine (not to scale)

Table 3.1 Major joint sets at Unki Mine (Unki, 2014)

Joint set	Dip (º)	Dip Dir (º)	Spacing (m)	Comment
J1	64	38	1.7	Major
J2	47	126	1.5	Major
J3	60	218	4.9	Major
J4	17	317	1	Major

Figure 3.11 and Figure 3.12 show a rose-plot in the form of a histogram wrapped around 360^{O} showing the orientations and abundance of the mapped discontinuities. As observed in these diagrams, there is a major East-West set of discontinuities as well as minor North-South sets.

Two main joint sets with shallow dips of 30º to 60º have been observed 1.5 m to 1.7 m above the hangingwall of the BMSZ. Joint Set 1 and 2 have steep to sub-vertical dips and north-south strike with dip direction predominantly to the east and west respectively. A shallower joint component of the same strike orientation dips 47° to the west.

Joint Set 3 is steep to sub-vertical group striking north-south with dip direction mainly west. Joint Set 4 is shallow dipping group with dip direction ranging from east-west. The footwall fault just below the high-grade mining zone is represented in this group.

The stereo-net contour plot in Figure 3.13 shows that steep dipping discontinuity sets are well defined both in terms of their strike and dip. The contours represent clusters of poles. The discontinuity sets trend North-South and East-West. The stereo-net also shows that the majority of the discontinuities are steeply dipping as the great circles are close to the center which represents the vertical plane.

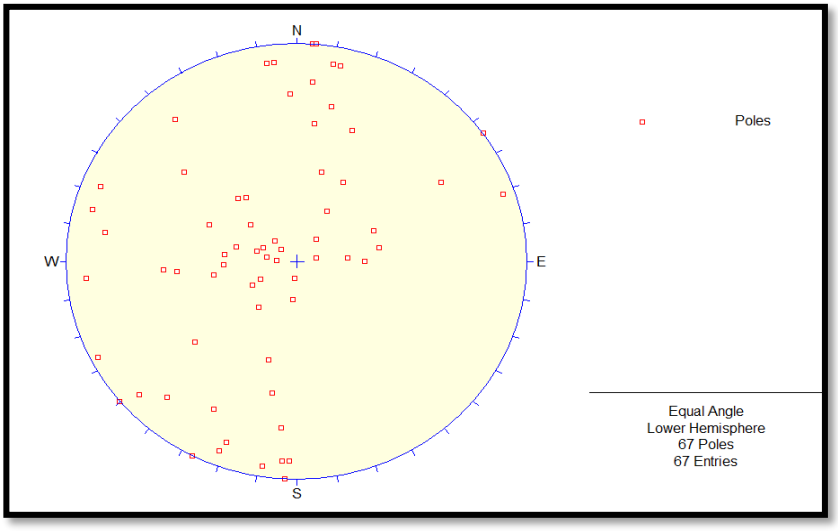

Figure 3.11 Joint poles plotted in terms of dip and dip direction

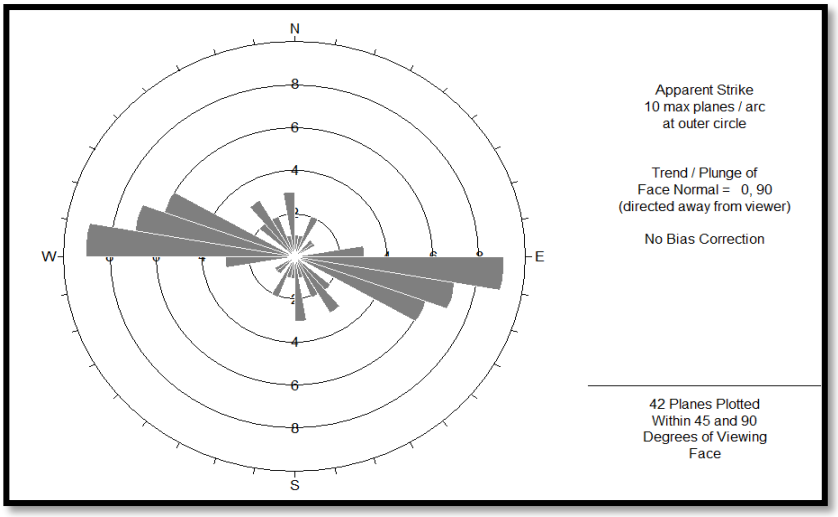

Figure 3.12 Joint rosette plot

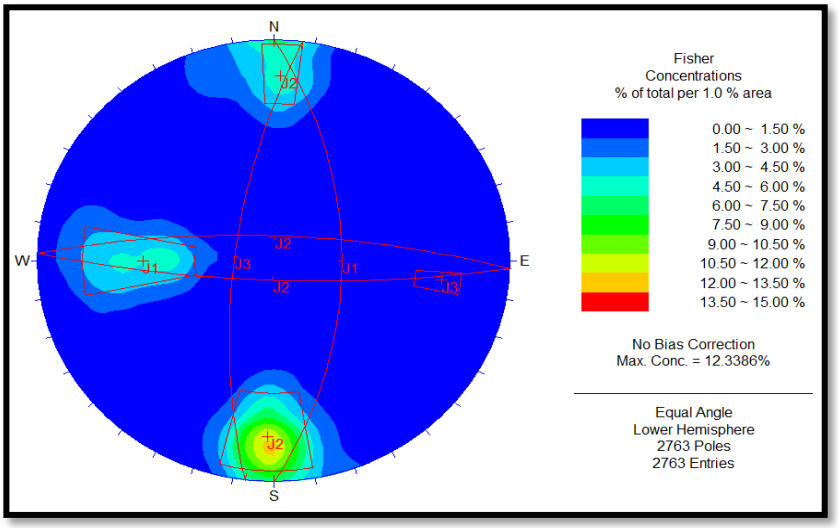

Figure 3.13 Contour plot of joint sets (Unki, 2014)

3.2.5. Flexural slip thrust faults/ Dome structures

The presence of flexural slip thrust faults in the Great Dyke was described earlier in the scientific literature. They are colloquially referred to as 'curved joints' and 'cooling domes' by the miners. These structures represent two particular threats to mining activities in the mining environment, namely FOG threat and pillar failure threat (Roberts and Clark-Mostert, 2010). The flexural slip thrust faults have a history of being the root cause of major FOGs during mining operations resulting in fatalities, injuries and losses of production (Roberts and Clark-Mostert, 2010).

According to Roberts and Clark-Mostert (2010), fault gouges are associated with flexural slip thrust faults. They went further to explain that if the bord and pillar mining method is employed and fault gouge is present in the vicinity of the reef, the integrity of the mining operations can be severely compromised and in some cases mining operations have been abandoned.

A flexural slip thrust fault causes FOG in two parts according to Roberts & Clark-Mostert (2010) by forming a layer-parallel portion of the fault, known as a flat and an inclined non planar surface, known as the ramp portion of the fault. Figure 3.14 is a schematic section illustrating the complexity of flexural slip thrust faults.

It is the ramp structures that are colloquially referred to as 'domes' and are known to have caused FOG fatalities, particularly where these structures intersect high angle joints, faults and veins. Figure 3.15 shows the actual FOG in a bord and pillar operation where the block that fell consisted of a ramp intersecting a steep joint.

Roberts & Clark-Mostert, (2010) mentions that the visual location of these dome structures before they fall can be difficult and some mines attempt to locate these structures using ground penetrating radar and borehole cameras and install recommended support as required. Apart from the obvious FOG hazards that these structures present, the spatial understanding of these structures in three dimensions and how they impinge on the mining excavations is important.

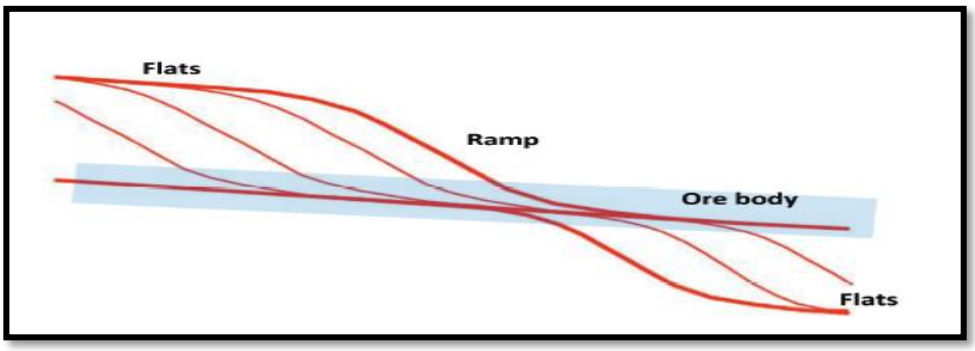

Figure 3.14 Schematic section showing multiple ramps and roof flats (Roberts and Clark-Mostert, 2010)

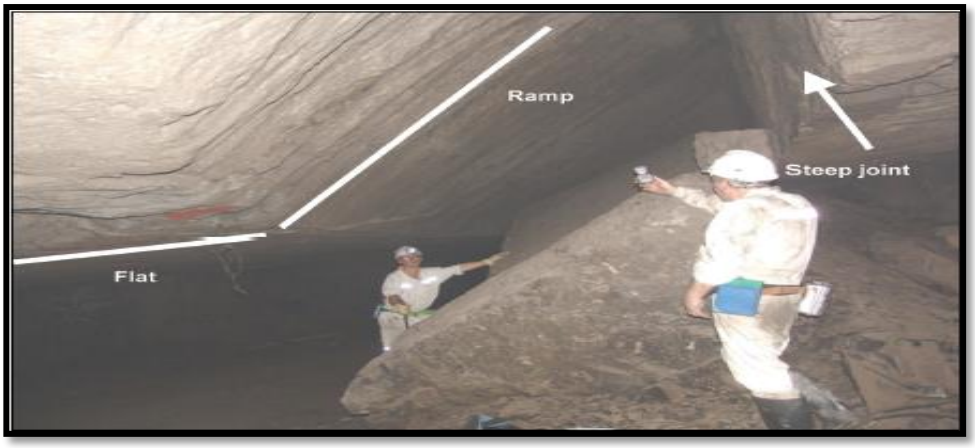

Figure 3.15 A fall of ground in a bord and pillar operation (Roberts and Clark-Mostert, 2010)

Figure 3.16 shows a triangular pyramid wedge averaging 4.2 m (l) x 3.2 m (w) x 0.5 m (h) weighing (22,780 kg) that dislodged in 1 North Strike at Unki Mine. The wedge collapsed after blast forming a cantilever beam hinged on two bolts on the last line of support.

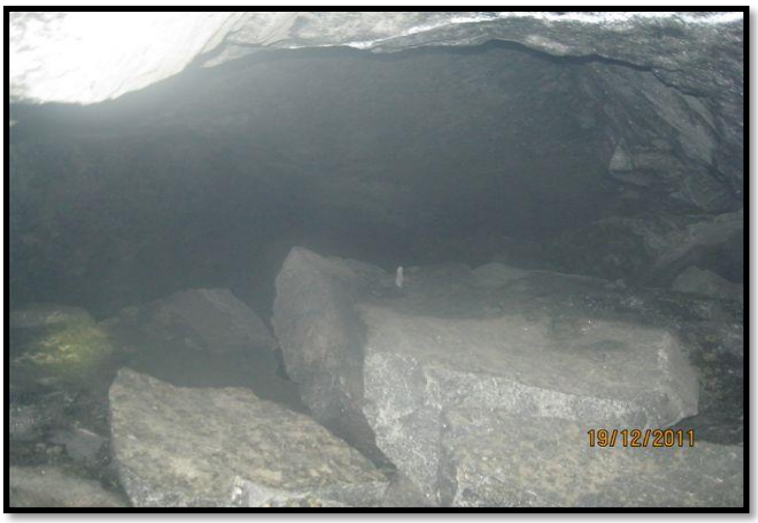

Figure 3.16 Unki mine FOG in 1NS due to dome structure (Unki, 2014)

Figure 3.17 shows the wedge that resulted in 2 North Strike FOG that was defined by 2 joints dipping at 58° NE and 62° SW as well as a granitic dyke in the South and a vertical joint to the North. This points that the FOGs are geologically controlled mostly.

Figure 3.17 FOG in 2 NS due to dome structure (Unki, 2014)

3.2.6. Dykes

Dykes are different rock types that cut across a parent rock. Vertical small dykes occur. These have little effect on the hangingwall stability, but again they should be identified and appropriate support recommended.

3.3. Chapter summary

Following this discussion in this section on geological features and their effects, it can be seen that mining spans and support strategies for mining operations at Unki Mine need to be modified to take into account the presence of these geological structures. Most of the FOGs recorded are geologically controlled as will be shown in the next chapter.

4. UNKI MINE FOG STATISTICS ANALYSIS

The previous chapter outlined the geological setting at Unki Mine on both regional and local environment. In this section, the FOG statistics for Unki Mine are discussed in detail in order to determine the support requirements. From 2010 to 2015, 24 FOG incidents were recorded in the Unki Mine FOG database. The incidents were filtered for example the FOG induced by conveyor belt suspended weight is excluded. The sample data used is small and this is likely to bring bias, irregular graphs and misrepresent the statistics. This sample was used anyway since this is the only available data.

4.1. Height of potential fall

The height of potential fall in a rock mass is the most critical parameter that influence support design. The fall-out heights were determined from in-situ measurements of dislodged rocks after falls. Mostly the fall-out height is used to determine the support resistance and energy absorption criteria that a proposed support system is supposed to meet (Ryder and Jager, 2002). Figure 4.1 shows twenty four cases of the Unki Mine FOG heights. At Unki Mine the fall out height is used to determine unit weight of FOG, the length of support bolts and spacing.

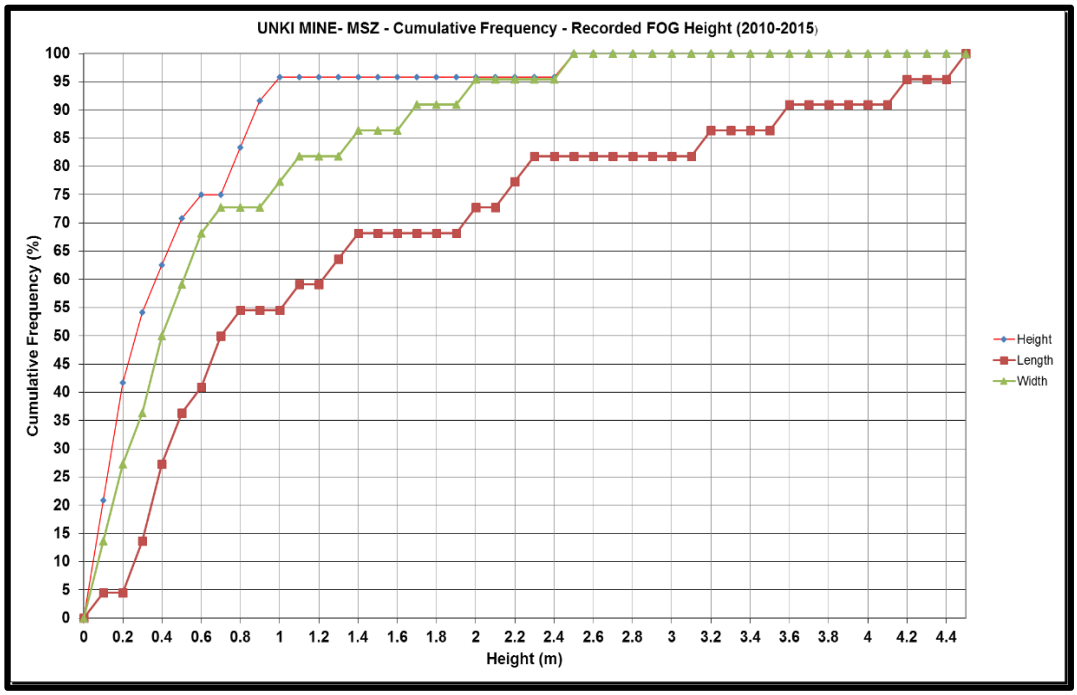

Figure 4.1 Unki Mine Cumulative Frequency - Recorded FOG Height (2010-2015)

The fall-out thickness data for the mine has been collected for rock falls only and there is nothing for rock bursts since this is a shallow mining environment where rock bursts are non-existent. The cumulative percentage fall-out heights are determined in Figure 4.1 and a support resistance criterion has to be set such that the support system caters for 95% of all potential rock falls (Stacey, 2001). Figure 4.1 shows that the fall-out height for the 95% level is at 0.9 m. The support resistance criterion is calculated using the Tributary Area Theory (TAT) where weight of rock to be supported is calculated by its volume, density and gravitational acceleration. The weight is then divided between a fixed number of support elements according to the attributable area (Ryder and Jager, 2002).

Figure 4.2 shows the frequency distribution for the fall out height. It shows that 10 out of 24 FOG incidents recorded are less than 0.1 m high. The frequency reduces as the fall out height increases.

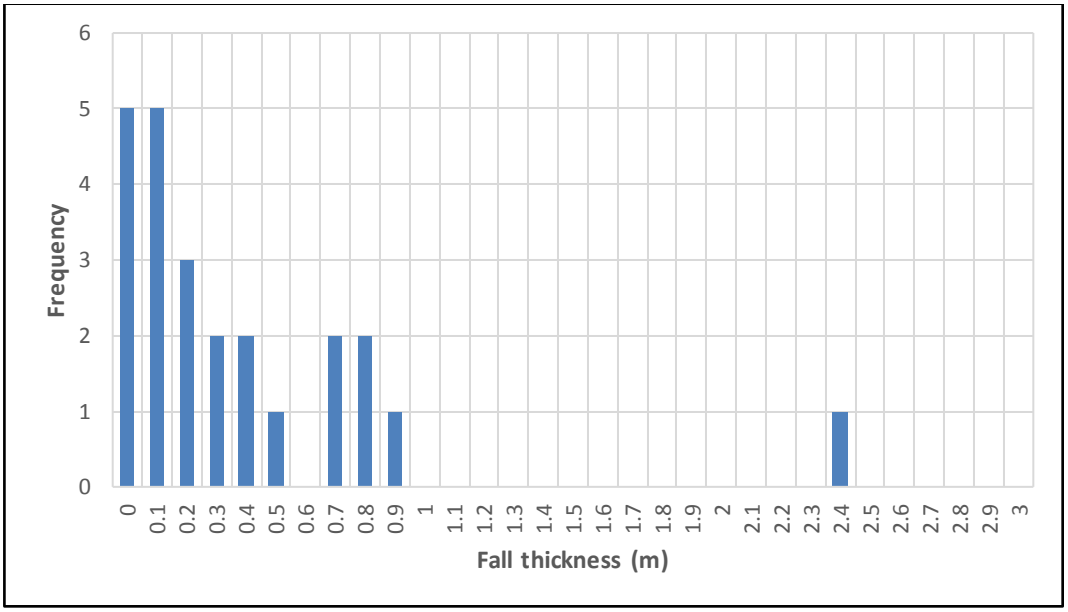

Figure 4.2 Unki Mine Frequency - Recorded FOG Height (2010-2015)

Figure 4.3 shows the FOG rock dimensions. The dimensions of all the FOG was 2.6 m (l) x 1.3 m (w) x 0.5 m (h) on average.

The descriptive statistics for the probability density function (PDF) and cumulative distribution (CD) for the FOG dimensions are shown in Appendix A, Figure A1 to Figure A5.

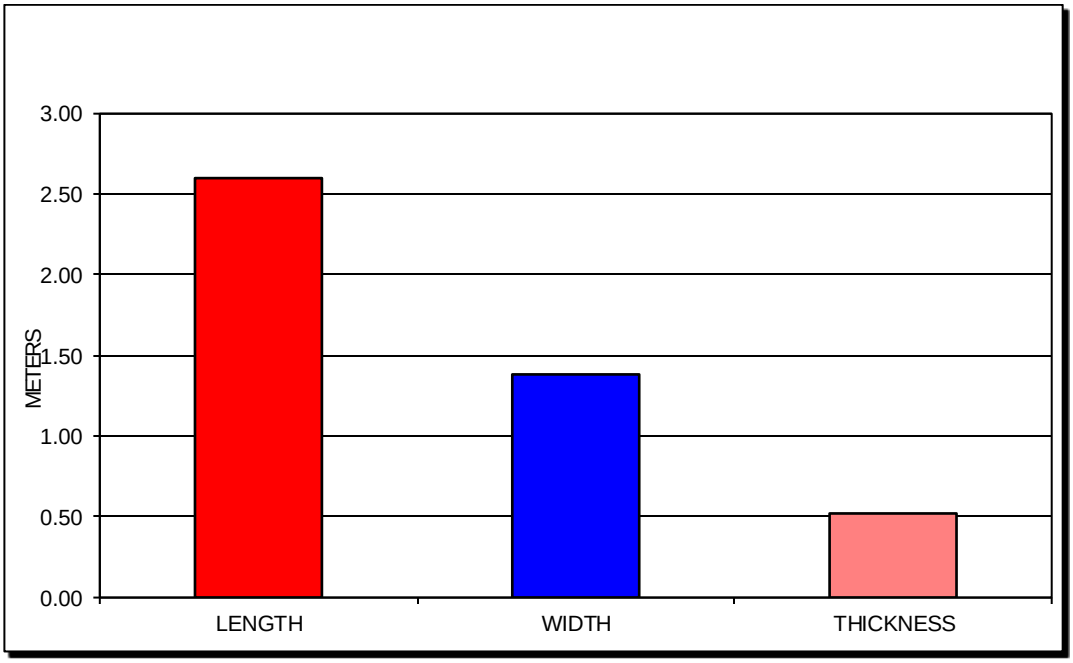

Figure 4.3 Unki Mine FOG Average Rock Dimensions

The mine's fall out heights were also measured against the distances from the face (Figure 4.4). The statistics show that the rocks with the highest fall-out thickness of 0.78 m are falling right at the face where the distance is less than 1m. This data shows the inadequacy of temporary support in the face area. Therefore the current design should be reviewed carefully.

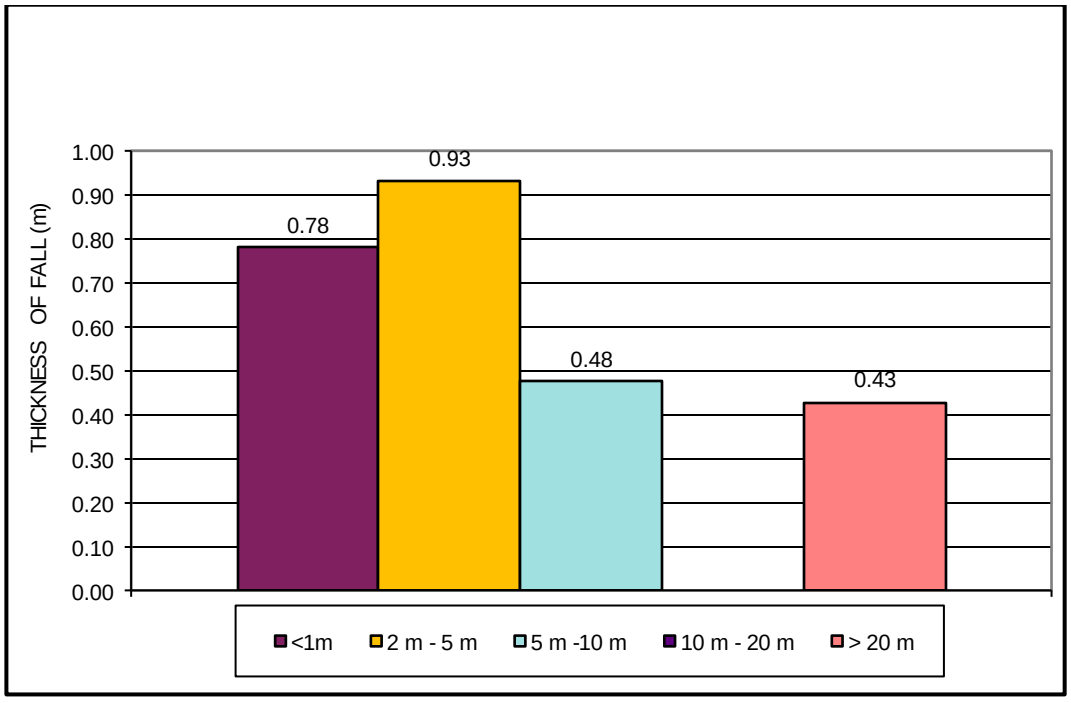

Figure 4.4 Fall out thickness at varied distances from face

This is mostly attributable to the fact that the area is unsupported and is associated with a lot of vibrations from drilling activities. The rocks with fall-out thickness of 0.93 m are falling from 2 m to 5 m from the face. The rocks with fall-out thickness of 0.48 m are falling from 5 m to 10 m from the face. At distances in excess of 20 m that is in the back areas, the rocks fall with a thickness of 0.43 m.

Figure 4.5 shows the top, middle and bottom sections of the 12 m bord at Unki Mine. The top and bottom sections are 3 m wide each. The middle section is 6 m wide.

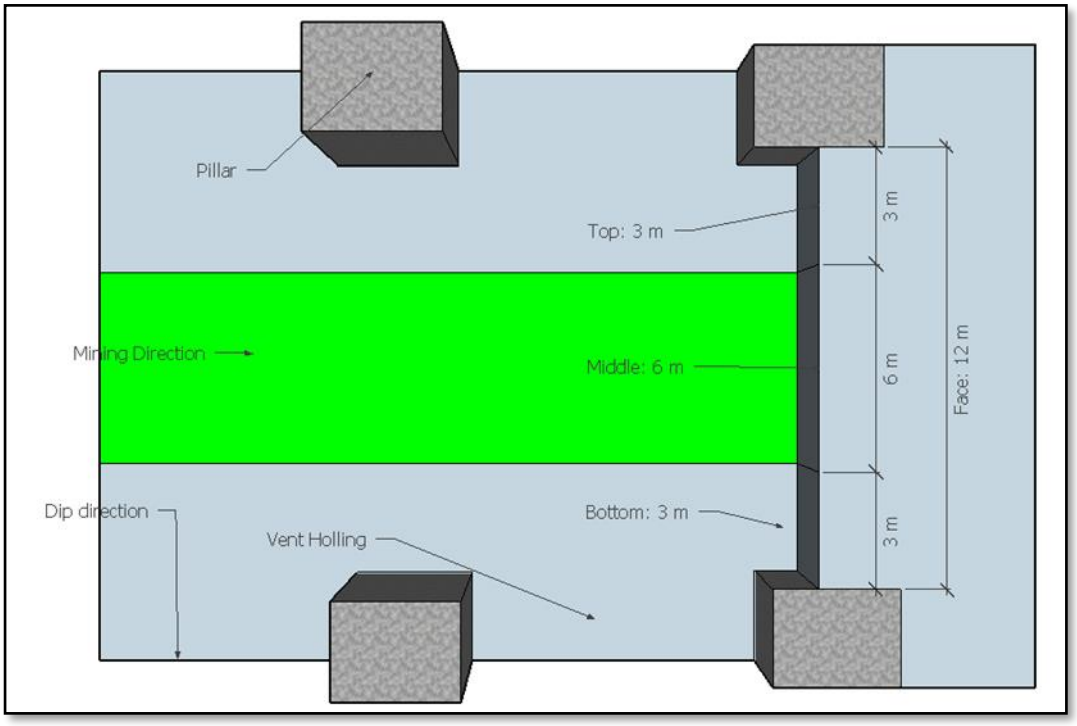

Figure 4.5 12 m bord section and face

The most problematic areas with FOG have been classified as shown in Figure 4.6. The statistics show that 46% of the rock falls occur at the center of the face most probably due to higher roof sag. On the other hand, 38% of the falls occur at the bottom of the face and only 4% at the top of the face. Face area nevertheless accounts for a combined 46% of all FOG and this shows the importance of face area that needs to be properly supported.

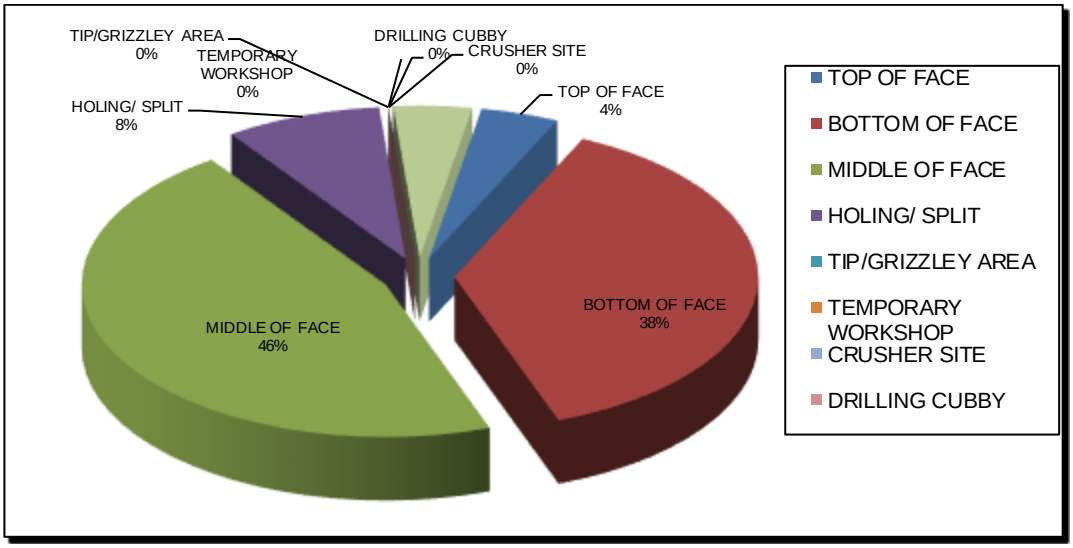

Figure 4.6 FOG Area – Stoping

4.2. Influence of geology on FOG statistics

Geological discontinuities such as dykes and faults have a significant influence on the FOG statistics as shown in Figure 4.7 and Figure 4.8. When the beam is cut across by a structure, it becomes a cantilever beam. The tensile stress for a cantilever is much higher than that in a clamped beam. Since there are more faults than dykes, the faults contributes 17% of the FOGs while dykes contributes only 8% of the FOGs. In blocky and highly fractured zones, the joints contribute 40% and fractures contribute 25% of the FOGs. In the support design process, the system has to address the FOG caused by low angle joints followed by faults and dykes.

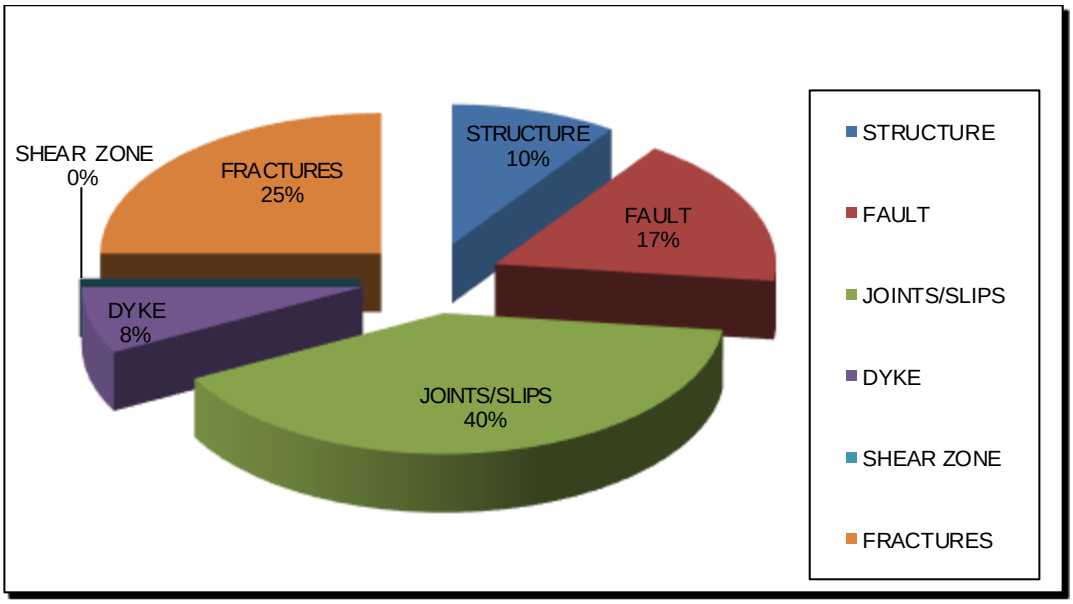

Figure 4.7 FOG due to geology

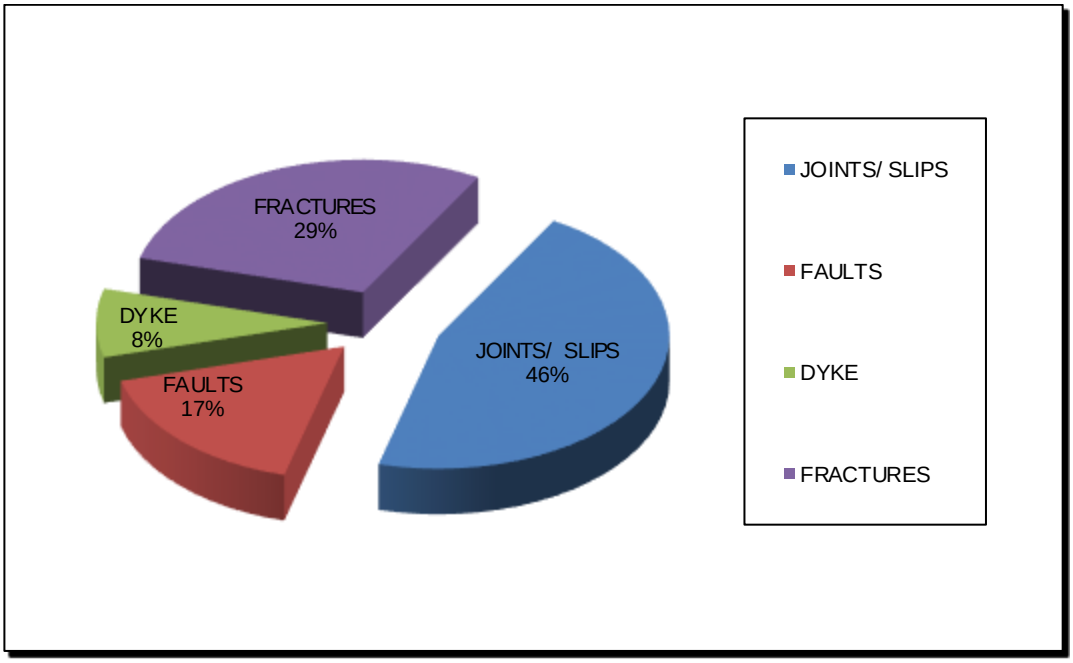

Figure 4.8 Fall boundaries

4.3. FOG during mining related tasks

Figure 4.9 shows that 25% of the FOG incidents occur during lashing with LHDs and the main contributor is the unsupported ground. Another 17% occur during supporting process. The 29% of the FOGs occurs at the time of blasting. This is where the dome structures collapse and keyblocks fall due to induced vibrations from the blast. Therefore the support design process must take into consideration the effects of blast induced vibrations.

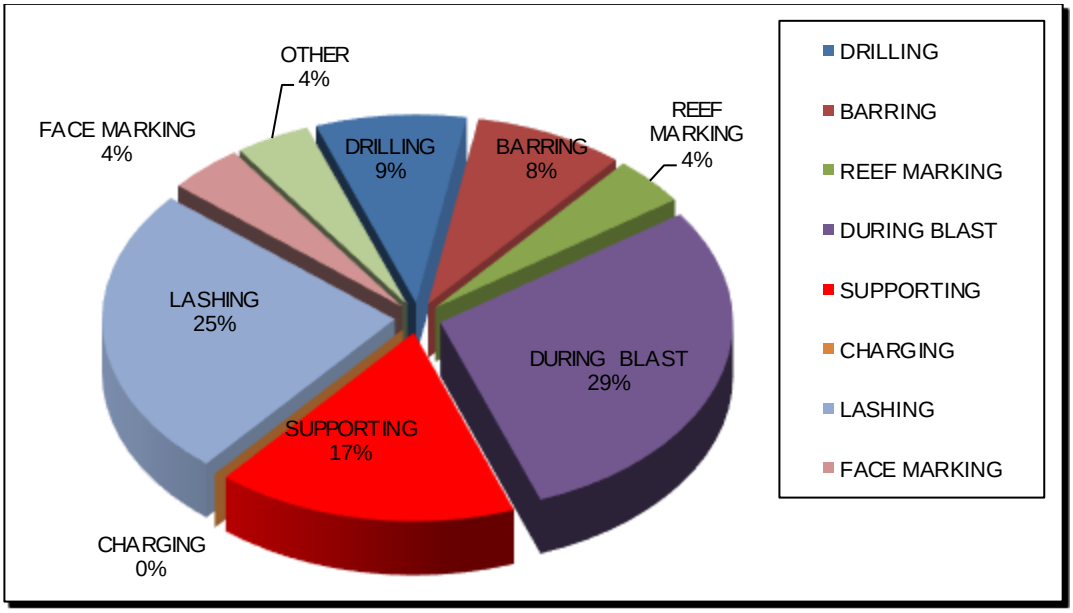

Figure 4.9 FOG during mining related tasks

Figure 4.10 shows that the LHD and drill rig operators are involved 37% in the FOG incidents at Unki Mine followed by lashers with 27% involvement and rock drill operators with 18%. This shows that more FOG incidents are caused by keyblocks falling as a result of vibrations from rig drilling and Jack hammer drilling.

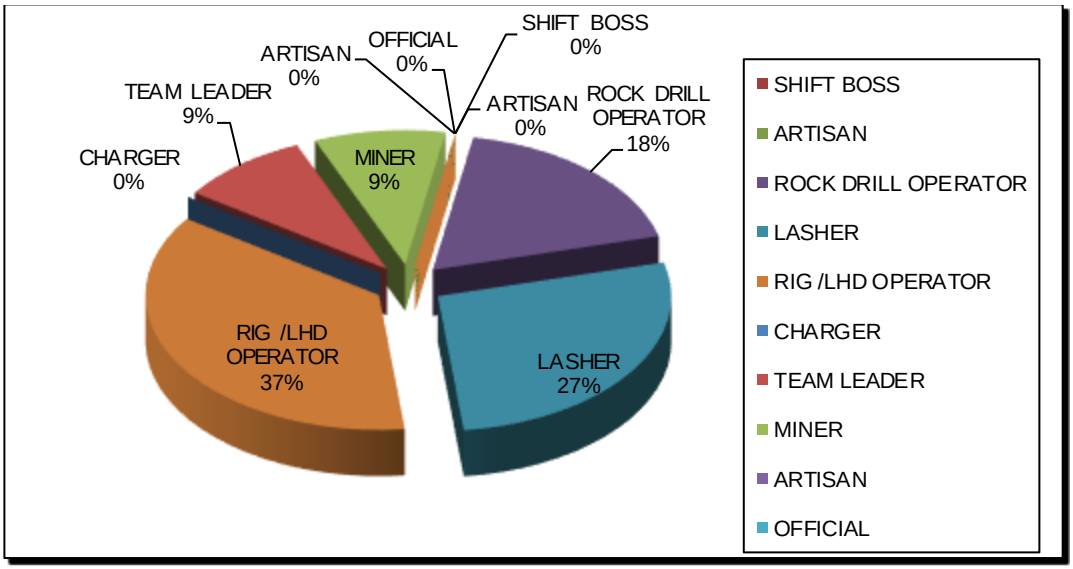

Figure 4.10 Injured/involved occupation during FOG

On analysing all the FOG incidents that caused injuries (Figure 4.11), it was found out that 22% caused head injuries, 7% caused neck injuries, 22% caused foot injuries, 14% caused leg injuries and 14% toe injuries.

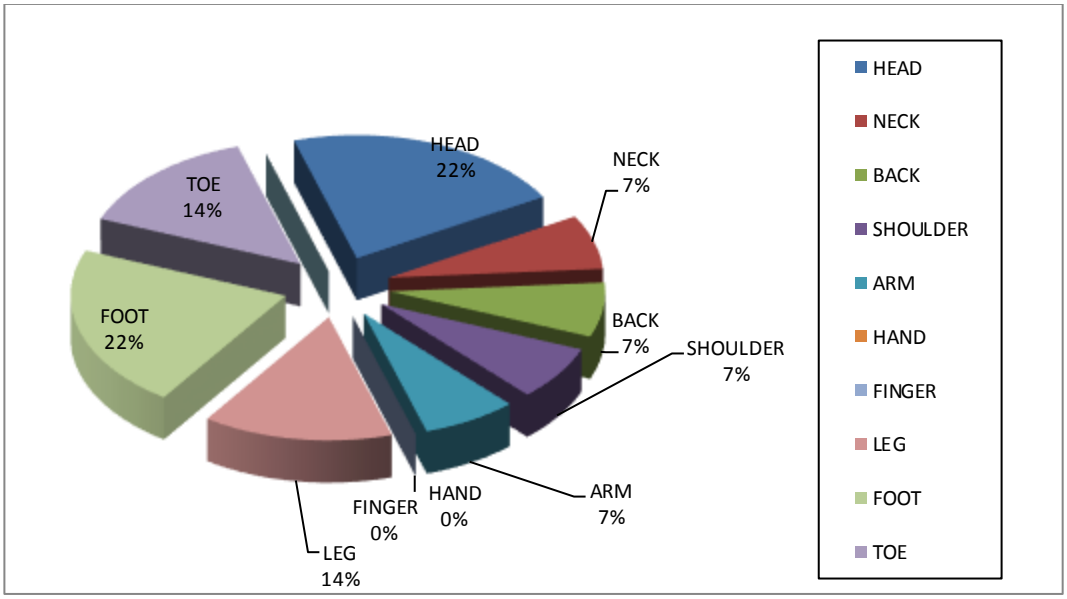

Figure 4.11 Body part injured due to FOG

On the severity of all the FOG incidents, Figure 4.12 shows that 20% were medical treatment cases, 12% were near misses, 16% caused serious injuries and 4% caused fatality. In-depth risk evaluation will be reserved for future studies

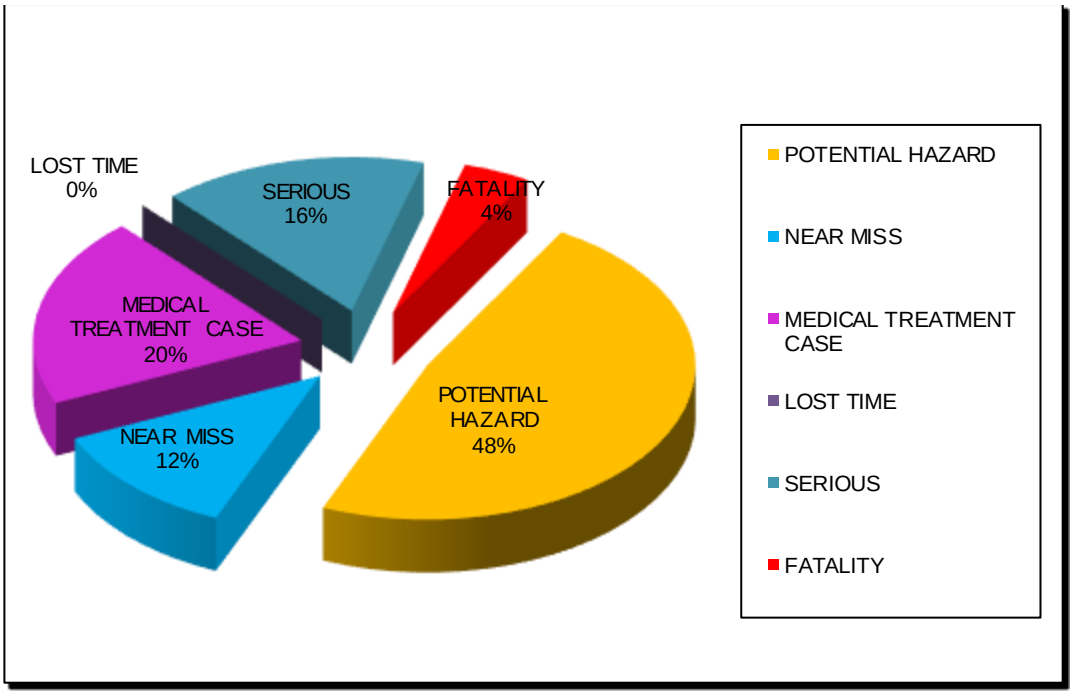

Figure 4.12 Severity of FOG

4.4. Effect of support on FOG

Figure 4.13 shows that 72% of all the FOG incidents are not associated with the support failure, 16% resulted from failing rock bolts, 11% was a result of poorly supported areas and no cases were reported for failing cable anchors. This means mostly keyblocks less than support spacing of 1.5 m x 1.5 m are falling between the installed bolts. Also the cable anchors shows that if installed they have never failed. The 3 m cable anchors proves to be the most effective type support currently being used because they do not fail.

Figure 4.14 shows the FOG incidents caused by the quality of support installed. After analysing all the FOG statistics that occurred in supported bords, 17% was a result of poor support installation and 83% shows that the support was to standard. The poor quality support could be caused by incorrect bolt spacing, using rock bolts with less capacity than demanded and using too short rock bolts that fail to pin blocks together.

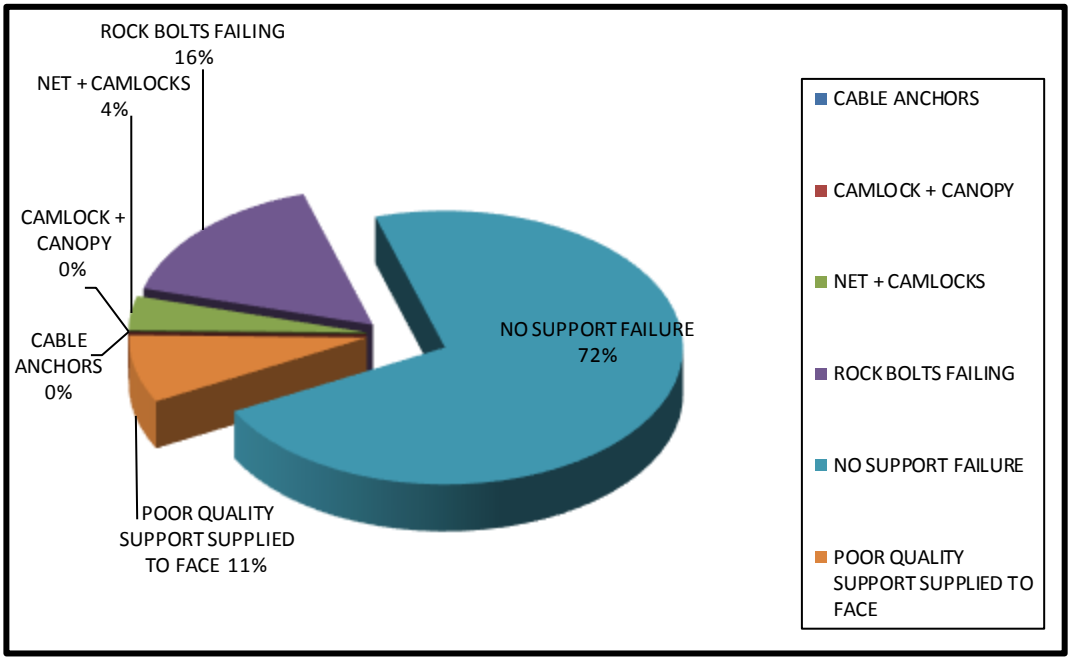

Figure 4.13 Effect of support quality on FOG

This shows that the FOGs resulted from the presence of dome structures that pulls and breaks the rock bolts (Figure 4.14). The support failed because the demand is higher than the bolt capacity. Although support installation is a problem, the major contributing factor to FOG is the span design itself. Even the places with proper support installation is failing, indicating the inadequacy of the current support design to provide adequate roof support.

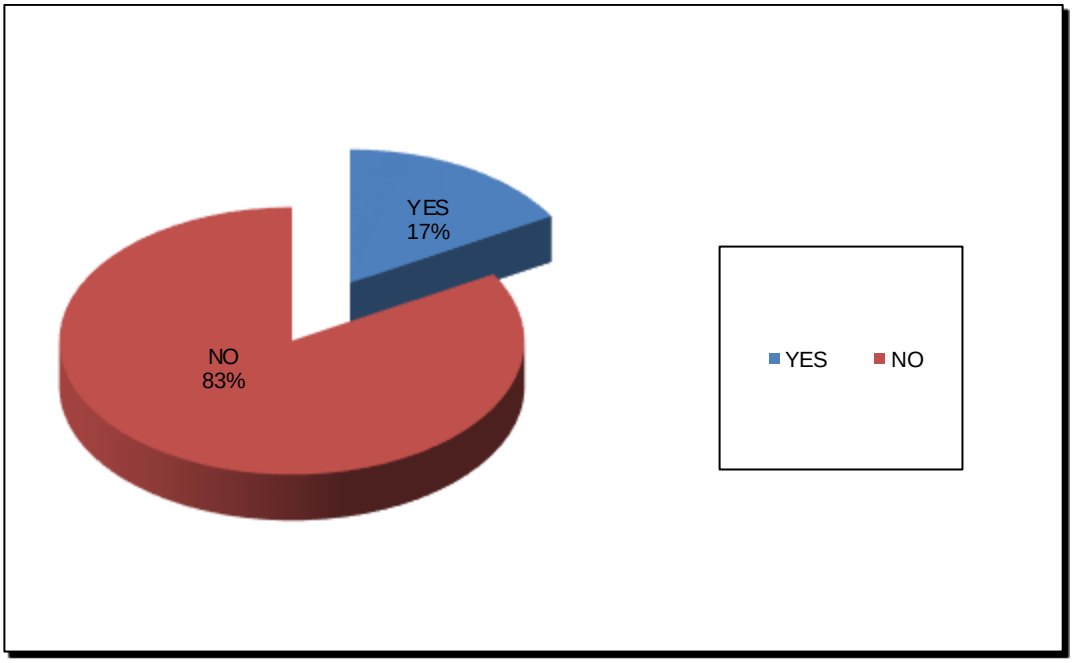

Figure 4.14 Effect of poor quality support installation on FOG

4.5. Chapter summary

This chapter dealt with FOG statistics from Unki Mine database that include FOG dimensions, the influence of geology on FOG and the effect of different support on FOG. It was found out that more FOG incidents were caused by rocks less than 0.1 m thick and these occur between support bolts. It was also found out that FOGs are partially triggered by vibrations from blast, rig drilling and Jack hammer drilling. The risk evaluation was not covered and that will be part of further research studies. The following chapter will focus on the laboratory testing of rocks to provide the input data into the numerical modelling software.

5. LABORATORY TESTING

This chapter will review the literature pertaining to the laboratory testing of mechanical properties of rocks in the area under study. The aspects referred to in this section include the importance of each test, the best way it can be done under laboratory conditions, specimen preparations, number of specimens needed and crucial rock engineering parameters which can be deduced from each test.

5.1. Mechanical properties of rocks

For one to be proficient in rock engineering design and prediction of rock mass behaviour, knowledge of how mechanical properties of rocks and rock masses are reliably determined in the laboratory needs to be firm. This section provides literature on these laboratory rock strength tests that are done as part of this research project.

Block samples of the immediate hangingwall rock, orezone and footwall zone were collected from the sections that experienced a high intensity of FOGs. Moisture loss was controlled by covering the samples with shrink wrap. Rock specimens to be tested included cylindrical samples. Preparation of cylindrical samples involved drilling cores of the required diameter according to the International Society for Rock Mechanics (ISRM) specifications and the sample diameter of 50 mm was used. The preparation also included cutting the cores to the required length and polishing the end surfaces so that they are flat and parallel. Testing was carried out within a month of sample collection.

The tests that were conducted included the following:

- Uniaxial compression strength tests.
- Brazilian tensile tests.
- Triaxial compressive strength tests.

The main properties to be determined include elastic modulus, compressive strength, tensile strength, triaxial strength, friction angle, shear strength, cohesion, density and Poisson's ratio. These properties will then be used in the design of robust support of excavations and design of stable spans at Unki Mine using numerical modelling softwares.

5.1.1. Uniaxial Compressive Strength test (UCS)

The aim of this test is to determine the UCS of a rock sample. It is used in strength classification and characterisation of intact rock. The UCS test gives an indication of the strength of a rock mass in which excavations are to be made, be it surface or underground.

According to Ryder and Jager (2002), a specimen of cross-sectional area (***A***) is loaded with an increasing force (***F***) until it 'fails'. The peak stress (***F/A***) at failure is called the UCS of the specimen, and is denoted by the symbol σ_c. Figure 5.1 shows the compression device. In addition to measuring the axial load, axial and radial strains or deformations are also measured via strain rosettes or gauges bonded to the specimen placed vertically and horizontally. Testing is conducted such that failure takes place within five to ten minutes of loading (Fairhurst and Hudson, 1999).

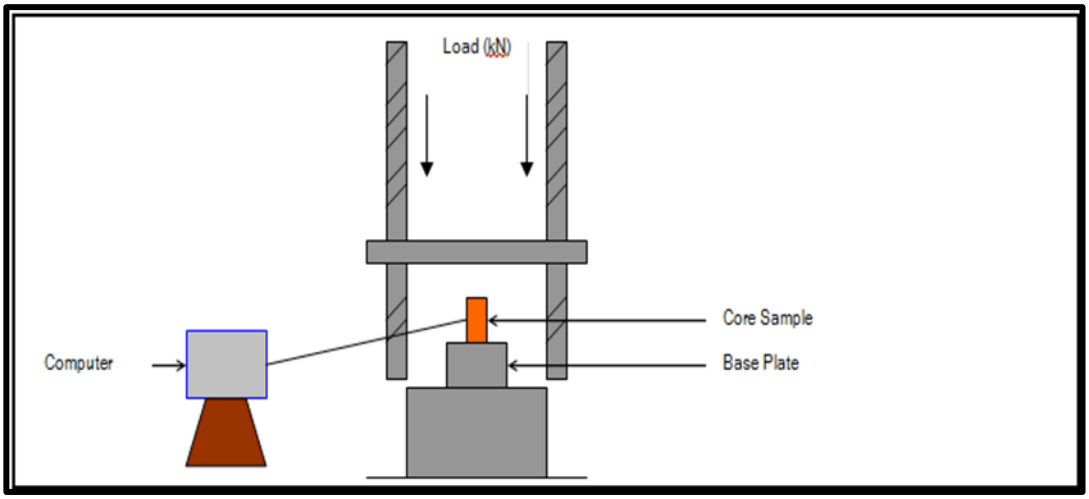

Figure 5.1 Core sample under load to determine the UCS

In the test, the stress-versus-strain curve for the axial and lateral direction is plotted. Average slope of the more-or-less straight line portion of the stress-strain curve is used to calculate the tangent or secant elastic modulus.

The specimen preparation in the UCS and Triaxial Tests are the same. Fairhurst and Hudson (1999) said "*the test specimens shall be right cylinders having a height-to-diameter ratio of between 2.0 and 3.0 and a diameter preferably of not less than approximately 50 mm. The diameter of the specimen shall be at least 20 times the*

largest grain in the rock micro-structure. The ends of the specimen shall be flat to ± 0.01 mm and shall not depart from the perpendicular to the longitudinal axis of the specimen by more than 0.001 radians. The sides of the specimen shall be smooth and straight to within 0.3 mm over the full length of the specimen. The diameter of the test specimen shall be measured to the nearest 0.1 mm by averaging at least two diameters measured at right angles to each other close to the top, the mid-height and the bottom of the specimen. The average diameter shall be used for calculating the cross-sectional area and later volume then density. The height of the specimen shall be determined to the nearest 1.0 mm. Specimens shall be stored for no longer than 30 days, and in such a way as to preserve, as much as possible, the natural water content. The number of specimens tested under a specified set of conditions should be sufficient to adequately represent the rock sample, and should be a function of the intrinsic variability of the rock".

A minimum of five specimens per set of testing conditions is recommended by Fairhurst and Hudson (1999). After the specimen is prepared, the strain or displacement measurement transducers or strain rosettes are attached to the specimen and the assembly is installed onto the lower platen in the load frame. A small preload is applied to the specimen in force control (Fairhurst and Hudson, 1999).

The force until failure will be obtained from the computer or the built-in load cell. Axial strain and radial strain may be recorded directly from strain indicating equipment or may be calculated from displacement readings depending upon the type of instrumentation used. In this case strain rosettes were used. The compressive strength, $\boldsymbol{\sigma_c}$ is calculated as shown in the following equation:

$$\boldsymbol{\sigma_c} = \frac{\boldsymbol{F}}{\boldsymbol{A}} \qquad (8)$$

Where, $\boldsymbol{F}$ is the compressive force on the specimen or maximum load,

$\boldsymbol{A}$ is the initial cross-sectional area,

In this test procedure, compressive stresses and strains are considered positive.

Axial strain, $\boldsymbol{\varepsilon_a}$, is calculated as shown below:

$$\boldsymbol{\varepsilon_a = \frac{\Delta l}{l_0}} \quad (9)$$

Where: $\boldsymbol{\Delta l}$ is the change in measured axial length (positive for a decrease in axial length)

$\boldsymbol{\Delta l_0}$ is the axial length of specimen prior to loading.

Radial strain is determined either by measuring the changes in specimen diameter or by measuring the circumferential strain. In the case of measuring the changes in diameter, the radial strain, $\boldsymbol{\varepsilon_d}$ is calculated as shown below:

$$\boldsymbol{\varepsilon_d = \frac{\Delta d}{d_0}} \quad (10)$$

Where: $\boldsymbol{\Delta d}$ is the change in diameter (negative for an increase in diameter)

$\boldsymbol{d_0}$ is the diameter of the specimen prior to loading.

The Young's modulus, $\boldsymbol{E}$, of the rock is defined as the ratio of the change in axial stress to the change in axial strain as shown in the following equation.

$$\boldsymbol{E = \frac{\sigma}{\varepsilon_a}} \quad (11)$$

Young's modulus is expressed in units of stress, i.e. Pascal (Pa) but the most appropriate multiple unit is the megapascal (MPa) or gigapascal (GPa).The most common methods of establishing the Young's modulus value are as follows. Tangent Young's modulus, $\boldsymbol{E_t}$ is measured at a stress level which is some fixed percentage of ultimate strength. It is generally taken at a stress level equal to 50% of the UCS. Average Young's modulus, $\boldsymbol{E_{av}}$ is determined from the average slopes of the more-or-less straight line portion of the axial stress-axial strain curve. Secant Young's modulus, $\boldsymbol{E_s}$ is usually measured from zero stress to some fixed percentage of the compressive strength, generally at 50% (Fairhurst and Hudson, 1999). Poisson's ratio (**v)** is the absolute value of the ratio of the diametric or transverse strain to the axial strain in compressive loading and is calculated as shown below:

$$\boldsymbol{\nu = \left|\frac{-\text{radial strain}}{\text{axial strain}}\right|} \quad (12)$$

5.1.2. Triaxial strength test

The triaxial strength test is done to determine the strength of cylindrical rock specimens subjected to triaxial compression. The test simulates the behaviour of rock underground, because it applies confining pressure to the sample during loading. The major stress is applied along the axis of the cylindrically shaped rock sample by the Amsler testing machine (Bieniawski and Hawkes, 1978). Minor stress is applied around the curved surface by the fluid pressure through the synthetic rubber jacket. From the results of this test the values of internal friction and cohesion of the rock material can be calculated.

The sample preparation for triaxial strength test is the same as for the UCS test described in section 5.1.1. A soft Amsler loading machine is used for applying and measuring the axial load in the rock specimen. It must be of sufficient capacity to fail the specimen at the selected confining pressure. A triaxial cell is needed to apply confining pressure to the specimen (Ulusay, 2014). The procedure is that the end cap of the Hoek triaxial cell is removed and the specimen is inserted in the high strength synthetic rubber jacket. After inserting the specimen in the jacket, platens and load spreader pads are placed at either ends of specimen. The tightened assemblage is positioned at the bottom platen of the testing machine, and then the lower platen raised until the cell is just supported in the machine (Ulusay, 2014).

Confining pressures of 5, 10, 15, 20 and 25 MPa are used successively in order to determine the strength at which the specimen fails. The confining pressure at Unki Mine underground conditions must be considered since the orebody dips at 14^{O}. The increase in depth also changes the confining stress and affects the rock strength.

For triaxial strength test, the specimen is loaded axially at a steady rate so that failure occurs within 5 minutes. The load is released completely, keeping the axial pressure greater than radial pressure so as to prevent rupturing the synthetic rubber jacket and the above step is repeated for all the samples. The results are plotted on an Axial Pressure (σ_1) vs Confining Pressure (σ_3) graph over the range of confinement. Figure 5.2 shows the Mohr-Coulomb criterion in σ_1 vs σ_3 space.

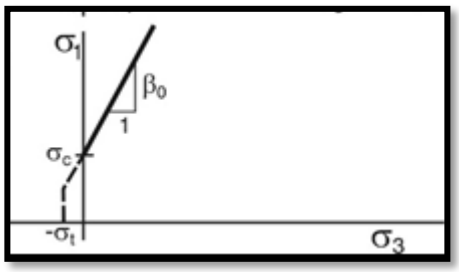

Figure 5.2 Mohr-Coulomb in σ_1-σ_3 space (Lightfoot, 2000)

If a near-linear strengthening relationship is found to apply in a σ_1 vs σ_3 space, the values of the $\boldsymbol{\sigma_1}$ intercept $\boldsymbol{\sigma_c}$ and slope $\boldsymbol{\beta_o}$ are read off. The angle of internal friction $\boldsymbol{\phi_i}$ and cohesion $\boldsymbol{C_0}$ are calculated from the following equations according to Ryder and Jager (2002).

$$\boldsymbol{\sigma_1 = \sigma_c + \beta_0 \sigma_3} \quad (13)$$

$$\boldsymbol{\beta_0 = \frac{1+\sin \emptyset_i}{1-\sin \emptyset_i}} \quad (14)$$

$$\boldsymbol{\sin \emptyset_i = \frac{\beta_0 - 1}{\beta_0 + 1}} \quad (15)$$

$$\boldsymbol{\emptyset_i = arc\ sin \frac{\beta_0 - 1}{\beta_0 + 1}} \quad (16)$$

$$\boldsymbol{c_0 = \sigma_c \frac{1-\sin \phi_i}{2 * cos\ \phi_i}} \quad (17)$$

Where:

β_0 is the calculated gradient of the line of best fit drawn through the σ_1 vs σ_3 space.

σ_c is the vertical intercept of the line of best fit drawn through the σ_1 vs σ_3 space.

5.1.3. The Brazilian test/ Tensile strength test

This test is intended to measure the uniaxial tensile strength of rock specimen indirectly. The justification for the test is based on the experimental fact that most rocks in biaxial stress fields fail in tension when one principal stress is tensile and the other finite principal stress is compressive with a magnitude not exceeding three times that of the tensile principal stress. Also the test is much easier to perform rather than the direct tensile strength test (Bieniawski and Hawkes, 1978). The suggested apparatus to achieve this is illustrated in Figure 5.3. This is a suitable compression testing machine to measure the applied load with the required

accuracy. Two steel loading jaws are designed so as to contact a disc-shaped rock sample at diametrically-opposed surfaces over an arc of contact. The loading rate is set so that failure would occur within 5 minutes. To achieve this, a loading rate of 200 N/s is recommended. The specimen is loaded to failure and is assessed for mode of failure. At least 10 test samples are needed (Bieniawski and Hawkes, 1978).

Bieniawski and Hawkes (1978) stated that "*the test specimens should be cut and prepared using clean water. The cylindrical surfaces should be free from obvious tool marks and any irregularities across the thickness of the specimen should not exceed 0.025 mm. End faces shall be flat to within 0.25 mm and parallel to within 0.25 °. The specimen diameter shall not be less than NX core size, approximately 50 mm, and the thickness should be approximately equal to the specimen radius*".

The results are tabulated and the indirect tensile strength of the specimen is calculated from the following equation:

$$\sigma_t = \frac{2F}{\pi LD} \qquad (18)$$

Where F = Maximum load at failure (N).

L = Length or thickness of specimen measured at the center (mm).

D = Diameter of specimen (mm).

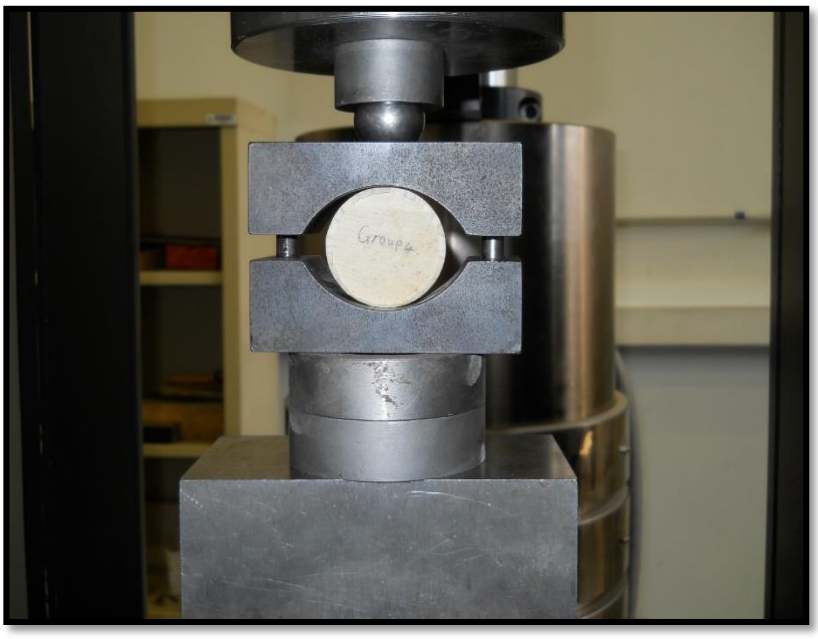

Figure 5.3 Brazilian tensile strength testing apparatus

5.2. Results of laboratory tests

Laboratory testing was carried out successfully and Table 5.1 shows the results. The laboratory results were used to determine descriptive statistics for the hangingwall, ore zone and footwall. The geotechnical characteristics of the hangingwall is very important in order to determine the type and quantity of support to be used. These results will be used as input data in the support design.

Table 5.1 Summary of laboratory results

PARAMETER	HANGINGWALL			ORE ZONE	FOOTWALL
	GABBRONORITE	WEBSTERITE-PYROXENITE	PEGMATOIDAL PLAGIOCLASE PYROXENITE	PLAGIOCLASE PYROXENITE	MYLONITISED AND BRECCIATED PLAGIOCLASE PYROXENITE
UCS (MPa)	201 (5 Samples)	263 (5 Samples)	225 (5 Samples)	216 (5 Samples)	194 (5 Samples)
Tensile strength (MPa)	10.5 (10 Samples)	9.1 (10 Samples)	11 .4 (10 Samples)	20.2 (10 Samples)	7.0 (10 Samples)
Young's Modulus (GPa)	100.5	38.0	125.0	65.0	30.2
Poisson's ratio (v)	0.30	0.27	0.25	0.24	0.29
Cohesion (MPa)	33.5	33.0	35.7	33.2	25.2
ϕ Friction angle (°)	48.6	49.4	53	49.0	40.0
Unit weight (g/cm^3)	2.89	3.07	3.26	3.27	2.89

The immediate hangingwall consists of a layer of pegmatoidal pyroxenite and therefore lies in the tensile zone in the back areas. Pegmatoidal pyroxenite layer occurs anywhere from about 0.6 m to 2 m above the BMSZ and could have some parting potential due to the larger grain-size perhaps allowing splitting along crystal cleavage planes. It has a UCS of 197 MPa minimum and 250 MPa maximum with 225 MPa on mean as shown in the probability density function in Figure 5.4.

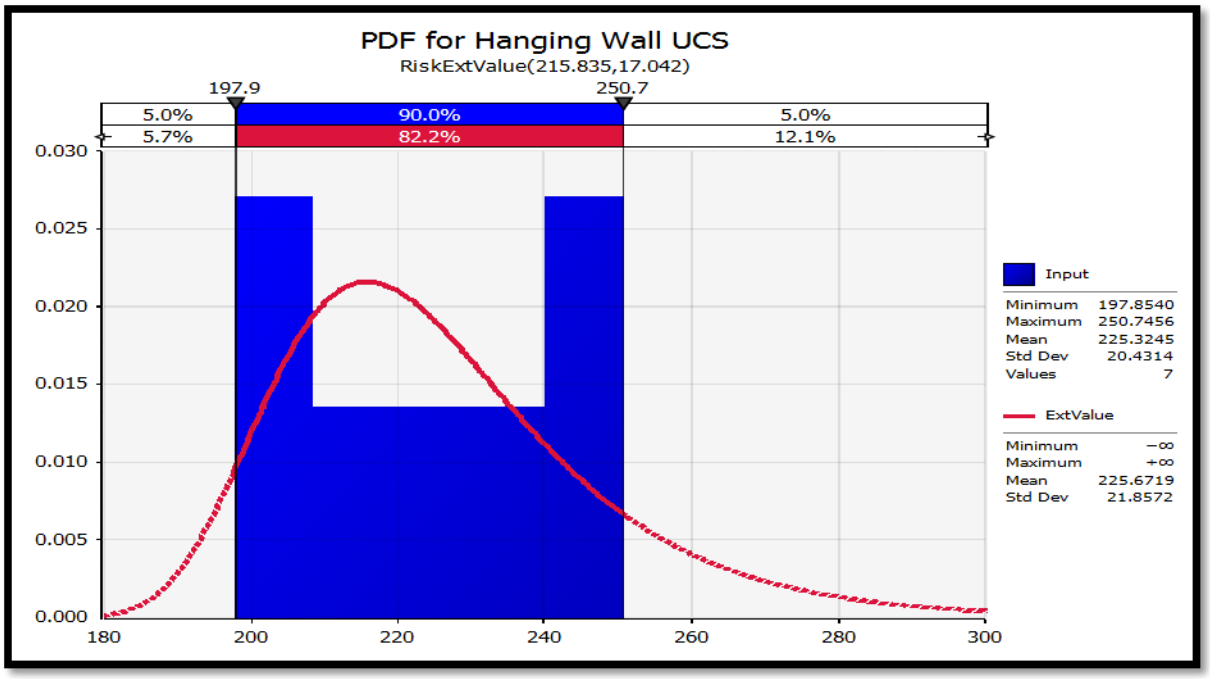

Figure 5.4 Probability Density function (PDF) for Hangingwall UCS

The ore zone consists of plagioclase pyroxenite layer where mining takes place and the pillars are formed. Plagioclase pyroxenite is a hard and tough rock with a UCS of 216 MPa on average as shown in Figure 5.5. Plagioclase pyroxenite is highly jointed and these joints lower rock mass strength. The extent of joints may cause unstable conditions to develop in large spans.

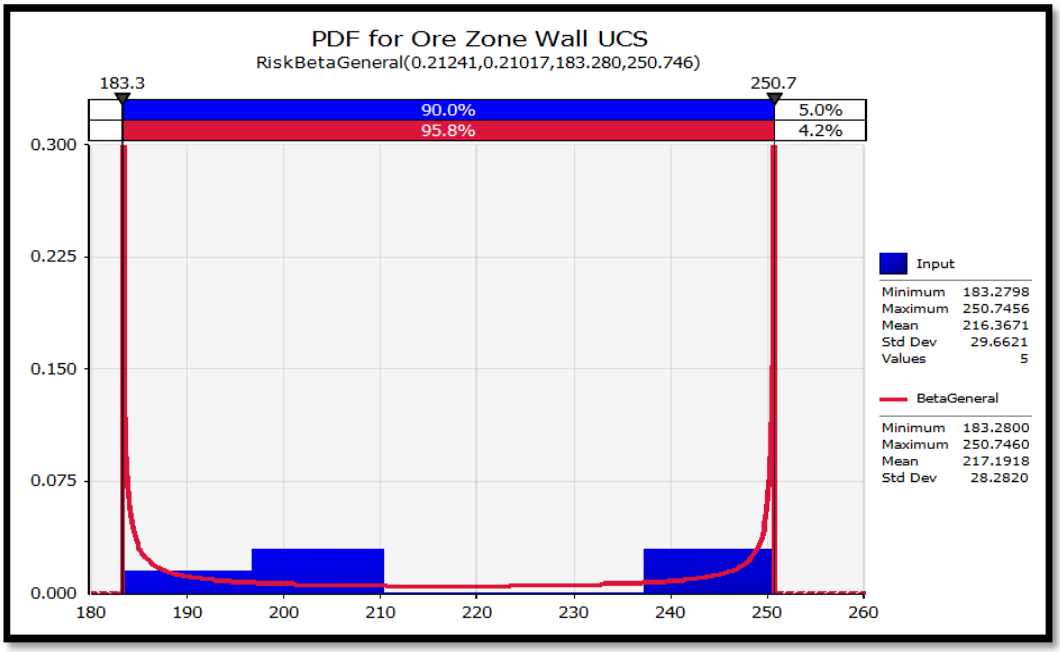

Figure 5.5 Probability Density function (PDF) for Orezone UCS

The footwall zone consists of a shear zone of chloritized talc. The zone is 300 mm thick but in some places it is frequently thinner or thicker. The average UCS is 194 MPa with a minimum of 183 MPa and a maximum of 205 MPa as shown in Figure 5.6.

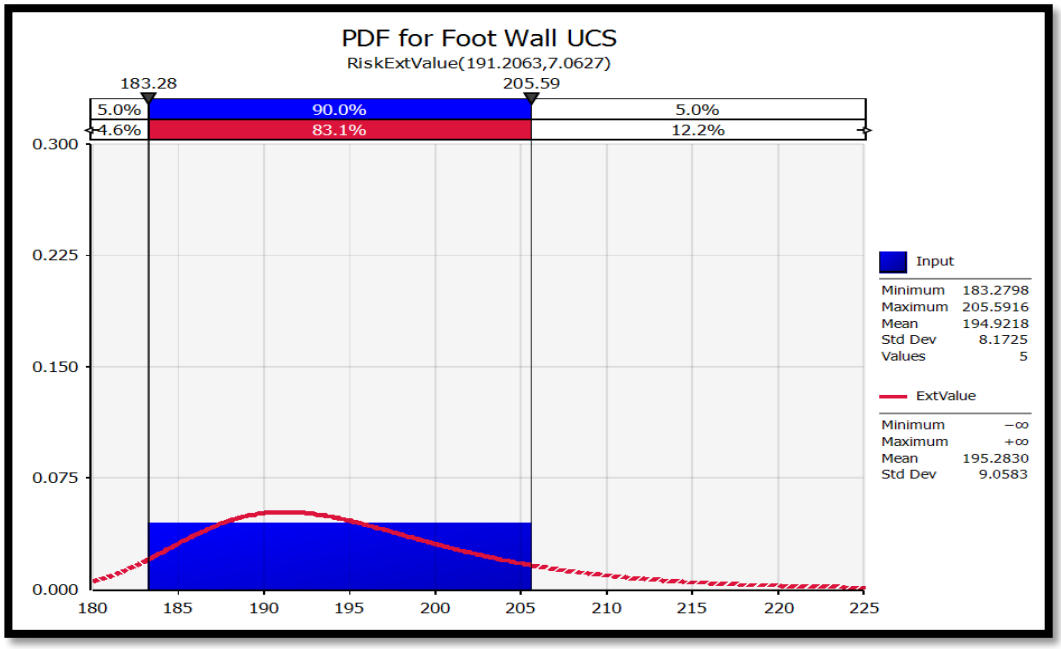

Figure 5.6 Probability Density function (PDF) for Footwall UCS

In Appendix B, Table B1 shows the lab test results on UCS and Table B2 shows the results for Triaxial Compressive Strength (TCS) test. Figure B1 shows the UCS sample pictures after failure and Figure B2 shows the TCS sample pictures before the lab tests. All the samples tested conformed to the ISRM guidelines after the tests.

5.3. Chapter summary

This chapter presented the different laboratory tests of rock samples. The tests included the uniaxial compressive test, triaxial strength test and the Brazilian test. The results were discussed and presented in the form of a table for the hangingwall, orezone and footwall. These results will be used in the next chapter as input data in the support design process. Numerical modelling would provide the opportunity to design the span and support taking into account these parameters and conditions.

6. NUMERICAL MODELLING METHODOLOGY AND RESULTS

This section will discuss the modelling procedure followed in Phase^2 and J-Block. The results of the stress and deformation distributions will then be discussed for the Unki Mine bord and pillar. The discussions will consider elastic and in-elastic behaviour. After analysing the results, a comparison will be made between different analysis and underground observations.

6.1. Numerical modelling in Phase² overview

Phase^2 is a two dimensional elasto-plastic finite element stress analysis program for underground excavations in rock. The program helps in the calculation of stresses and displacements around underground openings and in solving a wide range of mining and geotechnical problems that include excavation design, slope stability, groundwater seepage, probabilistic analysis, consolidation, and dynamic analysis capabilities (Rocscience, 2015).

According to Rocscience (2015), complex, multi-stage models can be easily created and quickly analysed. Progressive failure, support interaction and a variety of other problems can be addressed too.

Phase^2 offers a wide range of support modelling options. Liner elements can be applied in the modelling of shotcrete, concrete, steel set systems, retaining walls, piles, multi-layer composite liners and geotextiles. Liner design tools include support capacity plots which allows to determine the safety factor of reinforced liners. Bolt types include end anchored, fully bonded, cable anchors, split sets and grouted tiebacks (Rocscience, 2015).

The pre-processing module was used for entering and editing the model boundaries, support, insitu stress, boundary conditions, material properties and creating the finite element mesh as shown in Appendix C, Figure C1. Loading in underground is due to the weight of overlying rocks. After the excavation, the stresses redistribute and a new equilibrium state is reached causing failure in some instances depending on the new state of stress.

The Phase^2 compute engine performs the required finite element calculations in less than a minute as shown in Appendix C, Figure C2. During this process, equilibrium

is established until the unbalanced forces reach a pre-defined value. Once the computations are done, the results are viewed in Interpret as shown in Appendix C, Figure C3. The interpret module helps in interpreting the computed results (Rocscience, 2015).

6.1.1. Modelling procedure in Phase²

The numerical modelling procedure in Phase² for bord and pillar mining allows the user to construct the model geometry, discretise it into finite elements, solve the problems and display the results in accordance with the following steps:

a. Start Phase² program → File → New →Analysis → Project settings → Set general and Stage parameters.
b. Enter external boundaries of the model.
   Boundaries → Add external and enter all coordinates.
   Boundaries → Add the material boundaries, which will define the rock mass layers.
   Boundaries → Add stage boundaries to define the location of the stope and access roads within the orebody.
c. Mesh Setup parameters.
   Mesh → Discretise and Mesh → Refine the mesh in the area of pillars using advanced mesh regions check box.
d. Set the boundary conditions. The portion of the external boundary representing the ground surface.
   Displacements → Free → Right click and restrain X-Y both left and right.
e. Define Material Properties. This is specifying the properties of the different materials in the model as determined from the laboratory testing.
   Properties → Define Materials → Define elastic properties and strength parameters.
f. Define the in-situ stress field.
   Loading → Field stress → Gravity → Use actual ground surface → Specify horizontal field stress for each material.
   Advanced button → Apply custom field stress

g. Assigning Properties.

This allows to specify the stratigraphy of material layers in the model. In conjunction with the Stage tabs at the bottom left of the view. The complete model phase should appear in the last stage. The model is saved before analyzing.

Stage 1: Have correct material stratigraphy

Stage 2: Excavate main and ledging declines and connections

Stage 3: Excavate the bords

File → Save (Name is given).

h. Run the analysis.

Analysis → Compute.

i. To view the results of the analysis:
Select: Analysis → Interpret. This will start the Phase^2 Interpret program.

6.1.2. Modelling results in Phase^2

There were two models that were created. The first one is located at 100 m below the surface. The second one is located at 200 m below the surface. In each model there are stages created and described as follows:

Stage 1 ⟶ Different material stratigraphy (Insitu rockmass)

The rock material stratigraphy is arranged according to the actual Unki mine stratigraphy as shown in Figure 6.1. This was an isotropic elastic material type analysis.

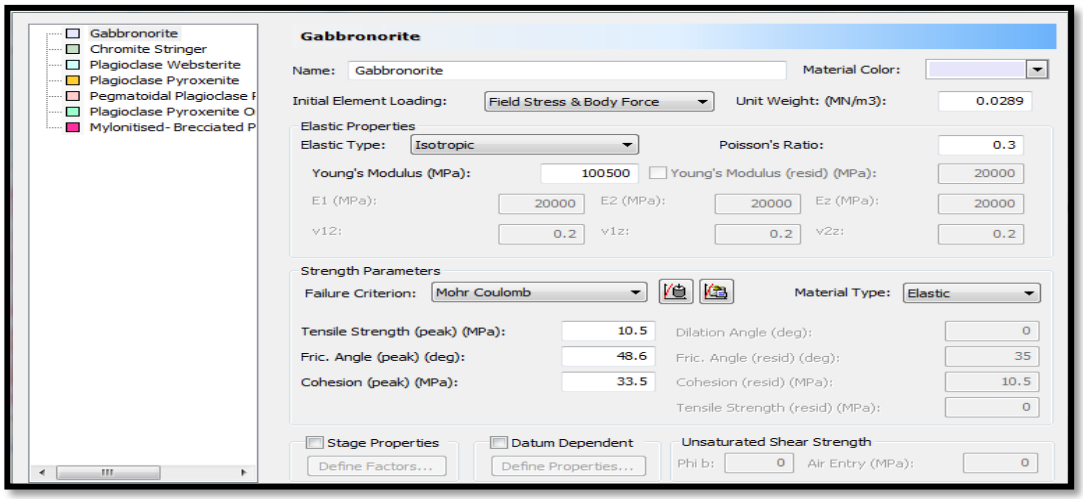

Figure 6.1 Materials stratigraphy used to model

Figure 6.2 shows the position of materials in the model. The colour coding is shown in Figure 6.1 stratigraphy.

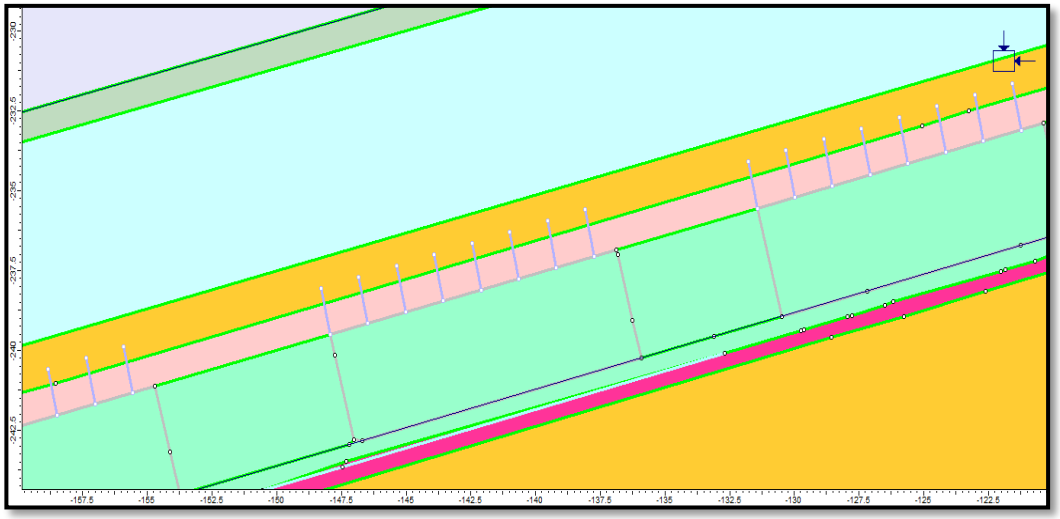

Figure 6.2 Position of materials stratigraphy

Stage 2 ⟶ Excavated bords

Figure 6.3 shows the excavated bords in the model when mining has taken place. The model has been meshed at this stage. The mesh element length was refined to 2.7 m.

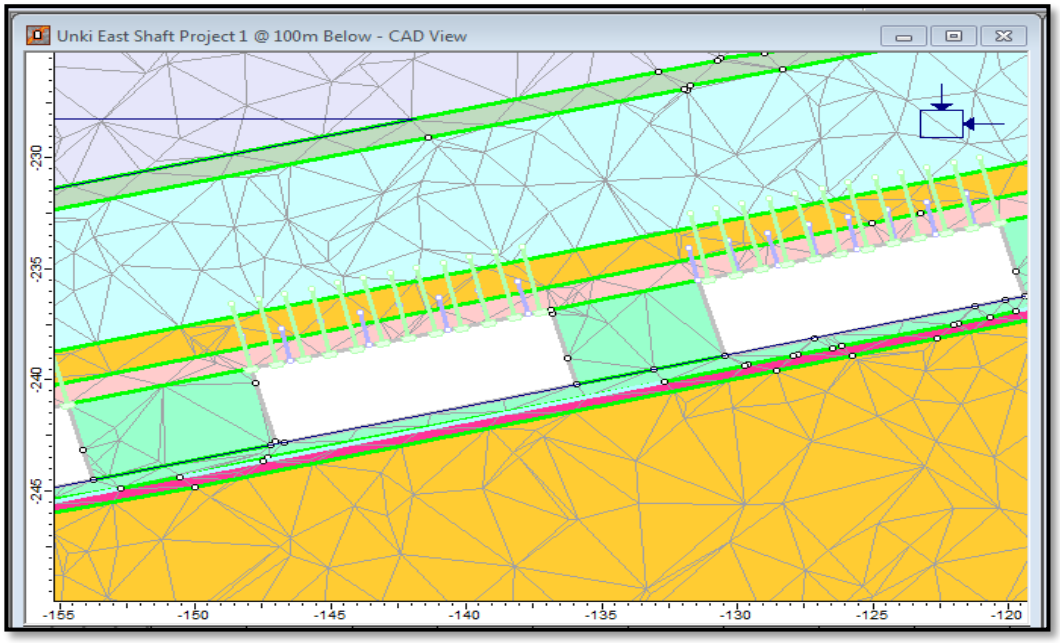

Figure 6.3 Excavated bords

Stage 3 ⟶ Joint network is added

Figure 6.4 shows the joint network that has been added to the model. Joints within the hangingwall are typically altered (mostly serpentinised), and even asbestos occurs within them from time to time. There are four dominant joint directions at Unki Mine, namely E-W, N-S, NNE-SSW. The joint frequency in the hangingwall is low. Two joint sets with shallow dips of 60^0 and 30^0 have been observed 1.5 m or less above the hangingwall of the BMSZ. The shallow dipping joints in the hangingwall (occurring closer to faults) are of concern to hangingwall stability, particularly where they are highly altered and form wedges when combined with the dominant joint sets. Stope face parallel/sub-parallel joints are quite common at Unki. Where they occur they give a shiny serpentinised striated appearance to the face (Mandingaisa, 2014).

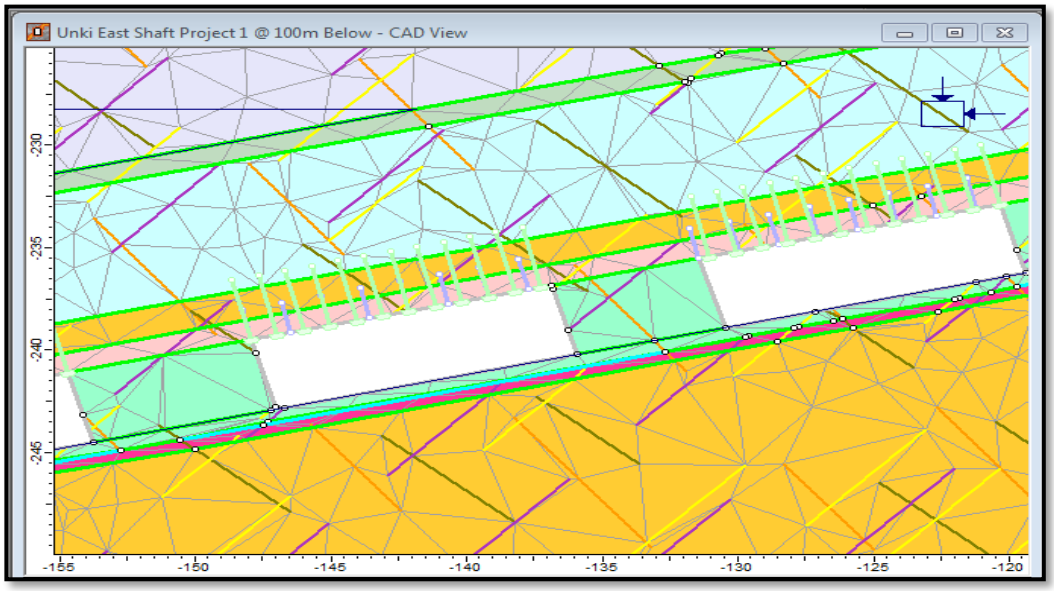

Figure 6.4 Joint network

J_1 and J_2 are approximately orientated on strike and dip respectively. They form an orthogonal pair and it is therefore conceivable that J_2 will be parallel to the face; with both J_1 and J_2 parallel to the pillar walls. This orientation is neither favourable to hangingwall stability nor to pillar stability (Mandingaisa, 2014).

Stage 4 ⟶ Support is added

Figure 6.5 shows the bords with primary support composed of 1.5 m long rock bolts spaced at 1.5 m x 1.5 m grid. This is the current mine support standard for good ground in A-class. The bolt has 150 kN yield strength.

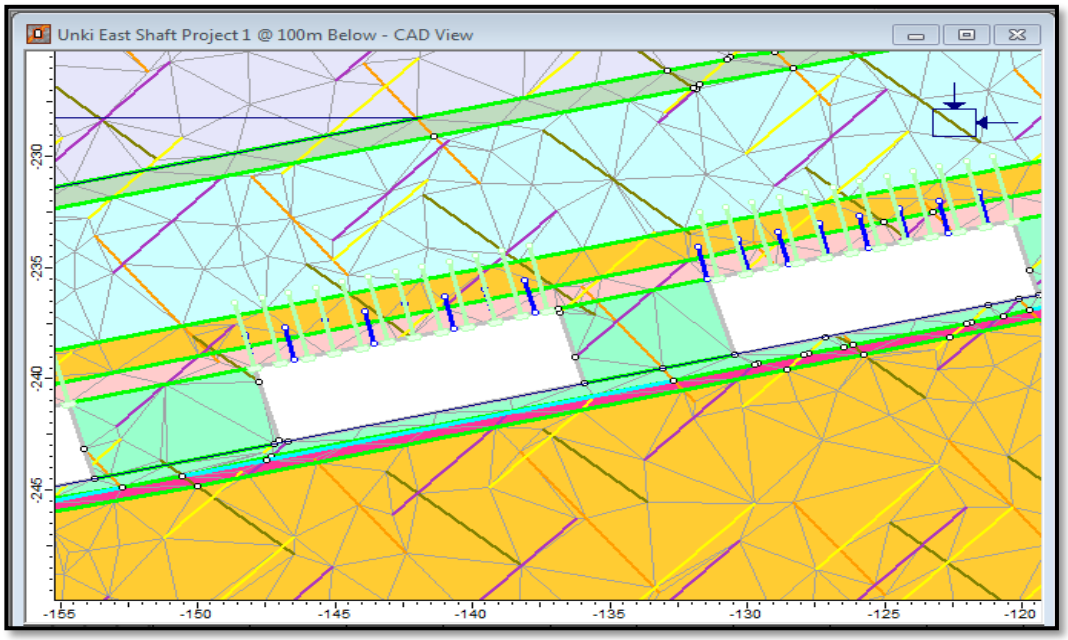

Figure 6.5 Primary support

Stage 5 ⟶ More robust support is added

Figure 6.6 shows the bords with secondary support composed of 3 m long cable anchors spaced at 2 m x 2 m grid. The 3 m cable anchor has 250 kN yield strength. The results that were obtained after running the compute process are as shown in Section 6.1.2.1.

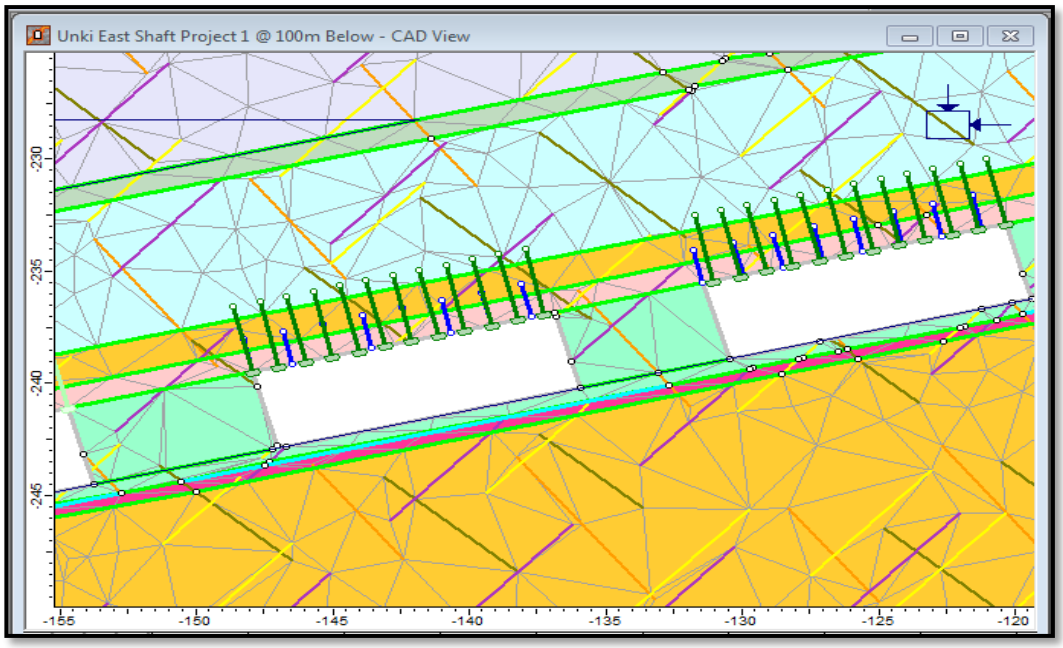

Figure 6.6 Secondary support

6.1.2.1. Sigma 1

Figure 6.7 is a contour plot of the major principal stress for the model at 100 m below surface before the excavation is made. The model at 200 m below surface had a 7 MPa uniformly distributed stress laid normal to its surface (Figure 6.8). The major principal stress is horizontally oriented and the minor principal stress is vertically oriented and the stresses increase as depth increases below the surface for contour plots in **Figure 6.7** and Figure 6.8. Mohr-Coulomb failure criterion was used in the models.

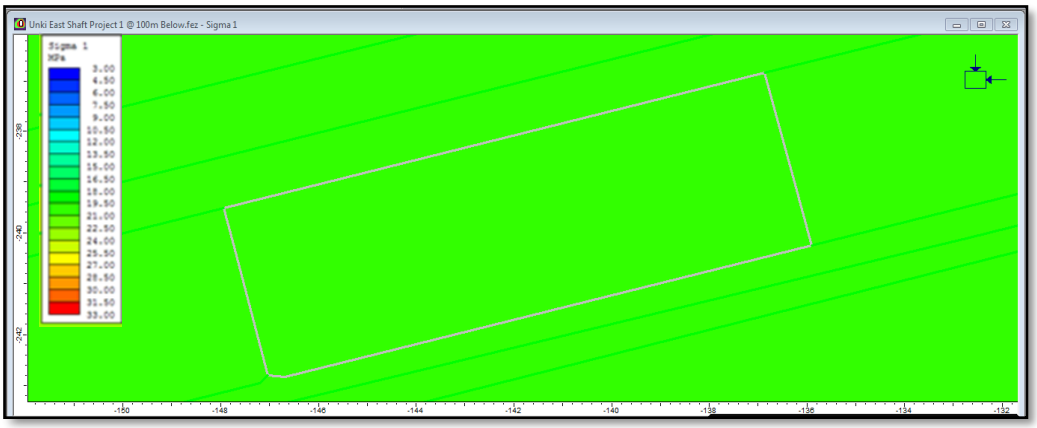

Figure 6.7 Sigma 1 Contour plot before excavation at 100 m below surface

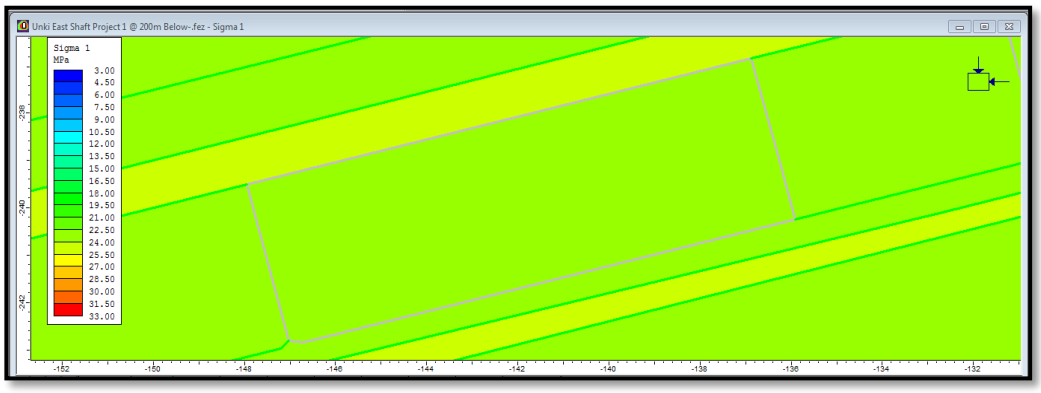

Figure 6.8 Sigma 1 Contour plot before excavation at 200 m below surface

The Sigma 1 stress trajectories are shown to change orientation from horizontal to 45^{O} around the excavation and revert back to horizontal with increasing distance from the excavation as shown in Figure 6.9 and Figure 6.10. The Sigma 1 stresses are highly concentrated on the up dip hangingwall to pillar contact and down dip footwall to pillar contact. Failure is most likely to occur at these locations with stress over 200 MPa. Rock strength is exceeded at these locations.

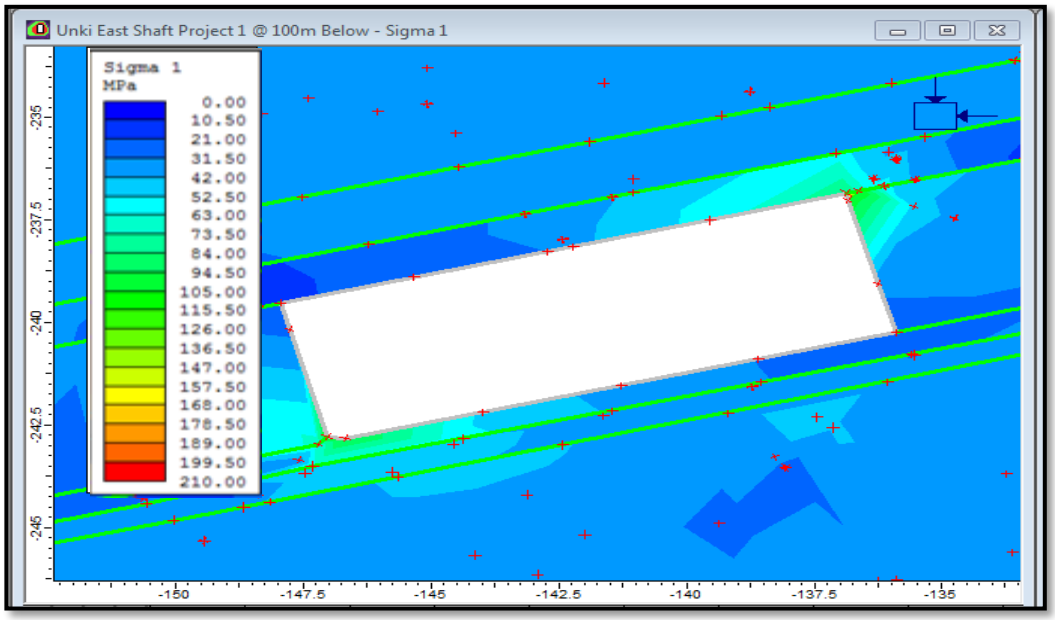

Figure 6.9 Stress trajectories for Sigma 1 contour plots after excavation of bords at 100 m below surface

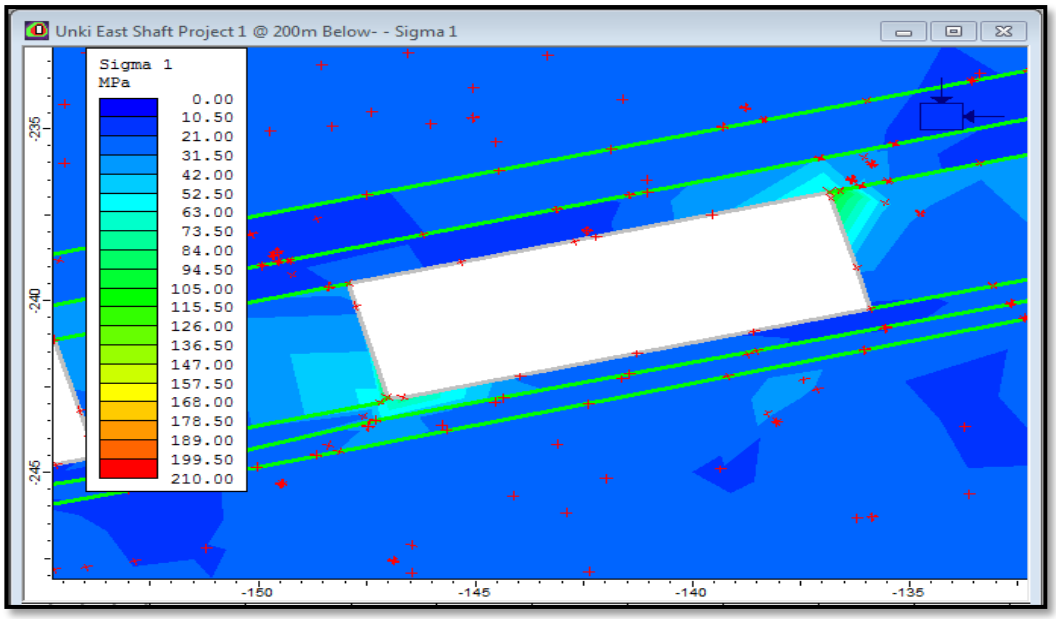

Figure 6.10 Stress trajectories for Sigma 1 contour plots after excavation of bords at 200 m below surface

6.1.3.2 Total Displacement

The total displacement for the excavations at stage 2 is generally high at the center of the bords than at the sides or pillar contacts. There is more displacement at the excavation 200 m below surface which is 10.25 mm (Figure 6.12) than at the excavation 100 m below surface which is 3.53 mm (Figure 6.11). The displacement at 200 m below surface (Figure 6.12) is more in vertical direction than the displacement at 100 m (Figure 6.11) which is more in horizontal direction. This

means failure is also likely to occur at the middle of the bord with displacement in excess of 3.5 mm if the hangingwall tensile stress is exceeded.

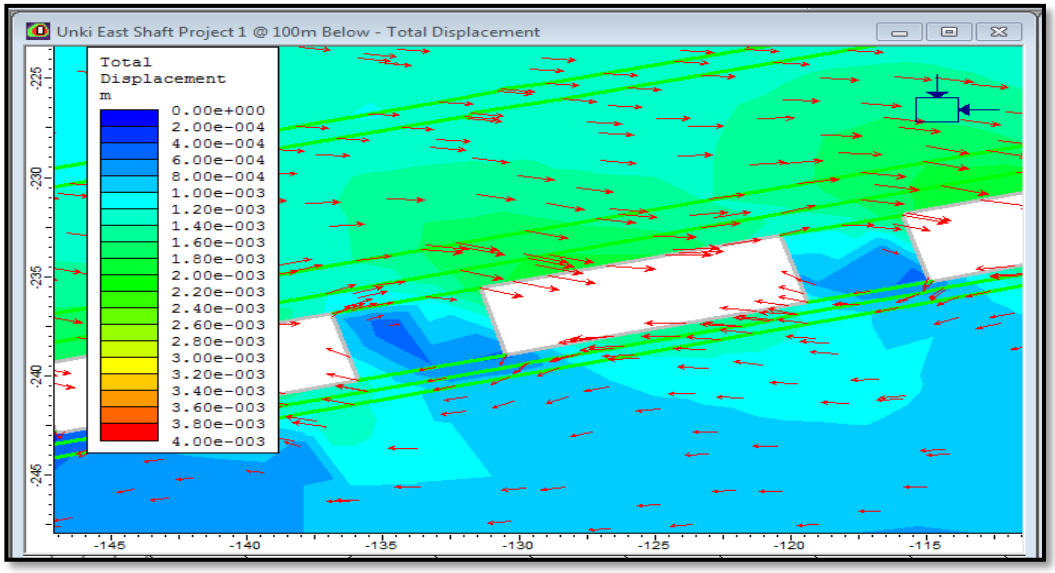

Figure 6.11 Total displacement contour plot at 100 m below surface

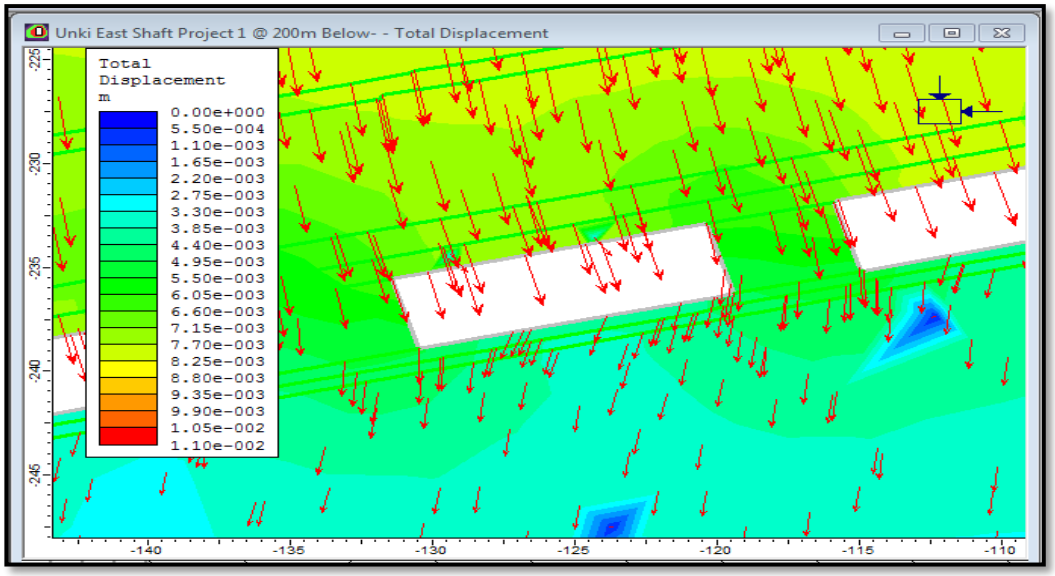

Figure 6.12 Total displacement contour plot at 200 m below surface

6.1.3.3. Strength Factor

The strength factor at stage 6 is mostly lower than 1.5 with a value of 0.63 at shallow depth less than 100 m below surface (Figure 6.13). The strength factor increases to 1.89 at greater depth of 200 m below surface (Figure 6.14). The yielding is in the roof of the bord posing potential failure especially at shallow depth. There are 3 yielded joints at shallow depth of 100 m below surface (Figure 6.13) compared to only 1 yielded joint at greater depth of 200 m below surface (Figure 6.14).

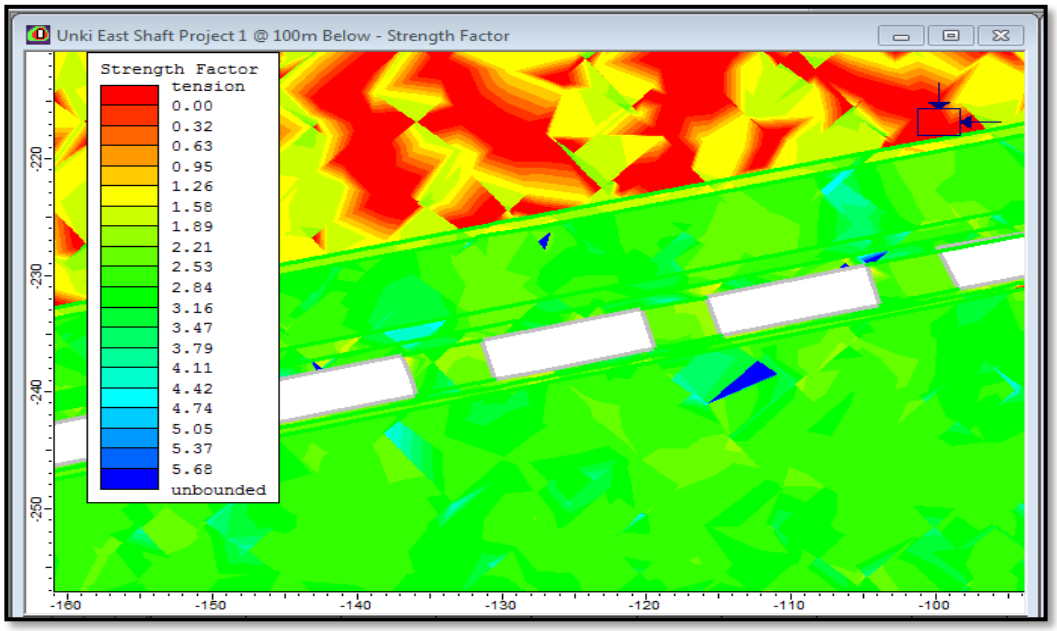

Figure 6.13 Strength Factor contour plot at 100 m below surface

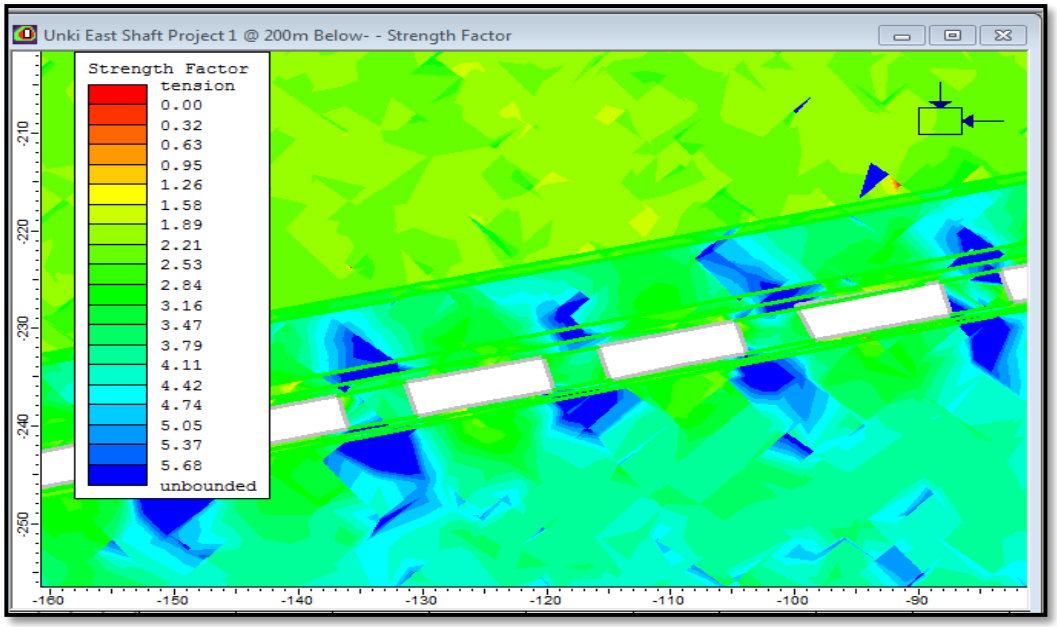

Figure 6.14 Strength Factor contour plot at 200 m below surface

6.1.3.4. Support quality

The support capacity in a 12 m bord is poorly suited since it allows wedges with a potential to fall. The standard support of 1.5 m long rock bolts spaced at 1.5 m x 1.5 m grid proves to be insufficient to provide adequate support (Figure 6.15). The support quality improves with bord width reduced to 8 m. The only wedge produced is actually sitting on the pillar partially and there is no wedge with potential to fail. The variability in wedge occurrence in this case is not considered. The standard

support used in this case is 1.5 m long rock bolts spaced at 1.5 m x 1.5 m grid (Figure 6.16). To improve the support in a 12 m bord, some 3 m grouted cable anchors has been added as secondary support (Figure 6.17). In this model, all the wedges with the potential to fall are now supported.

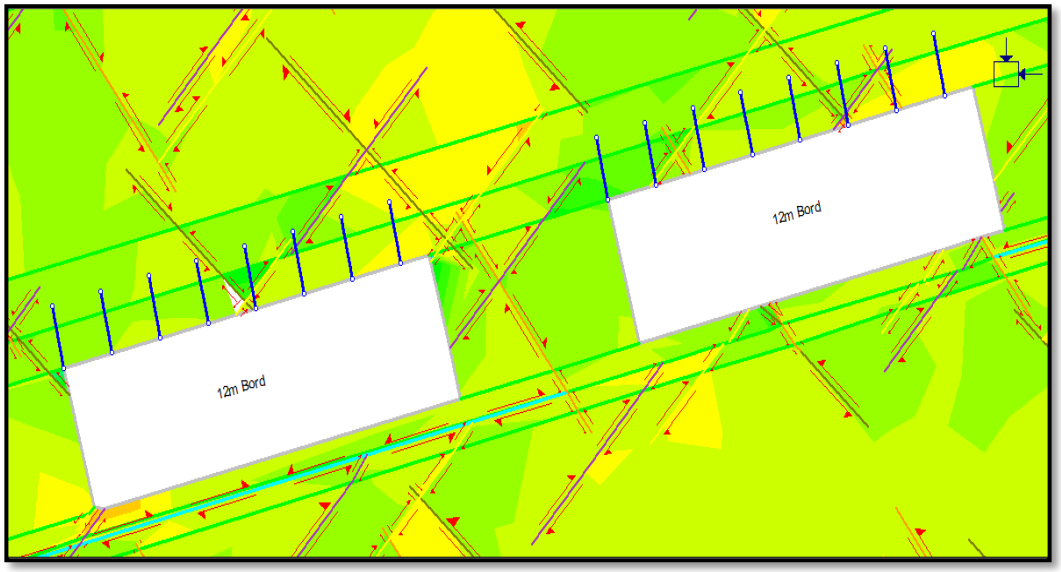

Figure 6.15 Support quality in 12 m bord using 1.5 m long rock bolts

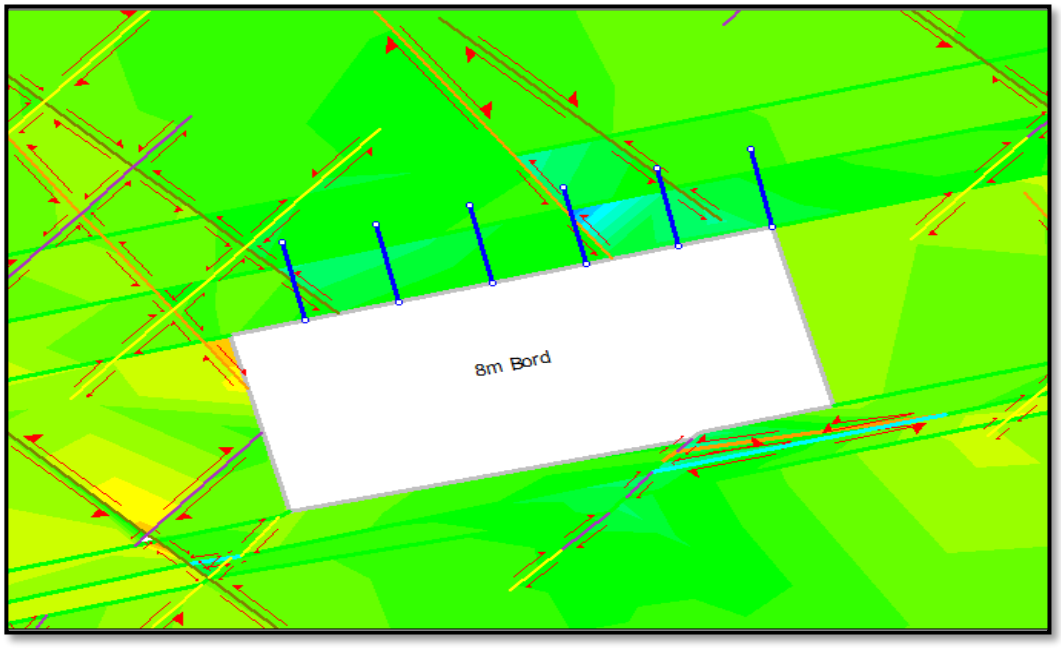

Figure 6.16 Support quality in 8 m bord using 1.5 m long rock bolts

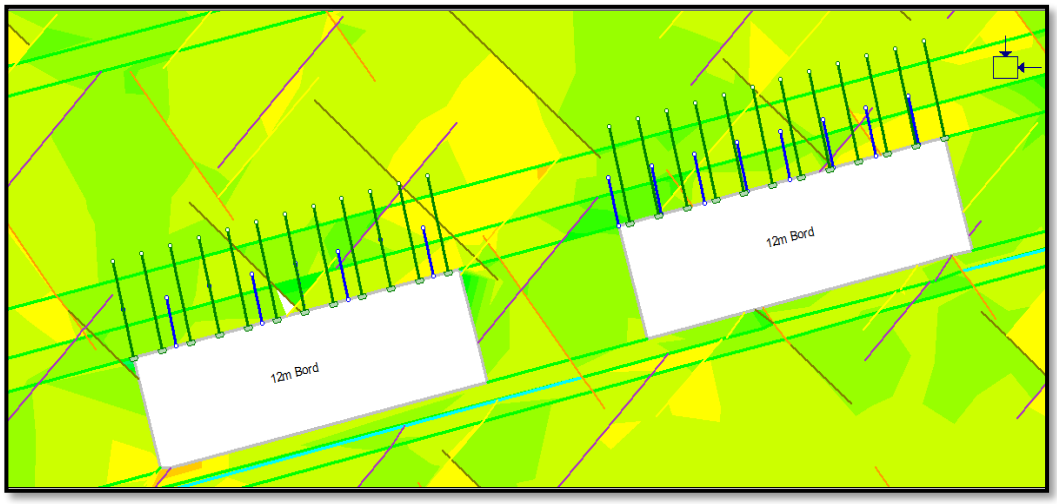

Figure 6.17 Robust support design in a 12 m bord using 3 m cable anchors

6.2. Numerical modelling in J-Block overview

J-Block is a probabilistic keyblock stability programme that can be used in the probabilistic assessment of gravity driven rock falls and the evaluation of support effectiveness (Stacey and Gumede, 2007). The program uses three statistical discontinuity sets to generate possible keyblocks with between four and six faces in the hangingwall and sidewall. The program makes use of joint length and joint orientation data to generate a given number of blocks (Esterhuizen and Streuders, 1998). In the J-Block program, it is assumed that a block may contain smaller blocks resulting in large blocks which are limited in size by the length of the joint. The program then determines whether the identified keyblock will cause failure of the support elements and the corresponding failure mode (Stacey and Gumede, 2007). Once J-Block has identified a keyblock, it is placed at random positions in a pre-defined excavation and checks whether the block is located over a support unit. If a keyblock is located between supports it will fail. If a keyblock is over one or more supports it may fail, depending on the strength of the support and the weight of the block. The J-Block program also considers installed support and the location of personnel to calculate the rockfall hazard distribution and likely injury rates (Kotze, 2012).

6.2.1. Block generation procedure

J-Block software was used to statistically simulate potential keyblocks that could occur in an area traversed by joints. The effect of the different support systems was then evaluated by obtaining the number of unstable blocks falling after support is installed. This provides a potential rockfall distribution for each support type.

6.2.2. J-Block input parameters

The input parameters for J-Block are listed in Table 6.1, Table 6.2 and Table 6.3 and have been taken from Unki Mine underground mapping and measurements. The density of the keyblocks was taken to be 3 150 kgm^{-3}. The mean friction angle for all the joints vary from 16° to 25°.

Table 6.1 Block joint input parameters for dip and dip direction

Joint Set	Dip (°)				Dip Direction (°)			
	Mean	Std Dev	Min	Max	Mean	Std Dev	Min	Max
J1	64	26	37	90	38	30	8	68
J2	47	29	18	77	126	26	99	152
J3	60	27	32	87	218	31	187	249
J4	17	03	14	20	317	27	290	344

Table 6.2 Block joint input parameters for cohesion and friction angle

Joint Set	(Cohesion)/ Strength (MPa)				Friction Angle (°)			
	Mean	Std Dev	Min	Max	Mean	Std Dev	Min	Max
J1	1.660	0.200	1.460	1.860	16.1	5	11.1	21.1
J2	0.258	0.020	0.238	0.278	24.9	1.3	23.6	26.2
J3	1.870	0.600	1.270	2.470	24.4	1.6	22.8	26.0
J4	0.208	0.030	0.178	0.238	24.1	1.3	22.8	25.4

Table 6.3 Block joint input parameters for joint spacing and length

Joint Set	Joint Spacing (m)				Joint Length (m)			
	Mean	Std Dev	Min	Max	Mean	Std Dev	Min	Max
J1	1.7	0.35	1.35	2.05	6.20	0.97	5.23	7.17
J2	1.5	0.11	1.39	1.61	6.36	1.27	5.09	7.63
J3	4.9	0.19	4.71	5.09	6.01	0.21	5.80	6.22
J4	1	0.48	0.52	1.48	6.70	1.96	4.74	8.66

The joint friction angle and is observed to be as low as 16^{o} and cohesion less than 1.68 MPa for weak soft and highly altered serpentinised joints. The highest friction angle was 24.9^{o} and cohesion of 1.87 MPa and this was for less altered and no infill gouge material. Failure of the joint gouge material is promoted by squeezing and eventually falls by sliding. Joint set 1 and 3 defines the most problematic set running along the bord lengths and along strike of the ore body.

6.2.3. Modelling results in J-Block

J-Block software records all relevant information pertaining to each block in terms of shape, geometry, area, volume, length, height and shear strength for each surface bounding the block (Kotze, 2012). The primary keyblock size indicates discrete keyblocks that do not contain any joints inside. This generally represents solid rock. The secondary keyblock size indicates keyblocks that consist of combined discrete blocks (Kotze, 2012). The program assumes the individual joint dip and dip directions follow a normal distribution with a standard deviation of one sixth the range (Kotze, 2012). This ensures that 95% of the random samples will lie within the stated range.

In the modelling, eleven scenarios were used. Scenario 1 is a model that constitutes a 12 m bord with no support. Scenario 2 is a model that constitutes a 12 m bord with existing support of 1.5 m long rock bolts at a spacing of 1.5 m x 1.5 m grid. Scenario 3 is a model that constitutes a 12 m bord in scenario 2 with additional 3 m cable anchors at a spacing of 2 m x 2 m grid. Scenario 4 is a model that constitutes an 8 m bord with existing support of 1.5 m long rock bolts at a spacing of 1.5 m x 1.5 m grid. Scenario 5 is a model that constitutes an 8 m bord with 3 m cable anchors installed on a 2 m x 2 m grid as shown in Table 6.4. Scenario 6 and 7 is a model that constitutes a 6 m VH with existing support of 1.5 m long rock bolts at a spacing of 1.5 m x 1.5 m grid and 3 m cable anchors respectively. Scenario 8 and 9 is a model that constitutes a 6 m CD with existing support of 1.5 m long rock bolts at a spacing of 1.5 m x 1.5 m grid and 3 m cable anchors respectively. Scenario 10 and 11 is a model that constitutes a 5 m MD with existing support of 1.5 m long rock bolts at a spacing of 1.5 m x 1.5 m grid and 3 m cable anchors respectively. The 1.5

m grouted long bolt has a capacity of 15 tons and the 3 m grouted cable anchor has a capacity of 25 tons.

Table 6.4 Support scenarios for different excavations

Scenario No.	Excavation Width	Description of support variables
1	12 m bord	No support.
2	12 m bord	Standard support 1.5 m resin bolts at 1.5 m x 1.5 m grid.
3	12 m bord	Standard support 1.5 m resin bolts at 1.5 m x 1.5 m grid with additional 3 m cable anchors at a spacing of 2 m x 2 m grid.
4	8 m bord	Standard support 1.5 m resin bolts at 1.5 m x 1.5 m grid.
5	8 m bord	Standard support 1.5 m resin bolts at 1.5 m x 1.5 m grid with additional 3 m cable anchors at a spacing of 2 m x 2 m grid.
6	6 m VH	Standard support 1.5 m resin bolts at 1.5 m x 1.5 m grid.
7	6 m VH	Standard support 1.5 m resin bolts at 1.5 m x 1.5 m grid with additional 3 m cable anchors at a spacing of 2 m x 2 m grid.
8	6 m CD	Standard support 1.5 m resin bolts at 1.5 m x 1.5 m grid.
9	6 m CD	Standard support 1.5 m resin bolts at 1.5 m x 1.5 m grid with additional 3 m cable anchors at a spacing of 2 m x 2 m grid.
10	5 m MD	Standard support 1.5 m resin bolts at 1.5 m x 1.5 m grid.
11	5 m MD	Standard support 1.5 m resin bolts at 1.5 m x 1.5 m grid with additional 3 m cable anchors at a spacing of 2 m x 2 m grid.

6.2.3.1 Scenario 1 for 12 m bord no support

Figure 6.18 shows that the keyblocks of size 0.3 m^3 has the highest frequency of over 1 250 occurrences out of a total of 2 100 keyblocks generated. This ties well with the actual observations as recorded in the mine FOG database that the highest frequency of FOG is recorded up to 0.3 m height as shown in Figure 4.2. The keyblock size distribution and the observation that the occurrence of keyblocks

decreases with increasing keyblock size for all eleven scenarios are similar. Therefore, the keyblock size distribution graphs will not be displayed for the remaining cases. The POF is high for the blocks less than 0.3 m^3 and this failure is mostly between rock bolt support.

Figure 6.19 shows there is no support failure since support is not yet included in this model. Figure 6.20 shows how the blocks of different sizes failed. Some of the blocks failed by single plane sliding while a greater percentage failed by double plane sliding. The support system needed must provide a normal resistive force to prevent failure by sliding. Thorough barring down has to be done continuously to account for the keyblocks dropping out. There is no failure by rotation.

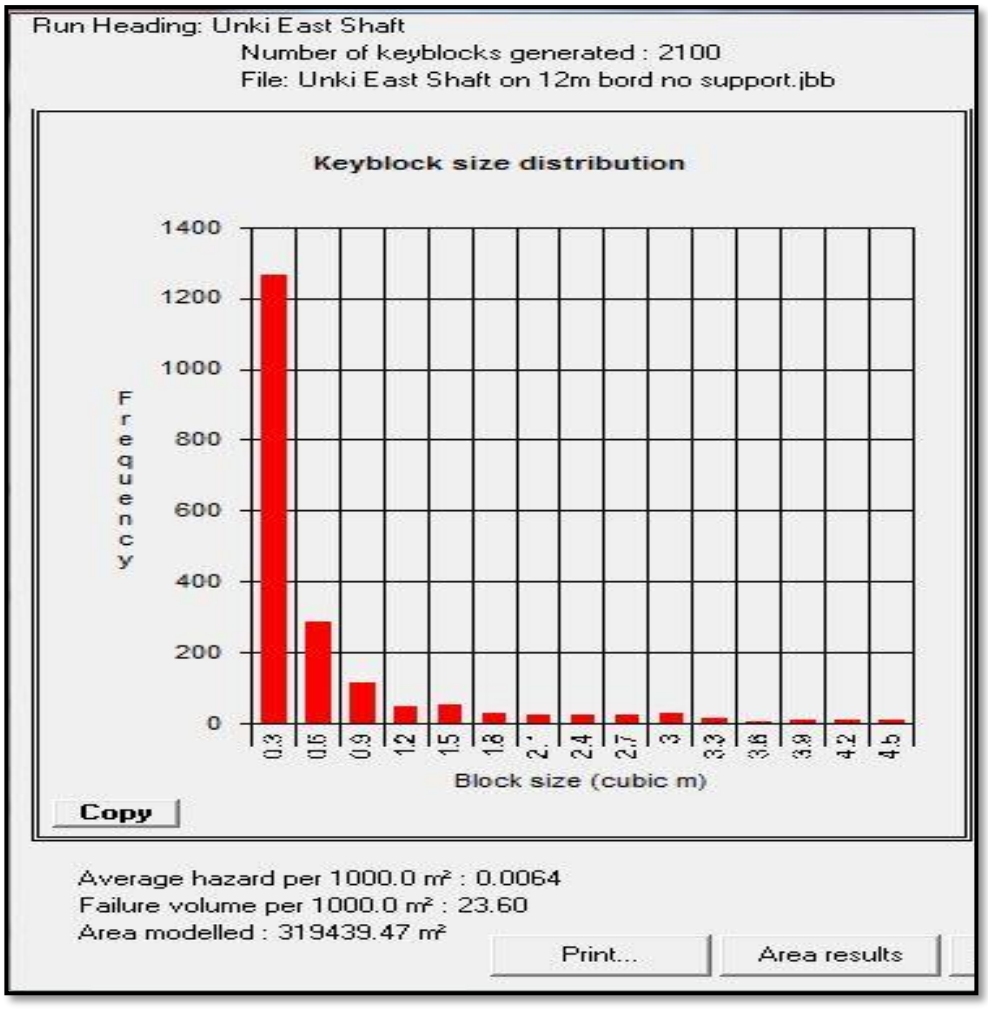

Figure 6.18 Keyblock size distribution for scenario 1

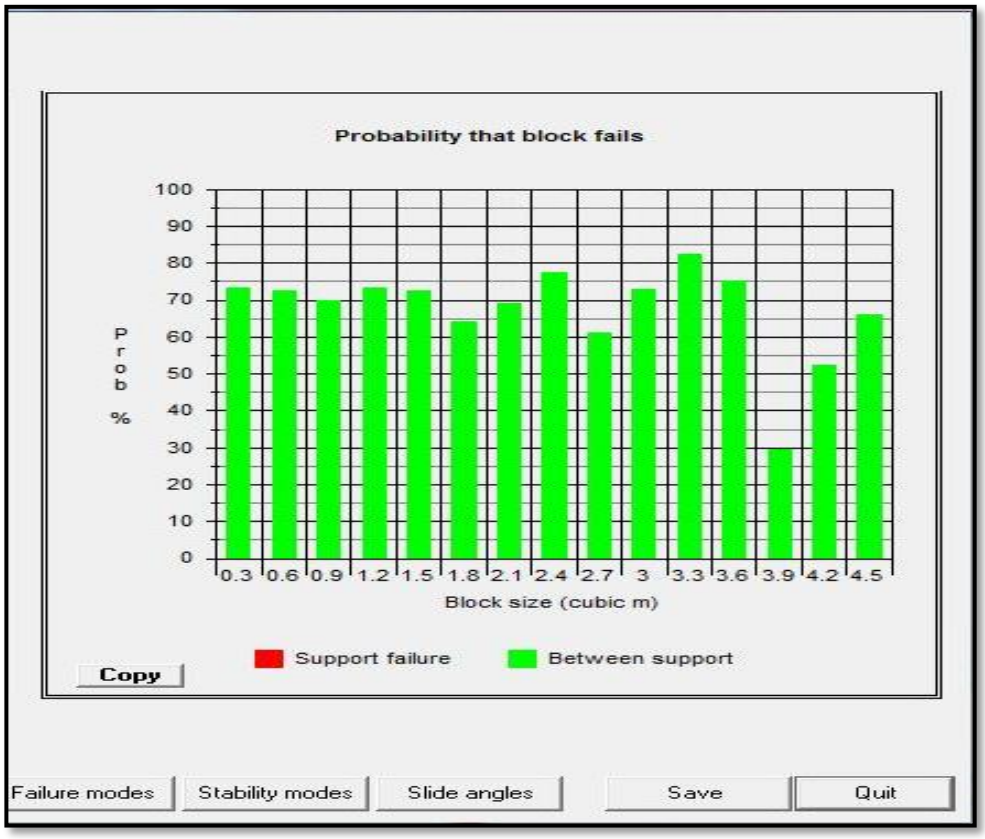

Figure 6.19 Probability of failure of keyblocks for scenario 1

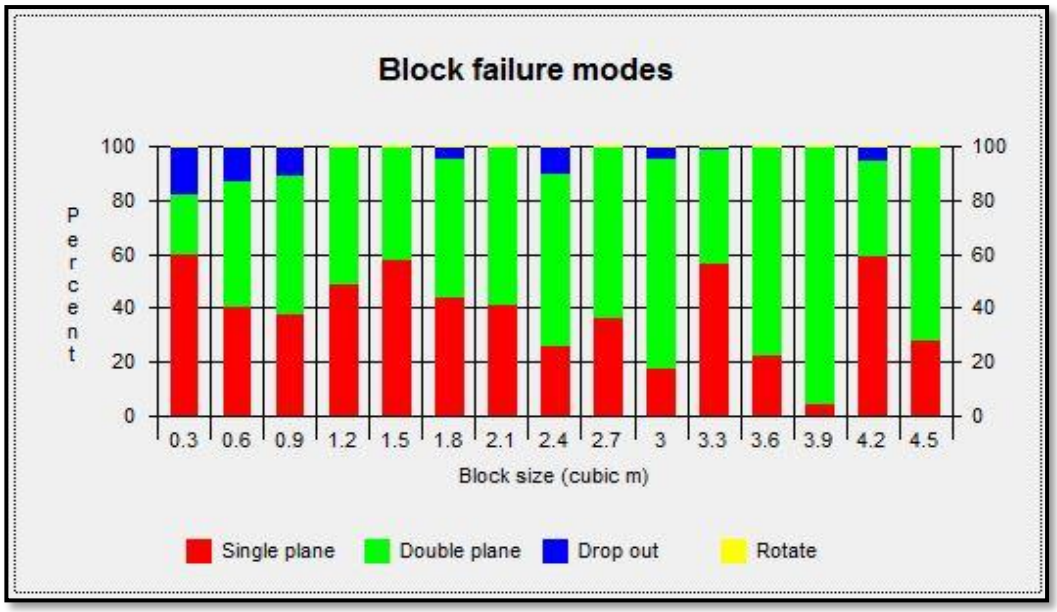

Figure 6.20 Block failure mode for scenario 1

The hazard index is observed to be high in the middle of the span as shown in Figure 6.21. This also ties well with the observations with 48% predominantly falling in the middle of the face area as shown in Figure 4.6. Appendix D, Figure D1 shows the keyblock fall percentage for scenario 1.

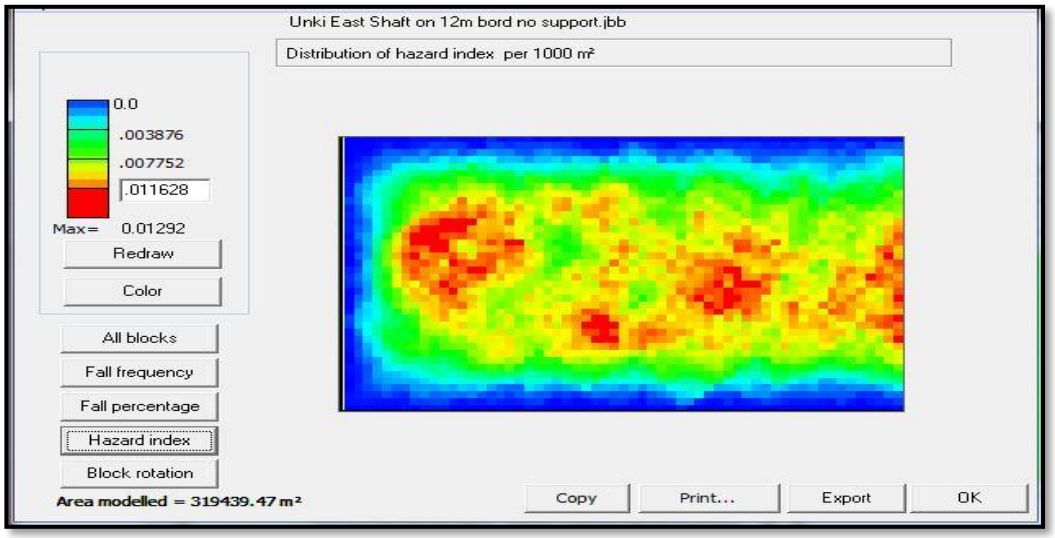

Figure 6.21 Hazard index for scenario 1

6.2.3.2 Scenario 2 for 12 m bord with existing support

Figure 6.22 shows the POF between support is high up to 0.9 m^3 keyblocks. The probability of support failure is high from 1.2 m^3 keyblocks. This means the failure of support could be caused by insufficient bolt capacity (150 kN) and length (1.5 m). A 150 kN bolt at 1.5 m x 1.5 m spacing would carry a 4.85 m^3 rock at a density of 3 150 km^{-3} and a height of 2.16 m assuming a rectangular prism geometry. All bolt failures in this case is due to insufficient bolt length. The short tendons in scenario 2 is 4.27%. Bolts are shorter than the key block height to pin it. Figure 6.23 shows the keyblocks fail by single plane, double plane, drop out and rotation.

Figure 6.22 Probability of failure of keyblocks for scenario 2

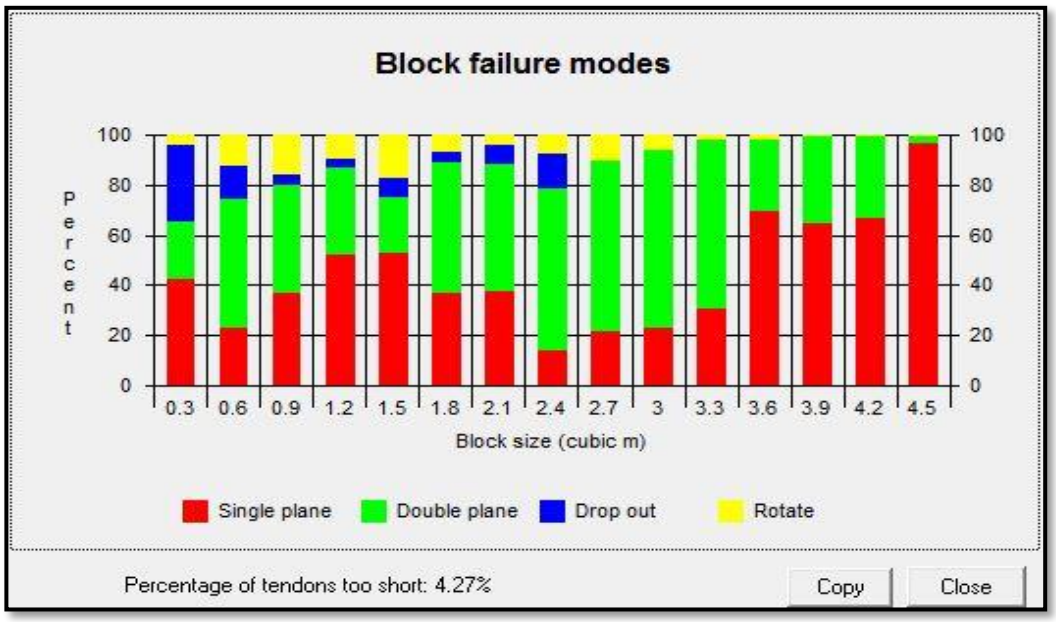

Figure 6.23 Block failure mode for scenario 2

The hazard index per 100 m^2 is observed to be high in the middle of the span as shown in Figure 6.24. Appendix D, Figure D2 shows the keyblock fall percentage for scenario 2.

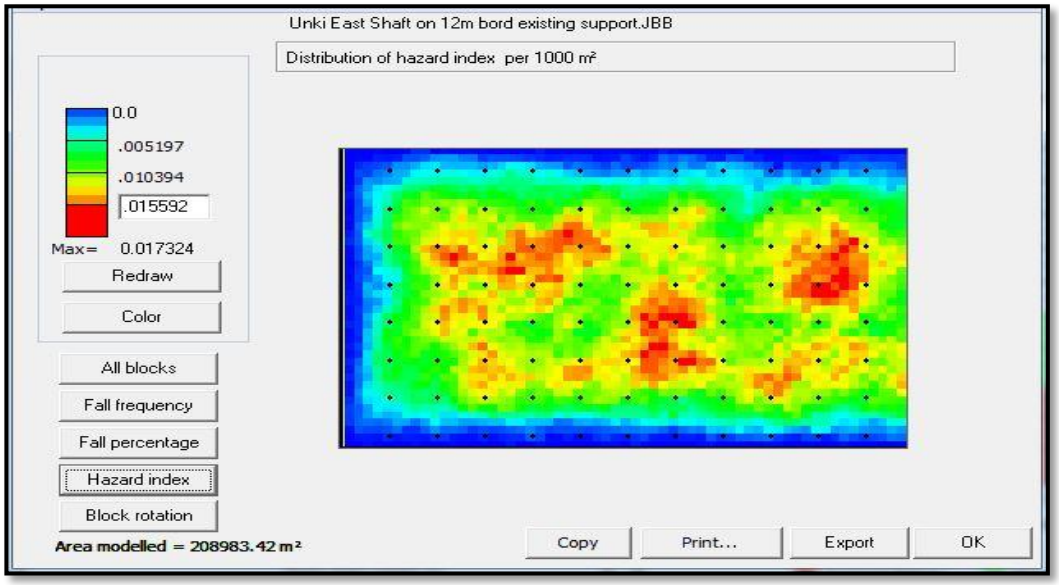

Figure 6.24 Hazard index for scenario 2

6.2.3.3 Scenario 3 for 12 m bord with 3 m long and 250 kN capacity cable anchors

Figure 6.25 shows the POF of support increasing with keyblock size and POF between support increases with decreasing keyblock size. A 250 kN bolt would carry up to 8 m^3 rock without failure. Bolt length should be at least 2 m at a spacing of 2 m x 2 m grid. Cable anchors are 3 m long and satisfy the requirement. However,

all bolt failures in this case is, again, due to variations in wedge heights that exceed the bolt length in the range of block size (up to 4.5 m^3) analysed. The short tendons are 2.21% in scenario 3 as shown in Figure 6.26. The short tendon failure is less for scenario 3 than scenario 2 (4.27%) because of the 3 m cable anchors used. A few larger keyblocks are now pinned and secured in competent ground in hangingwall by cable anchors.

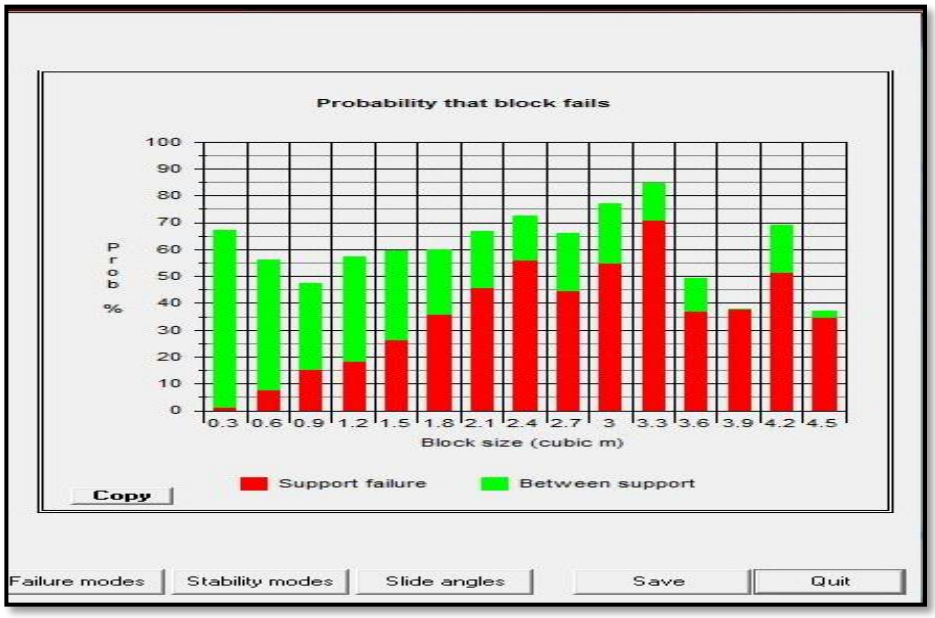

Figure 6.25 Probability of failure of keyblocks for scenario 3

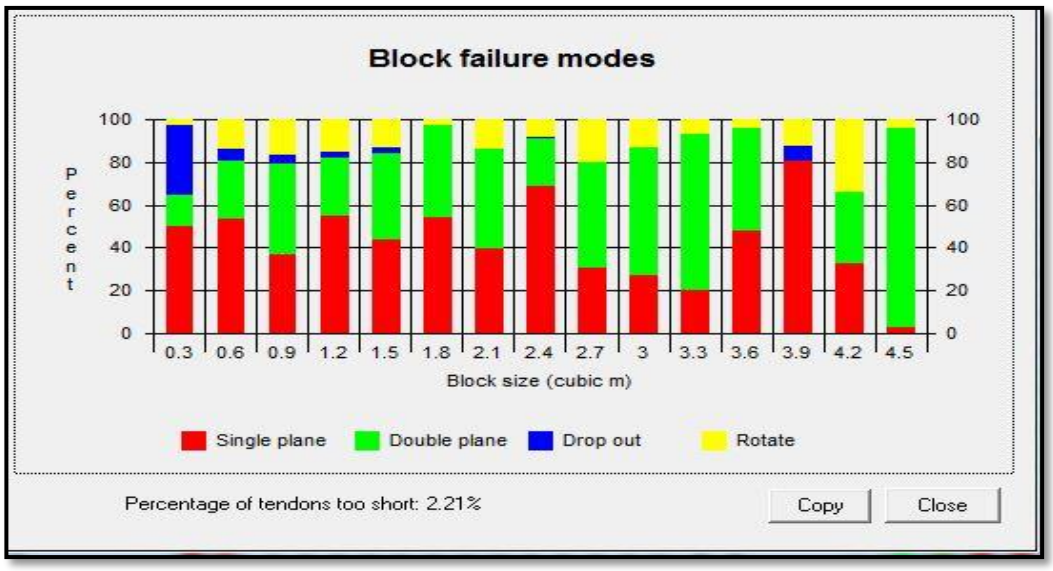

Figure 6.26 Block failure mode for scenario 3

The hazard index for scenario 3 is shown in Figure 6.27. Appendix D, Figure D3 shows the keyblock fall percentage for scenario 3.

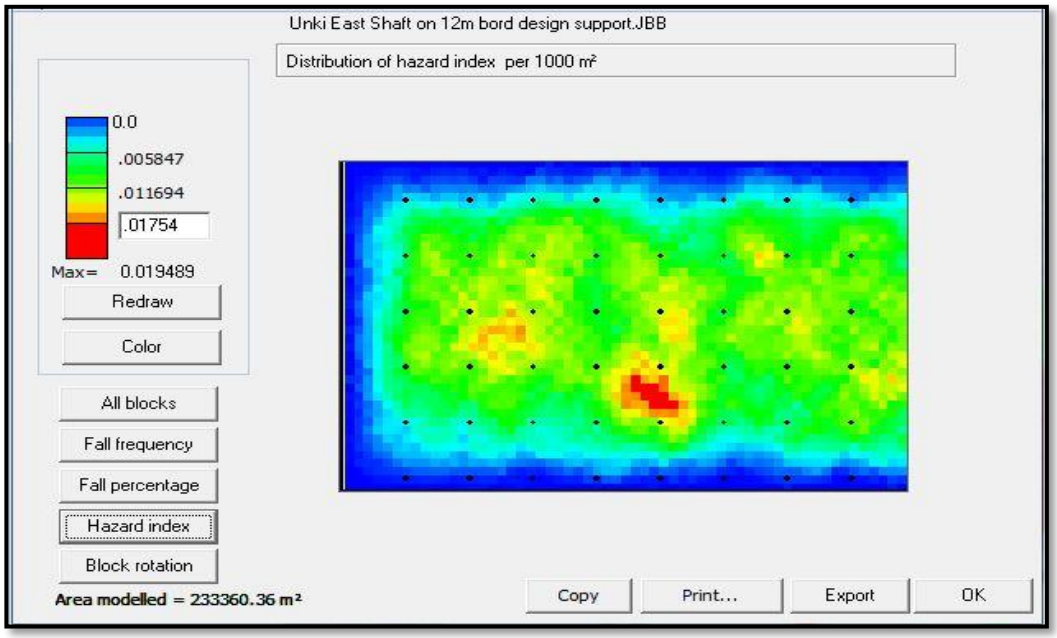

Figure 6.27 Hazard index for scenario 3

6.2.3.4 Scenario 4 for 8 m bord (strike conveyor) with existing support

The POF in support increases with increasing keyblock size due to the higher probability of insufficient length of the tendons. The POF between support is observed to increase with decreasing keyblock size as shown in Figure 6.28. The short tendons are 3.72% as shown in Figure 6.29.

Figure 6.28 Probability of failure of keyblocks for scenario 4

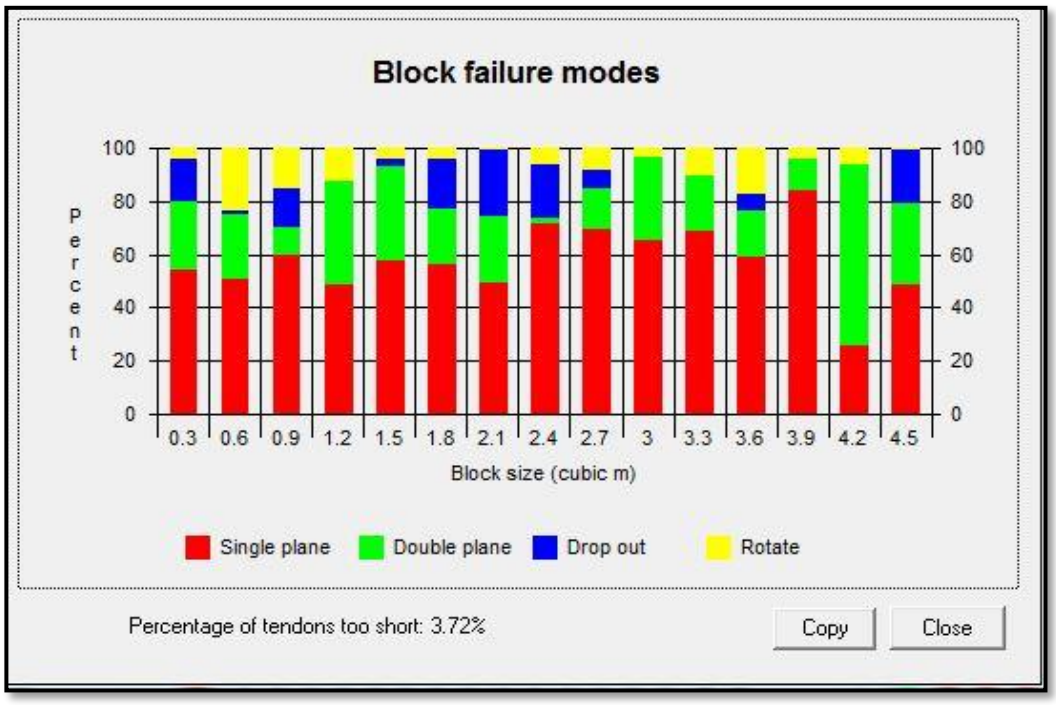

Figure 6.29 Block failure mode for scenario 4

The hazard index per 100 m^2 for scenario 4 is shown in Figure 6.30. Appendix D, Figure D4 shows the keyblock fall percentage for scenario 4.

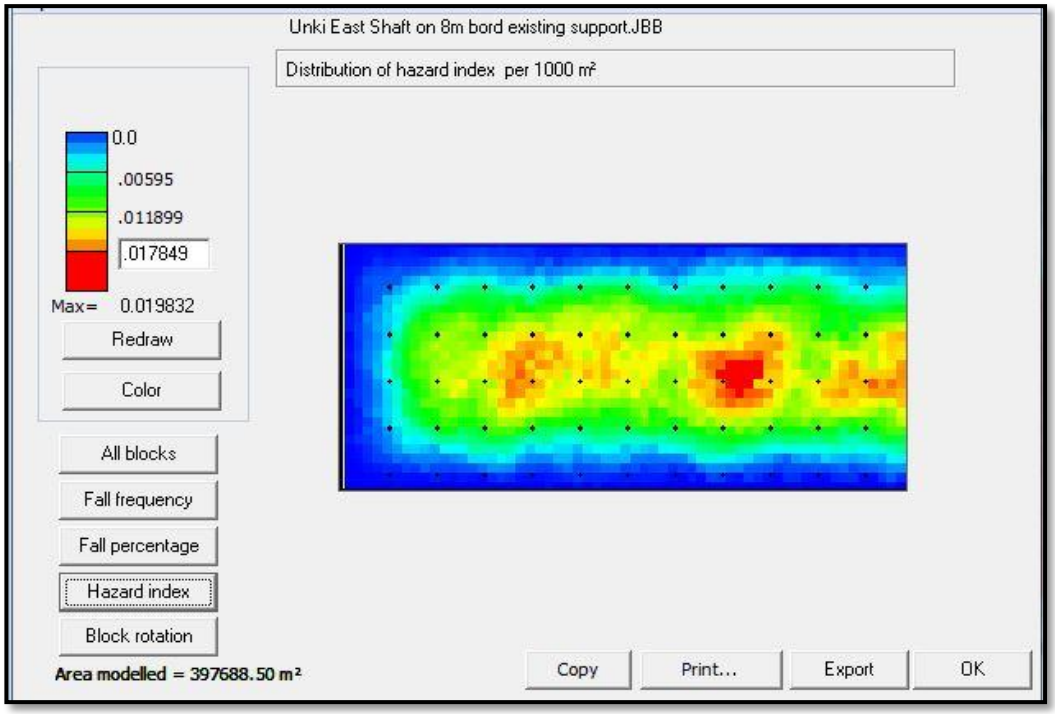

Figure 6.30 Hazard index for scenario 4

6.2.3.5 Scenario 5 for 8 m bord (strike conveyor) with cable anchors

The POF in support increases with increasing keyblock size. The POF between support is observed to increase with decreasing keyblock size as shown in Figure 6.31. The short tendons are 0.16% as shown in Figure 6.32.

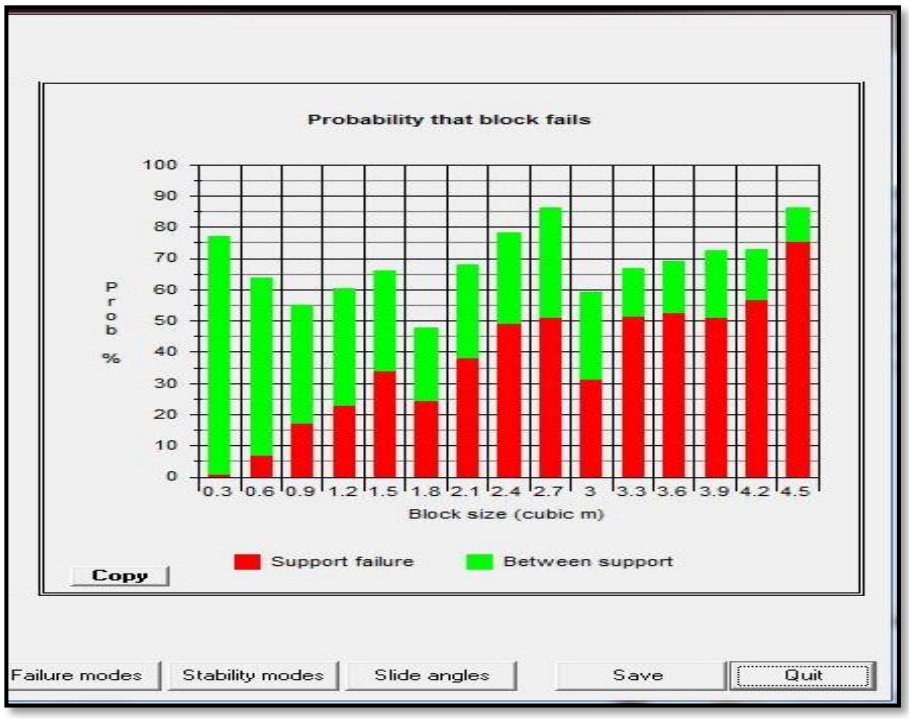

Figure 6.31 Probability of failure of keyblocks for scenario 5

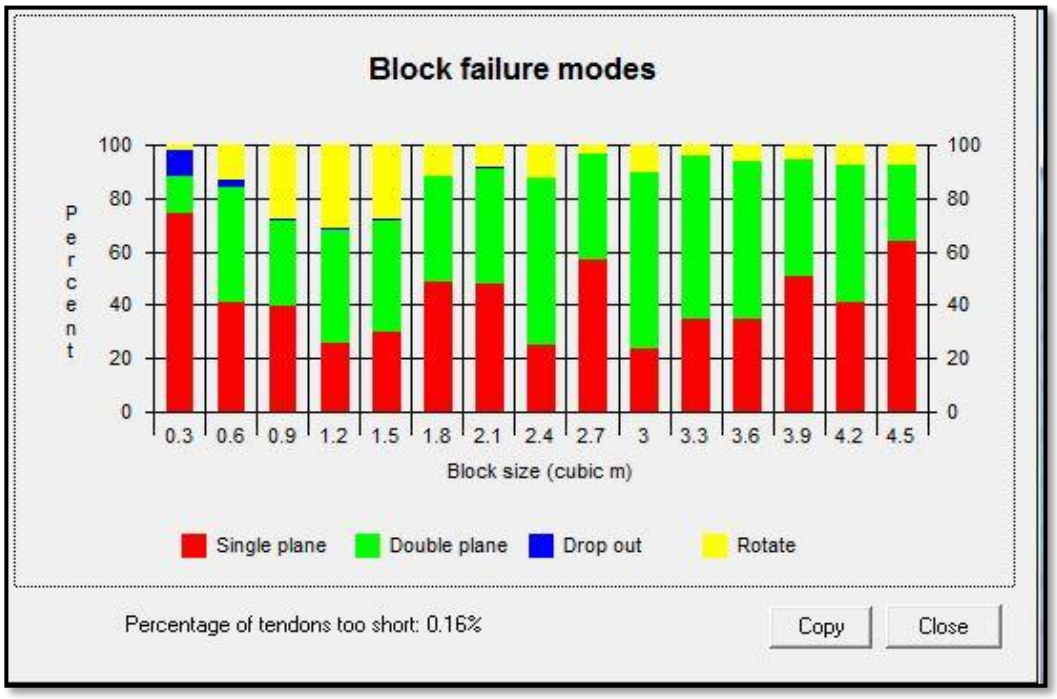

Figure 6.32 Block failure mode for scenario 5

The hazard index for scenario 5 is shown in Figure 6.33. Appendix D, Figure D5 shows the keyblock fall percentage for scenario 5.

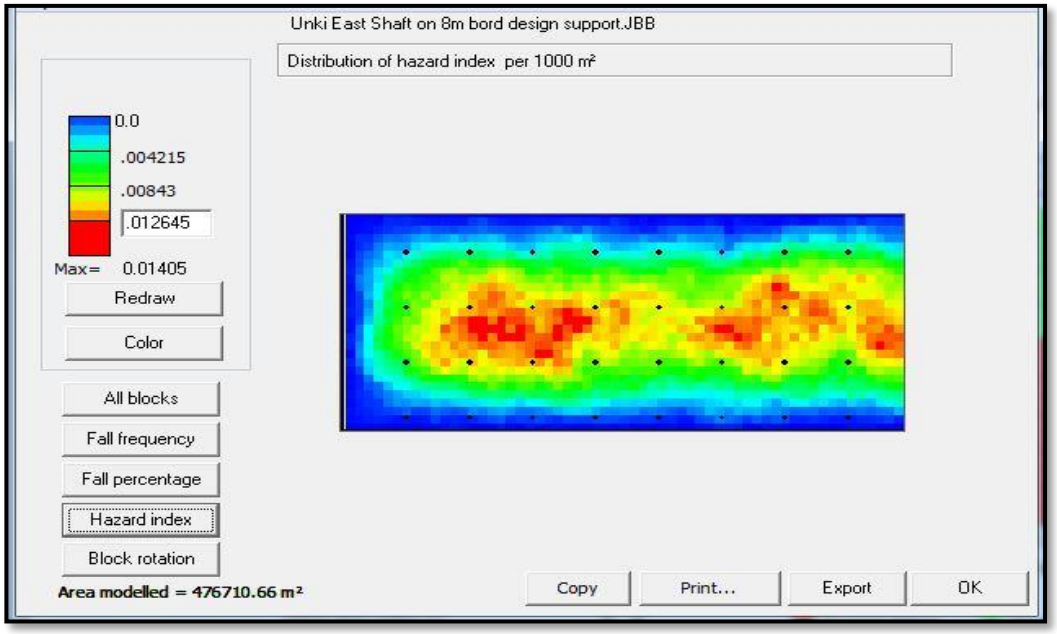

Figure 6.33 Hazard index for scenario 5

6.2.3.6 Additional Scenarios (Scenario 6 to Scenario 11)

The following Scenarios were also modelled and the results were found to be similar;

- 6 m VH with existing support.
- 6 m VH with cable anchors.
- 6 m CD with existing support.
- 6 m CD with cable anchors.
- 5 m MD with existing support.
- 5 m MD with cable anchors.

It was found that, for the above Scenarios;

- There is no support failure and there is no fall between support. Extra support is not needed since the POF is zero as shown in Figure 6.34.
- There are no short tendons as shown in Figure 6.35.
- The hazard index is zero as shown in Figure 6.36.
- Appendix D, Figure D6 shows no keyblock fall percentage for additional scenarios.

- There is no need to redesign the support for the additional scenarios since the support proved to be adequate.

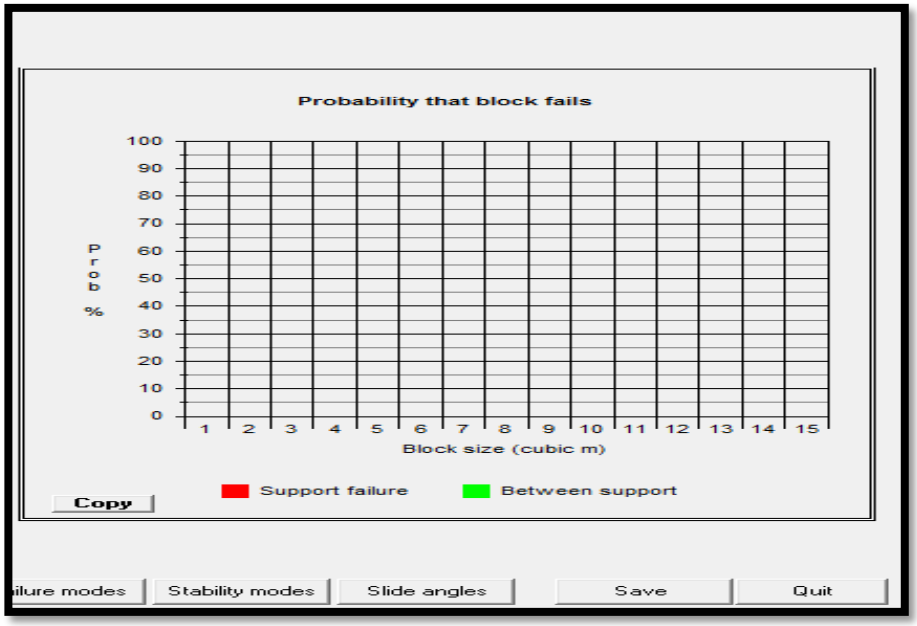

Figure 6.34 Probability of failure of keyblocks additional scenarios

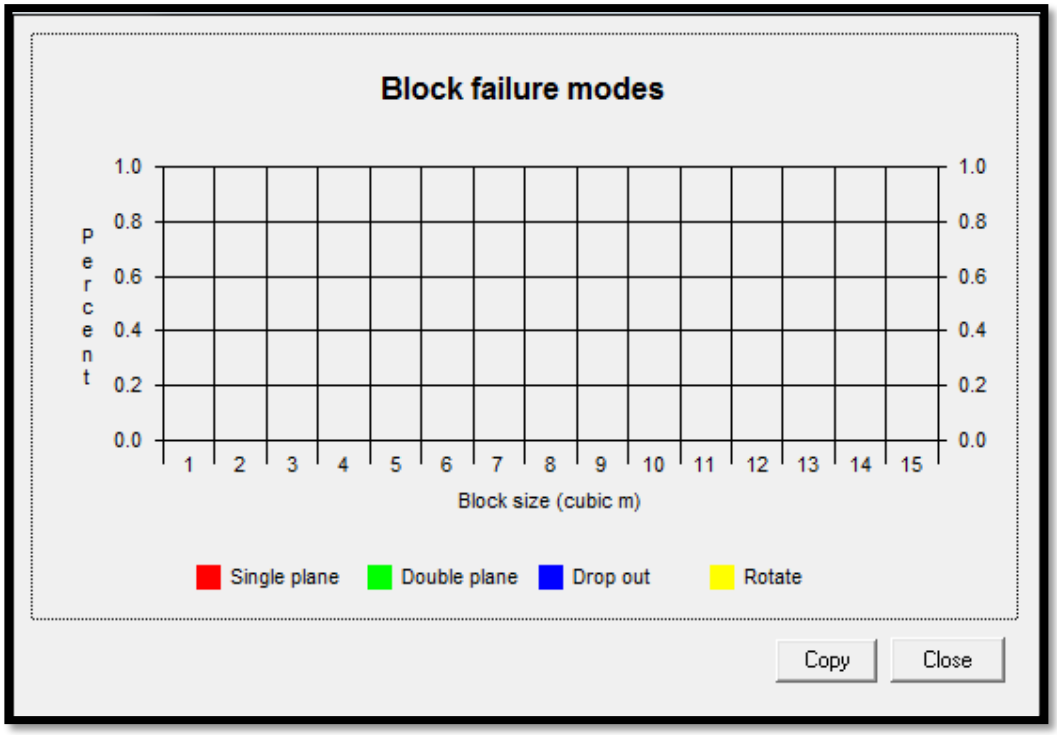

Figure 6.35 Block failure mode for additional scenarios

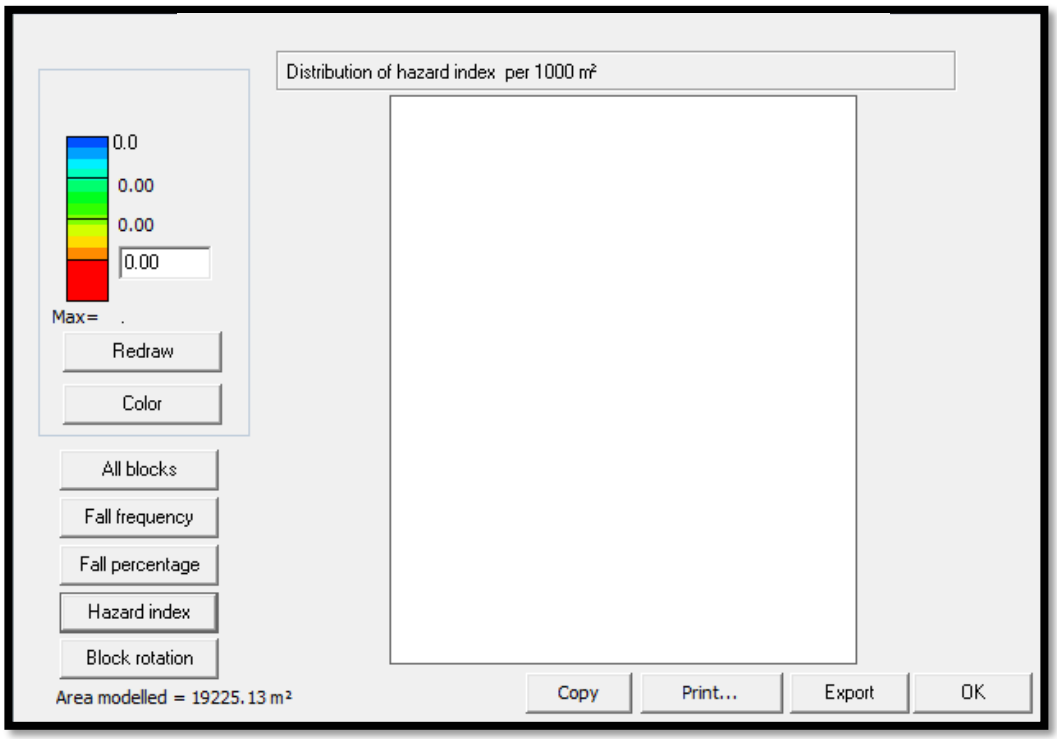

Figure 6.36 Hazard index for additional scenarios

6.3. Analyses of results and comparison to mine observations

This section will discuss and compare the results obtained from laboratory testing of rocks, analytical methods and the numerical modelling results obtained using Phase^2 and J-Block programs. The laboratory testing of rocks was done successfully in order to determine the rock properties as input to the numerical modelling. The summary of rock test results is shown in Table 5.1.

6.3.1. Beam analysis

This section shows the analytical results as discussed in Section 2.2 on behaviour of beams. The calculation is based on the following equation for clamped beams.

$$\sigma_t = \frac{\gamma L^2}{2t} \quad (19)$$

Where: γ is the unit weight of beam = 31 500 N/m^3,

t is the thickness of beam = 0.6 m (measured at tipping points),

L is the length of unsupported span = 12 m and 8 m.

6.3.1.1 Maximum tensile stress for 12 m bord clamped beam

$$\sigma_t = \frac{31\ 500\ x\ 12^2}{2\ x\ 0.6} = 3\ 780\ 000\ Pa = 3.78\ MPa$$

6.3.1.2 Maximum tensile stress for 8 m bord clamped beam

$$\sigma_t = \frac{31\ 500\ x\ 8^2}{2\ x\ 0.6} = 1\ 680\ 000\ Pa = 1.68\ MPa$$

The tensile strength for the immediate hangingwall for the pegmatoidal plagioclase was found to be 11.4 MPa from the laboratory results obtained in Table 5.1.

The maximum tensile stress from the clamped beam is 3.78 MPa for 12 m bord and 1.68 MPa for 8 m bord. This concludes that for a continuous clamped beam, the current span of 12 m at Unki mine is stable and no tensile failure is expected in the hangingwall. The calculation for cantilever beams is based on the following equation.

$$\boldsymbol{\sigma_t = \frac{3\gamma L^2}{t}} \qquad \textbf{(20)}$$

6.3.1.3 Maximum tensile stress for 12 m bord cantilever beam

$$\sigma_t = \frac{3\ x\ 31\ 500\ x\ 12^2}{0.6} = 22\ 680\ 000\ Pa = 22.68\ MPa$$

6.3.1.4 Maximum tensile stress for 8 m bord cantilever beam

$$\sigma_t = \frac{3\ x\ 31\ 500\ x\ 8^2}{0.6} = 10\ 080\ 000\ Pa = 10.08\ MPa$$

If the clamped beam is cut across by a fault, joint or dyke, it becomes a cantilever beam. The maximum tensile strength is calculated to be 22.68 MPa for 12 m bord. The maximum tensile strength is more than 11.4 MPa obtained from the laboratory tests. This means that the span at 12 m is unstable and tensile failure is anticipated in a cantilever beam. The FOS is 0.5 and this is lower than the recommended 1.5.

The maximum tensile stress is calculated to be 10.08 MPa for 8 m bord. The maximum tensile strength is less than 11.4 MPa obtained from the laboratory tests. This means that the span at 8 m is stable and no tensile failure is expected even if

the hangingwall is cut on one side by a fault or a dyke. The FOS is 1.13 and the recommended FOS is 1.5.

Therefore some of the FOG witnessed are caused by tensile beam collapse especially in 12 m bords cut across by geological structures like joints, faults and dykes.

6.3.2. Phase^2 modelling

Phase^2 modelling shows that the existing support of 1.5 m long rock bolts spaced at 1.5 m x 1.5 m grid in a 12 m bord is not enough to support the large wedges or domes created by low angle joints because the rock bolts are too short as shown in Figure 6.15. Using 3 m cable anchors improves the hangingwall stability because some of the wedges are pinned as shown in Figure 6.17. Reducing the bord from 12 m to 8 m increases the chances of unstable wedge to sit on a pillar thereby reducing the probability of having short tendons when using the existing support as shown in Figure 6.16.

6.3.3. Rockfall distribution from J-Block program

In order to assess the stability of the hangingwall of the area of interest, the stability program J-Block was run on the data collected from underground mapping at Unki Mine. A number of models were run using different block sets, mining directions and support standards.

6.3.3.1 Keyblock size fall probability

The histograms for keyblock size distribution shows the frequency the blocks occur in each size. Figure 6.19 shows that there is no rock size to cause support failure since there is no support at all in scenario 1. Larger number of 0.3 m^3 keyblocks falls between support and the number of occurrences decreases with increasing keyblock size for all the scenarios. It also means the hangingwall failure is mostly due to small, wedge-shaped blocks. To further prevent them from falling, areal support would be required. These small wedges will not be hazardous with less risk since they will mainly fall out during blasting time.

6.3.3.2 Keyblock failure mode

The failure mode graphs (Figure 6.20, Figure 6.23, Figure 6.26, Figure 6.29 and Figure 6.32) shows how keyblocks of different sizes fail. Scenario 1 to scenario 5 shows that the larger percentage fall by single plane followed by double plane failure. Failure by keyblock dropping out is slightly higher than for keyblock rotation.

Figure 6.20, Figure 6.23, Figure 6.26, Figure 6.29 and Figure 6.32 shows the percentage of tendons too short to support the keyblocks thereby causing poor and inadequate support. There is a decrease in the percentage of tendons failing to support from scenario 2 with 4.7% (Figure 6.23) to scenario 3 with 2.2% in a 12 m bord (Figure 6.26). This has been caused by increasing the tendon support length from 1.5 m rock bolts to 3 m cable anchors as shown in Figure 6.23 and Figure 6.26. Reducing the bord from 12 m to 8 m further reduce the percentage of short tendons drastically to 0.16% as shown in Figure 6.29 and Figure 6.32. Therefore reducing the bord from 12 m to 8 m and using 3 m cable anchors improves the quality of support. When the bord width is reduced to 6 m, there is no failure mode since there is no FOG occurring as shown in Figure 6.35 and for additional scenarios (scenario 6 to scenario 11). Therefore there is no additional support needed in VH, CD and MD except when highly jointed bad ground is intersected.

6.3.3.3 Fall percentage or probability of failure

The POF represents the number of keyblock falls at a point as a percentage of the total number of keyblocks generated over that point. POF shows the probability that a keyblock will be unstable if it is located at a particular position in the bord. There is reduction in POF from scenario 1 to scenario 2 of 79% to 74% respectively by simply supporting the bord with 1.5 m rock bolts spaced at 1.5 m x 1.5 m grid as shown in Appendix D, Figure D1 and Figure D2. This number is high because the smaller keyblocks generated are many compared to bigger keyblocks. These small keyblocks fall mostly between support.

Reducing the bord from 12 m to 8 m further reduce the POF from 74% to 62% for scenario 2 to scenario 4 as shown in Appendix D, Figure D2 and Figure D4. Reducing the bord from 12 m to 8 m and then replacing the 1.5 m long rock bolts

with 3 m cable anchors further reduced the POF from 62% to 60% for scenario 4 to scenario 5 as shown in Appendix D, Figure D4 and Figure D5. Further reducing the bord width to 6 m brought the fall percentage to zero as shown in Appendix D, Figure D6. This is a good trend in improving ground stability.

6.4. Chapter summary

This chapter presented the results from Phase^2 and J-Block during modelling. Different bord spans and support types were evaluated. It was found out that bord width and support type had the largest influence on hangingwall stability.

7. CONCLUSIONS AND RECOMMENDATIONS

The previous chapter presented the results for Phase^2 and J-Block modelling. This chapter covers the conclusions and recommendations arising from this study in relation to the results obtained after modelling.

7.1. Conclusions

The study to design robust support at Unki Mine will bring about some positive results in as far as support of underground bord and pillar mining is concerned. The following conclusions were drawn up from the study. Hangingwall instabilities at Unki Mine are largely geologically and span controlled rather than stress controlled as shown by Phase^2 modelling where the stress generated a FOS greater than 1.5.

The analytical clamped beam method proved that the hangingwall instability is not as a result of beam tensile failure in a 12 m bord. The calculated maximum tensile stress is less than the actual tensile stress of the immediate hangingwall strata obtained from the laboratory tests. Therefore there is no tensile failure anticipated in the hangingwall for clamped beams in a 12 m bord.

The analytical cantilever beam method proved the calculated maximum tensile stress is more than that obtained from the laboratory tests. This means that the span at 12 m is unstable and tensile failure is anticipated in a cantilever beam. If the bord is reduced to 8 m, the maximum tensile stress is less than that obtained from the laboratory tests. This means that the span at 8 m is stable and no tensile failure is expected even if the hangingwall is cut on one side by a fault or a dyke. Some of the FOG witnessed are caused by tensile beam collapse especially in 12 m bords cut across by geological structures like joints, faults and dykes.

J-Block modelling has indicated that span or bord size and type of support has influence on hangingwall instability. Phase^2 and J-Block modelling has shown that reducing the bord size bring improvements in hangingwall stability. The modelling has proved that replacing the existing support using 1.5 m long rock bolts for scenario 2 with 3 m cable anchors for scenario 5 further improves the hangingwall stability apart from reducing the bord. It was found out that reducing the bord width from 12 m to 8 m reduces the probability of intersecting the dome structures

associated with high risks. It was also found out that the existing support of 1.5 m bolts spaced at 1.5 m x 1.5 m grid is adequate to support spans of 6 m and below as in VH, CD and MD.

Both Phase^2 and J-Block modelling proved a high risk of having short support tendons with current support of 1.5 m long rock bolts which results in poor support conditions in 12 m and 8 m bords. This has been proved at Unki Mine where large FOG occurs in the form of a wedge with some failed support and evidence of short tendons. Using 3 m cable anchors and reducing the span to 6 m reduces the risk of having short support tendons.

7.2. Recommendations

In order to reduce FOG occurrences at Unki Mine, a major support system has to be implemented. The following recommendations were drawn up from this study.

- Reduce the bord width from current size of 12 m to less than 10 m with 8 m as the preferred size to improve hangingwall stability. This must be done in GCD1 and GCD3 in the upper zones of the mine where the ground condition is poor.
- The current support of using 1.5 m long resin rock bolts needs the addition of 3 m long cable anchors to reduce the risk of having short support tendons if the bord width is to remain at 12 m.
- The spacing of the support system could change from the current 1.5 m x 1.5 m grid to 2 m x 2 m grid when using 3 m cable anchors.
- It is strongly recommended for the rock engineering team to adopt faster and efficient way of collecting joint data to account for new geological conditions as mining progresses.

8. REFERENCES

Bieniawski, Z. and Hawkes, I. (1978) 'Suggested Methods for Determining Tensile Strength of Rock Materials', *International Journal of Rock Mechanics & Mining Sciences* , vol. I, no. 5, pp. 99-103.

Brady, B.H.G. and Brown, E.T. (2005) *Rock mechanics for underground mining*, 3rd edition, New York: Kluwer academic publishers.

Brown, R. and Mwatahwa, C. (2005) *Structural geology of the Unki platinum project area*, Shurugwi: Unpublished.

Chikuni, M. (2012) *Reef contour powerpoint presentation.*, Unki Mine.

Chunnett, G. and Mwatawha, C. (2008) *Middleridge Extraction Study Geology Report*, Harare, Zimbabwe: Platinum Exploration Ventures.

Eberhardt, E. (2003) 'Rock slope stability analysis- Utilisation of advanced numerical techniques', *Geological Engineering/ Earth and Ocean Sciences*, pp. 1-30.

Esterhuizen, G. and Streuders, S. (1998) 'Rockfall hazard evaluation using probabilistic keyblock analysis', *The South African Institute of Mining and Metallurgy*, pp. 59-64.

Fairhurst, C. and Hudson, J. (1999) 'Draft ISRM suggested method for the complete stress-strain curve for intact rock in uniaxial compression', *International Journal of Rock Mechanics and Mining Sciences*, vol. II, no. 36, pp. 279-289.

Goodman, R.E. and Shi, G. (1985) *Block theory and its application in rock engineering*, Prentice Hall.

Haile, A.T. and Jager, A.J. (1995) *Rock mass condition, behaviour and seismicity in mines of the Bushveld igneous complex*, Johannesburg, South Africa: SIMRAC Report GAP 027.

Hoek, E. (1989) *www.rocscience.com*, [Online], Available: https://www.rocscience.com/documents/hoek/corner/09_Factor_of_safety_and_probability_of_failure.pdf [15 March 2011].

Hoek, E. and Brown, E. (1988) 'The Hoek-Brown failure criterion - a 1988 update'", *Geotechnical Engineering Division ASCE*, pp. 31-38.

King, R.G. (2006) *Unki Support Layout*, Johannesburg: Angloplatinum.

Kotze, G. (2012) *JBlock training course*, Johannesburg: OHMS.

Lightfoot, N. (2000) *Numerical Modelling of Mine Works*, Pretoria: Department of Minerals and Energy.

Mahove, R. (2014) *Unki Mine FOG database update* , Shurugwi: Unpublished.

Mandingaisa, O. (2014) *Code of practice to combat rockfall and rocburst accidents*, Shurugwi: Unki Mine.

Maps (2013) *Google*, [Online], Available: https://maps.google.co.za/ [02 December 2013].

Mathemera, A. (2010) *Unki Mine Business Literacy Mining Department Presentation*, Shurugwi.

Mugwadi, N. (2012) *Unki Mine Business Literacy MRM Manual*, Shurugwi.

Potvin, Y. (1988) *Empirical open stope design in Canada*.

Roberts, M.K.C. and Clark-Mostert, V. (2010) 'Is there some commonality between the geological structures?', Johannesburg.

Rocscience (2015) *www.rocscience.com*, [Online], Available: http://www.rocscience.com/products/3 [2 May 2015].

Ryder, J.A. and Jager, J.A. (2002) *Rock Mechanics For Tabular Hard Rock Mines*, 1st edition, Johannesburg: The Safety in Mines Research Advisory Committee.

Stacey, T.R. (2001) *Best practice rock engineering handbook for "other" mines*, Braamfontein, South Africa: SIMRAC.

Stacey, T.R. (2012) *Numerical modelling techniques in rock engineering*, Johannesburg: Unpublished course notes.

Stacey, T. and Gumede, H. (2007) 'Evaluation of risk of rock fall accidents in gold mine stopes based on measured joint data', *The Southern African Institute of Mining and Metallurgy*, vol. 107, no. 1, pp. 345-350.

Stowe, C.W. (1968) 'The Geology of the Country South and West of Selukwe', *Geological Bulletin 59*, vol. II, pp. 181-185.

Swart, A.H. and Handley, M.F. (2004) *The design of stable stope panels for near-surface and shallow mining operations*, Pretoria.

Swart, A.H. and Handley, M.F. (2005) 'The design of stable stope spans for shallow mining operations', *The Journal of The South African Institute of Mining and Metallurgy*, vol. 105, April, pp. 275-286.

Swart, A.H., Stacey, T.R., Wesseloo, J., Joughin, W.C., Le Roux, K., Walker, D. and Butcher, R. (2000) *Investigation of factors governing the stability/ instability of stope panels in order to define a suitable design methodology for near surface and shallow mining operations*, Johannesburg: SIMRAC Project Report OTH 501.

Toyra, J. (2004) *Stability of Shallow Seated Constructions in Hard Rock- A Pilot Study*, Luleå, Sweden: Lulea University of Technology.

Ulusay, R. (2014) 'The ISRM Suggested Methods for Rock Characterization, Testing and Monitoring: 2007-2014', *International Journal of Rock Mechanics and Mining Sciences*, July, pp. 285-290.

Unki (2014) *Rock Engineering Department, Data Base*, Shurugwi.

Van der Merwe, N. (2010) *MINN4010 Course notes*, University of the Witwatersrand, Johannesburg: Unbublished.

Van der Merwe, N.J. and Madden, B.J. (2000) 'Rock Engineering for underground coal mining', *The South African Institute of Mining and metallurgy*, vol. 7, pp. 57-58.

Yilmaz, H. (2011) *Minn 4010 Rock engineering course notes*, University of the Witwatersrand, Johannesburg: Unpublished lecture notes.

9. APPENDICES

Appendix A. Descriptive statistics of FOG dimensions

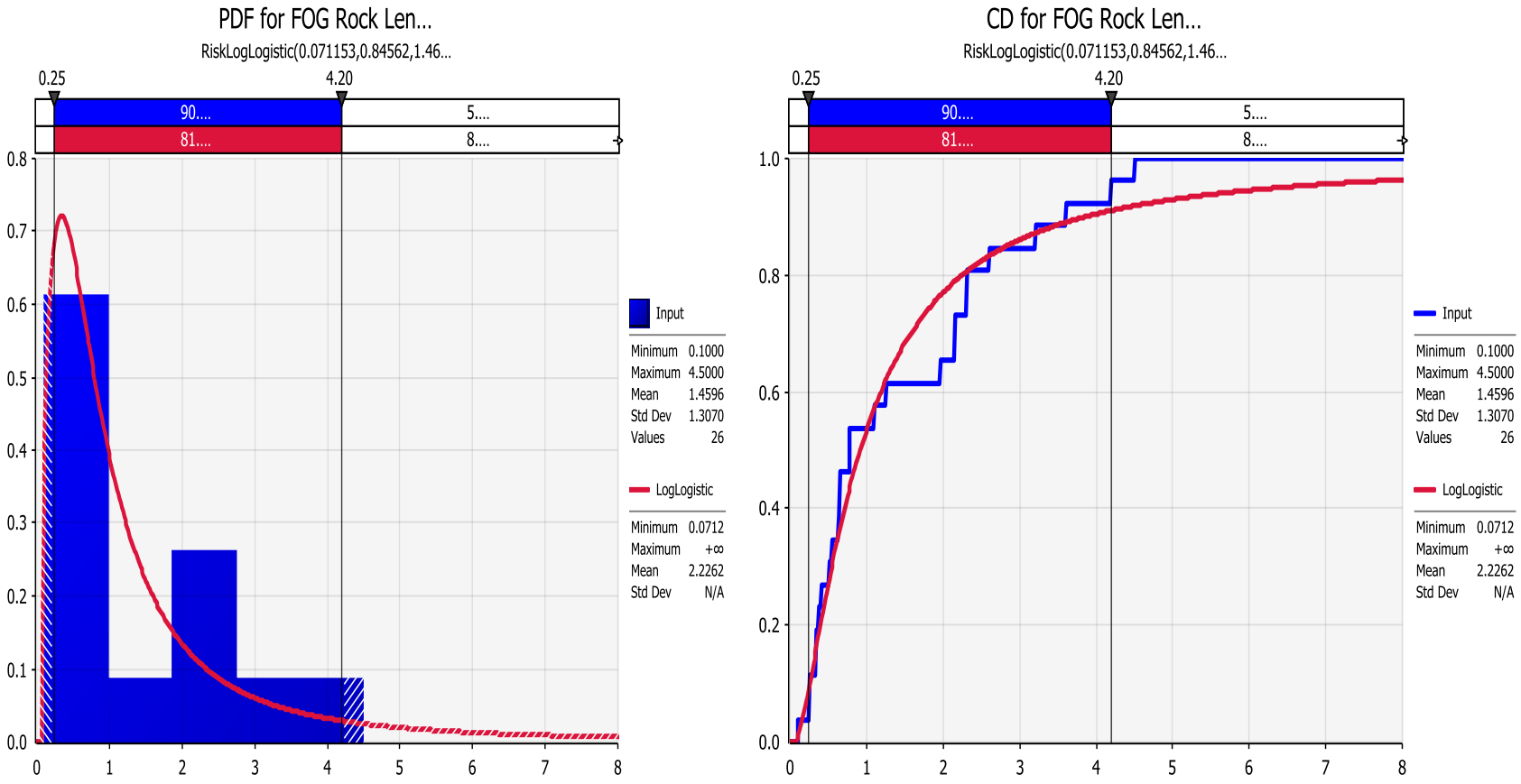

Figure A1. The PDF and Cumulative Distribution for the FOG length

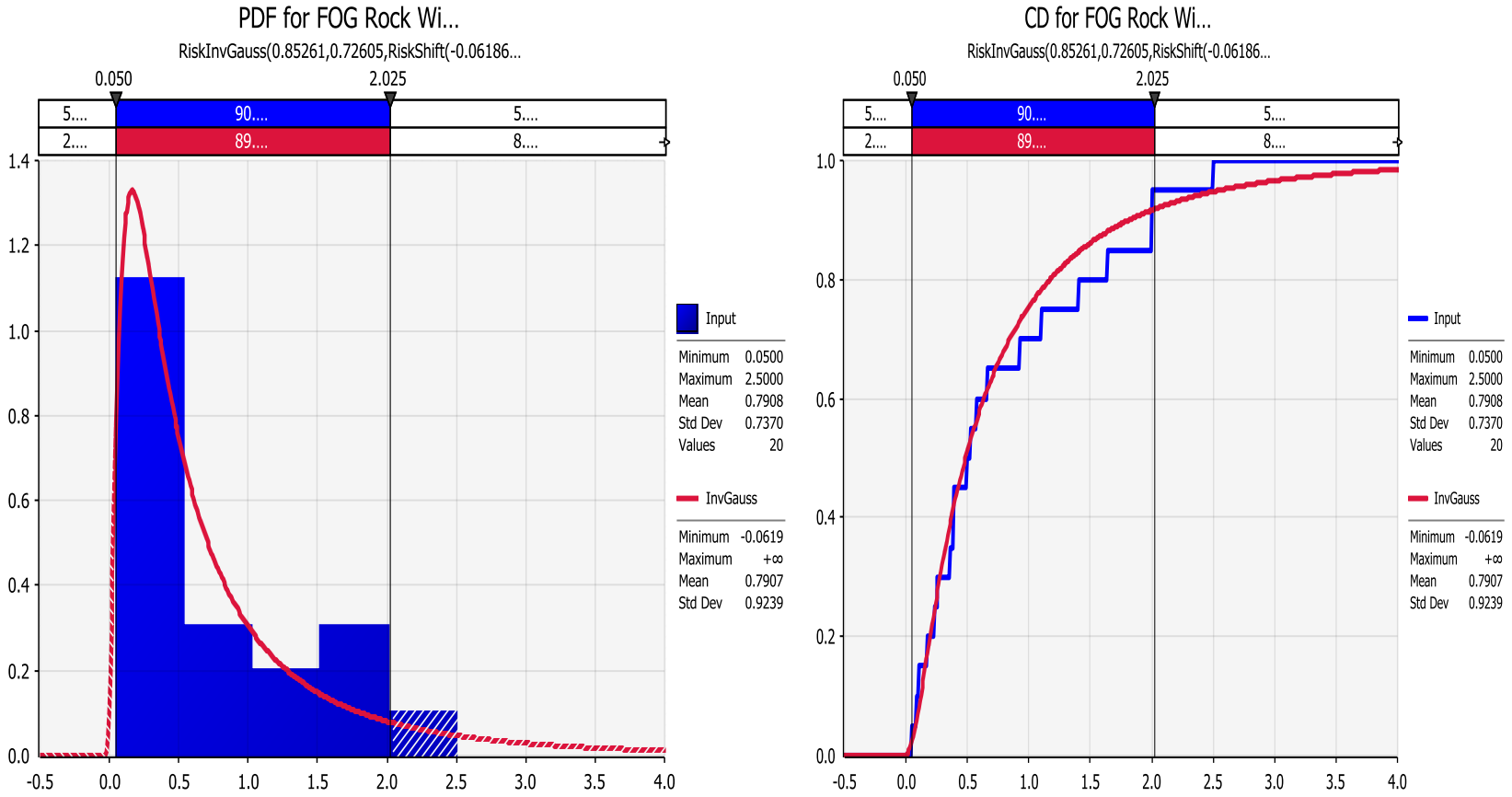

Figure A2. The PDF and Cumulative Distribution for the FOG width

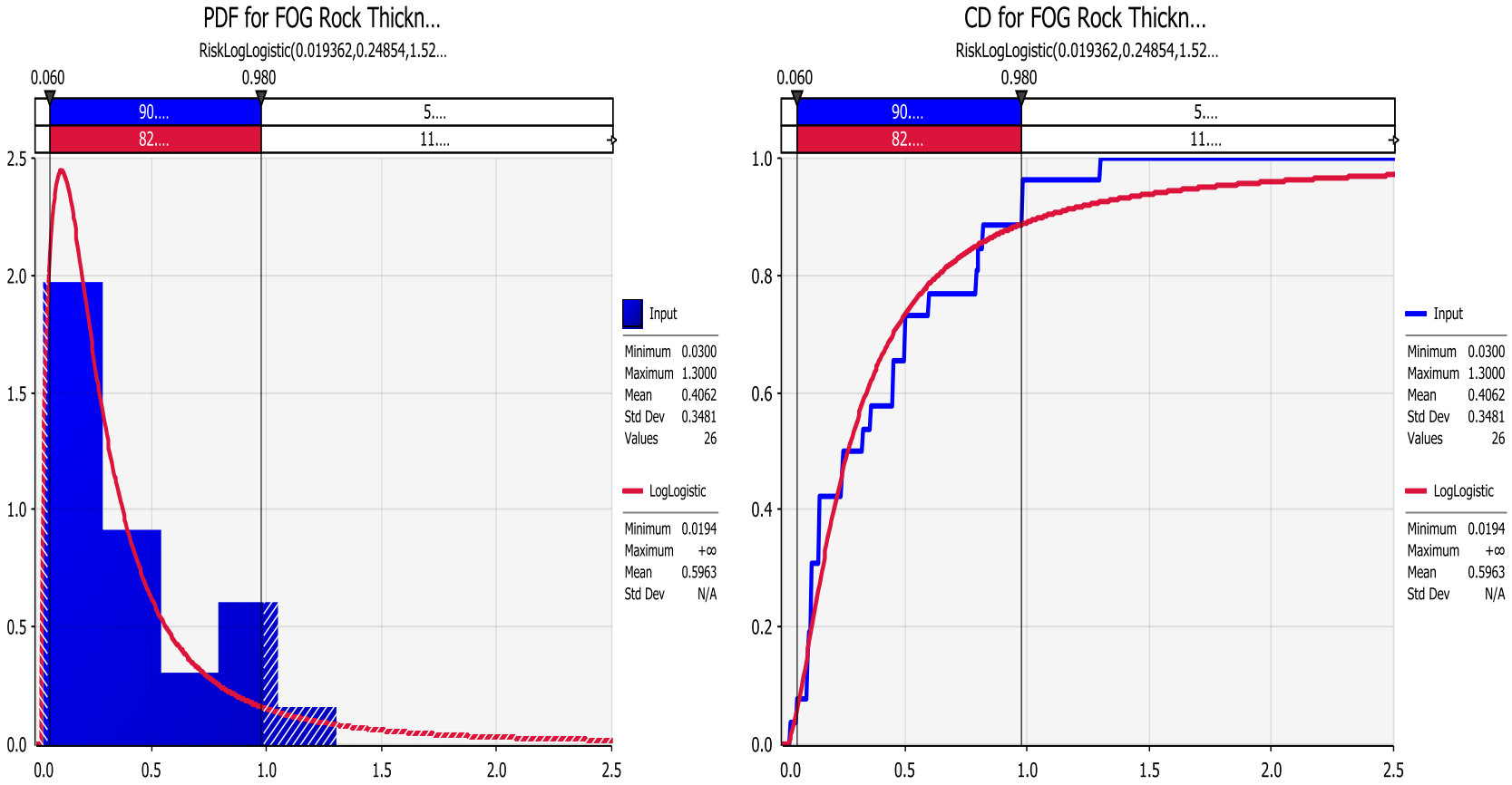

Figure A3. The PDF and Cumulative Distribution for the FOG thickness

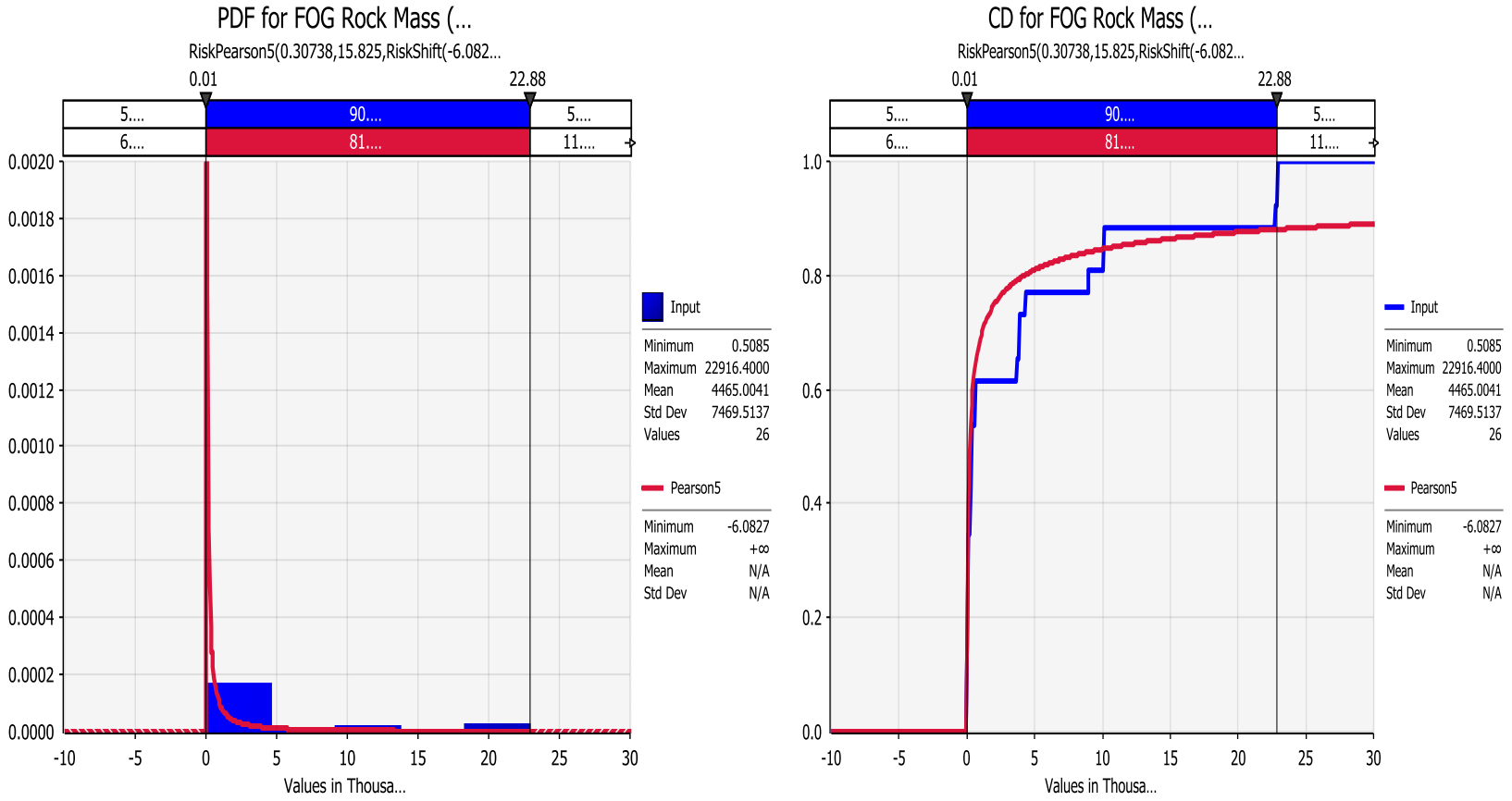

Figure A4. The PDF and Cumulative Distribution for the FOG mass

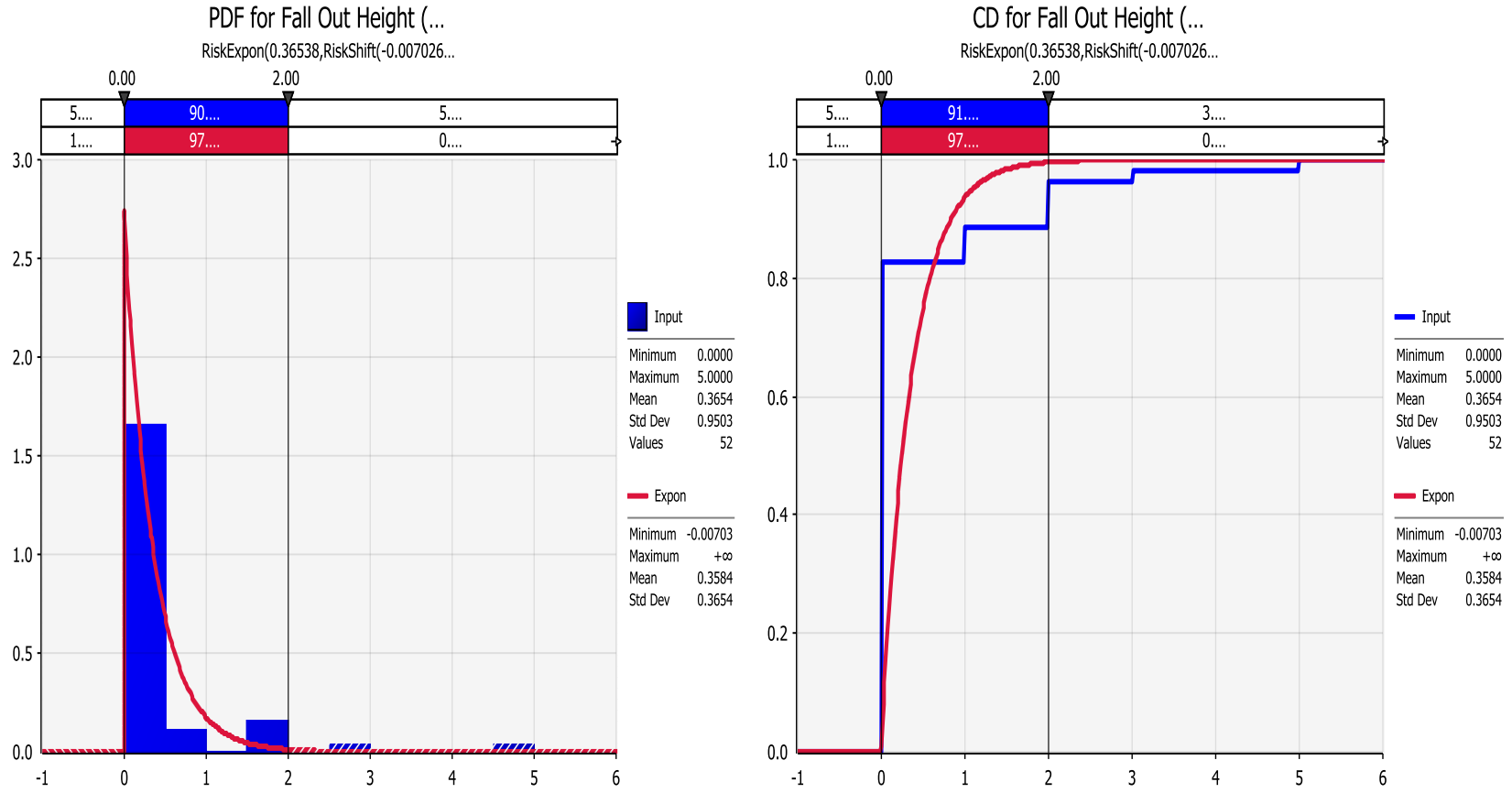

Figure A5. The PDF and Cumulative Distribution for the FOG fall out height

Appendix B. Laboratory tests

Table B1. Laboratory test results of uniaxial compression tests with elastic modulus and poisson ratio measurements by means of strain gauges

Client: Anglo Platinum — Sampling site: Uniki Mines, Zimbabwe — 11-02-2014

SPECIMEN PARTICULARS				SPECIMEN DIMENSIONS					SPECIMEN TEST RESULTS								
Rocklab Specimen No	Sample ID	Depth From.. To	Rock Type	Diameter	Height	Ratio of Height to diameter	Mass	Density	Failure Load	Strength (UCS)	Tangent Elastic Modulus @ 50% UCS	Secant Elastic Modulus @ 50% UCS	Poisson's Ratio Tangent @ 50% UCS	Poisson's Ratio Secant @ 50% UCS	Linear Axial Strain at Failure	Failure Code	Note
5618-		m		mm	mm		g	g/cm³	kN	MPa	GPa	GPa			mm/mm		
UCM-01-A				47.16	128.0	2.7	644.8	2.88	342.1	195.8	98.8	103.0	0.30	0.27	0.002615	XB	
UCM-01-B				47.22	127.9	2.7	647.5	2.89	336.3	192.0	99.5	104.0	0.30	0.28	0.002442	XA	
UCM-01-C	GN 1			47.23	128.5	2.7	652.4	2.90	321.1	183.3	102.0	107.0	0.31	0.28	0.002230	XB	
UCM-01-D				47.27	129.3	2.7	651.9	2.87	360.8	205.6	99.0	105.0	0.29	0.30	0.002738	XB	
UCM-01-E				47.18	128.0	2.7	644.1	2.88	345.9	197.9	102.0	105.0	0.31	0.30	0.002394	XB	
UCM-02-A				47.45	129.0	2.7	745.4	3.27	443.4	250.7	156.0	157.0	0.24	0.22	0.001839	XB	
UCM-02-B				47.24	128.8	2.7	734.6	3.25	428.3	244.4	153.0	159.0	0.25	0.24	0.001798	XA	
UCM-02-C	F/W2			47.09	129.0	2.7	736.8	3.28	396.6	227.7	161.0	164.0	0.23	0.23	0.001693	XA	
UCM-02-D				47.19	128.8	2.7	734.6	3.26	417.4	238.7	153.0	158.0	0.24	0.22	0.001925	XB	
UCM-02-E				47.40	127.8	2.7	733.7	3.25	374.7	212.3	132.0	140.0	0.26	0.25	0.001791	XA	

Note: All tests were conducted according to the ISRM's Specification.

Figure B1. Uniaxial compressive strength test sample photos after failure

Table B2. Laboratory test results of triaxial compressive strength tests with elastic modulus and Poisson's ratio measurements by means of strain gauges

Client: Anglo Platinum — Samping Site: Uniki Mines, Zimbabwe — 18-Feb-14

SPECIMEN PARTICULARS				SPECIMEN DIMENSIONS					SPECIMEN TEST RESULTS										
Rocklab Specimen No	Sample ID	Depth From.. To	Rock Type	Diameter	Height	Ratio of Height to Diameter	Mass	Density	Confining Pressure δ_3	Failure Load P	Strength (TCS) δ_1	Tangent Elastic Modulus @50% TCS	Secant Elastic Modulus @50% TCS	Tangent Poisson's Ratio @50% TCS	Secant Poisson's Ratio @50% TCS	Linear Axial Strain at Failure	Failure Code	Mohr-Coulomb Cohesion	Mohr-Coulomb Friction Angle	Note
5618-		m		mm	mm		g	g/cm³	MPa	kN	MPa	GPa	GPa			mm/mm		MPa	Deg.	
TCM-01-A				47.21	100.3	2.1	508.4	2.90	5.0	405.3	231.5	101.0	112.0	0.26	0.23	0.002964	XA			
TCM-01-B				47.26	99.91	2.1	503.5	2.87	10.0	467.4	266.4	93.1	101.0	0.28	0.27	0.004014	XA			
TCM-01-C				47.29	101.16	2.1	508.4	2.86	15.0	508.2	289.3	91.6	103.0	0.30	0.32	0.004599	XA			
TCM-01-D				47.31	100.56	2.1	512.5	2.90	20.0	570.1	324.3	87.4	97.3	0.24	0.19	0.005176	XA			
TCM-01-E	GN 1			47.24	99.86	2.1	509.8	2.91	30.0	602.5	343.8	85.7	104.0	0.21	0.27	0.006651	XA	33.2	49.4	
TCM-01-F				47.28	99.30	2.1	501.5	2.88	5.0	386.3	220.0	94.0	74.5	0.25	0.21	0.004391	XA			
TCM-01-G				47.21	100.50	2.1	507.1	2.88	10.0	473.4	270.4	98.3	110.0	0.38	0.26	0.003624	XA			
TCM-01-H				47.22	99.97	2.1	505.5	2.89	15.0	525.5	300.1	101.0	106.0	0.21	0.24	0.005437	XA			
TCM-01-I				47.28	100.32	2.1	508.4	2.89	20.0	586.2	333.9	84.7	107.0	0.18	0.22	0.006732	XA			
TCM-01-J				47.28	99.97	2.1	507.4	2.89	30.0	700.7	399.1	90.4	109.0	0.20	0.24	0.006218	XA			
TCM-02-A				47.14	99.4	2.1	567.3	3.27	5.0	438.1	251.0	159.0	161.0	0.25	0.23	0.002262	XA			
TCM-02-B				47.07	99.08	2.1	565.7	3.28	10.0	564.3	324.3	166.0	165.0	0.27	0.22	0.003357	YA			
TCM-02-C				47.19	100.99	2.1	574.6	3.25	15.0	663.3	379.2	149.0	161.0	0.17	0.21	0.003316	XA			
TCM-02-D				47.44	99.40	2.1	559.9	3.19	20.0	417.3	236.1	76.6	80.8	0.21	0.22	0.003765	XA			1
TCM-02-E	F/W2			47.37	100.21	2.1	576.9	3.27	30.0	798.9	453.3	153.0	165.0	0.37	0.32	0.005244	YA	35.7	53.0	
TCM-02-F				47.17	99.93	2.1	568.2	3.25	5.0	468.9	268.3	129.0	112.0	0.18	0.16	0.002905	XA			
TCM-02-G				47.20	100.77	2.1	576.7	3.27	10.0	529.3	302.5	153.0	164.0	0.28	0.26	0.003112	XA			
TCM-02-H				47.24	101.43	2.1	580.9	3.27	15.0	610.4	348.3	155.0	166.0	0.19	0.16	0.003270	XA			
TCM-02-I				47.17	100.79	2.1	574.5	3.26	20.0	701.5	401.4	126.0	135.0	0.25	0.26	0.005966	XA			
TCM-02-J				47.33	98.69	2.1	568.5	3.27	30.0	782.9	445.0	143.0	145.0	0.19	0.23	0.006268	2B			

Note: All tests were conducted according — TCS - stands for Triaxial Compressive Strength. — 1 - Specimen showing different density was not used for the analyses of both cohesion and friction angle.

Figure B2. Triaxial compressive strength test sample photos before tests

Appendix C. Modelling

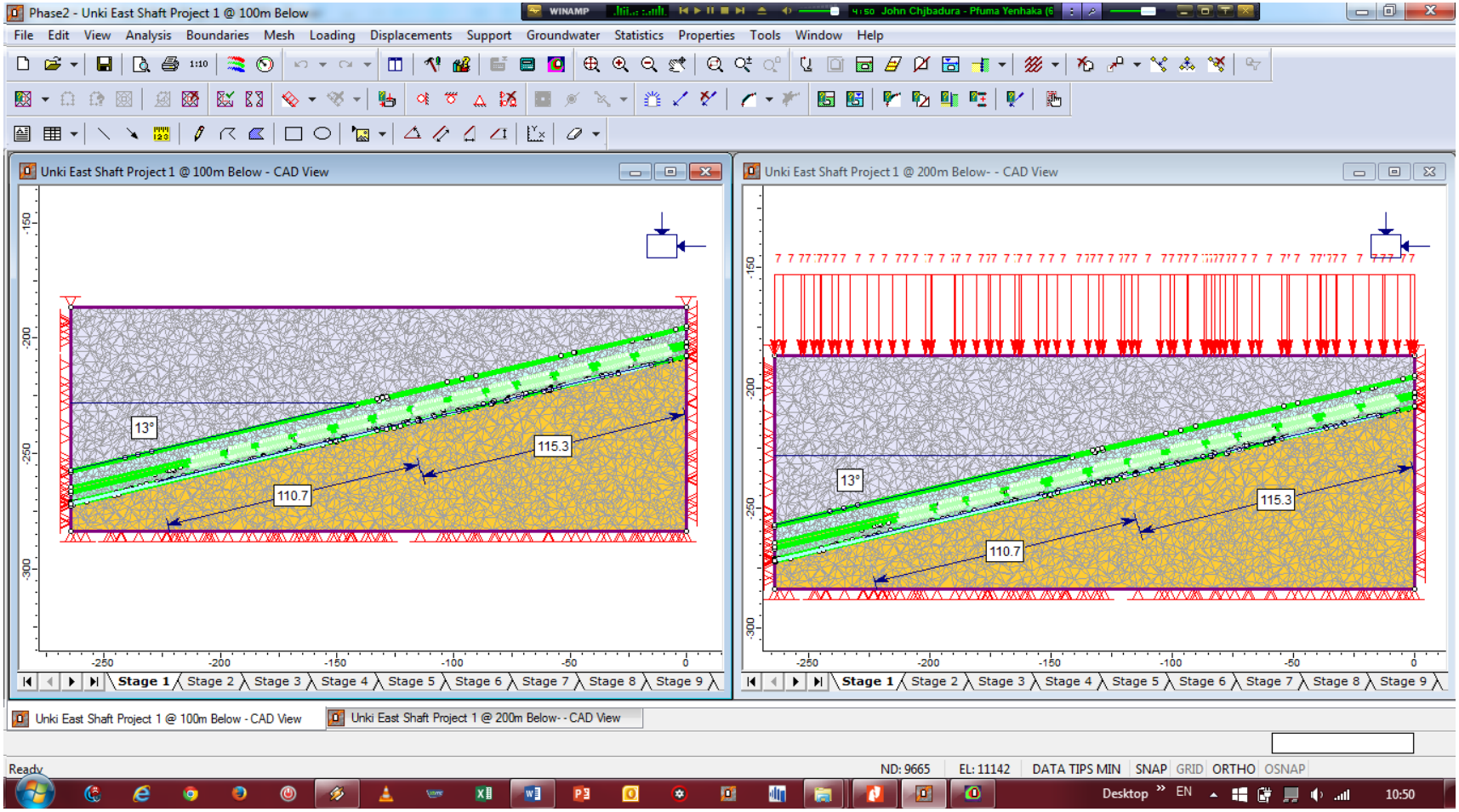

Figure C1. Modelling in Phase[2]

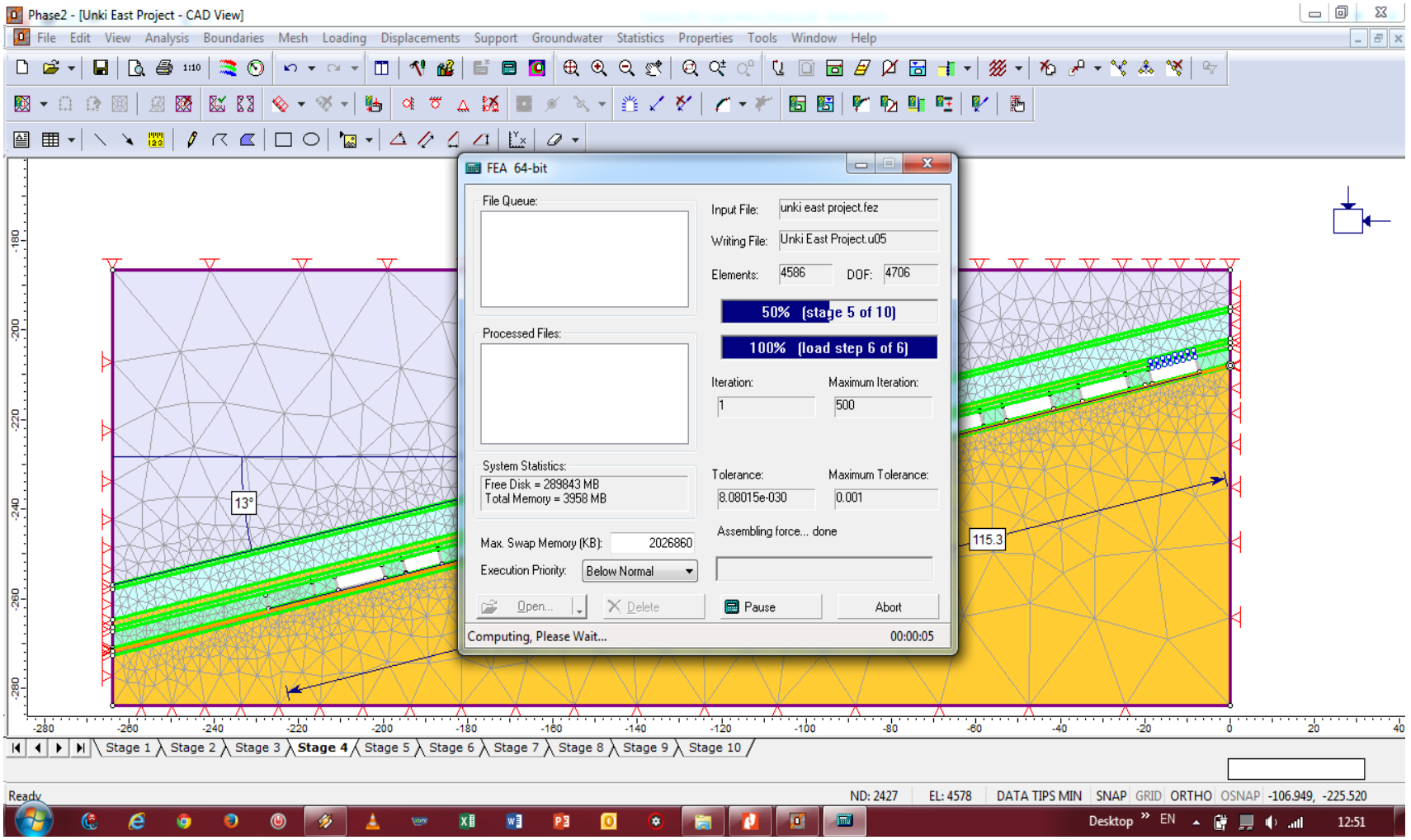

Figure C2. Computing in Phase[2]

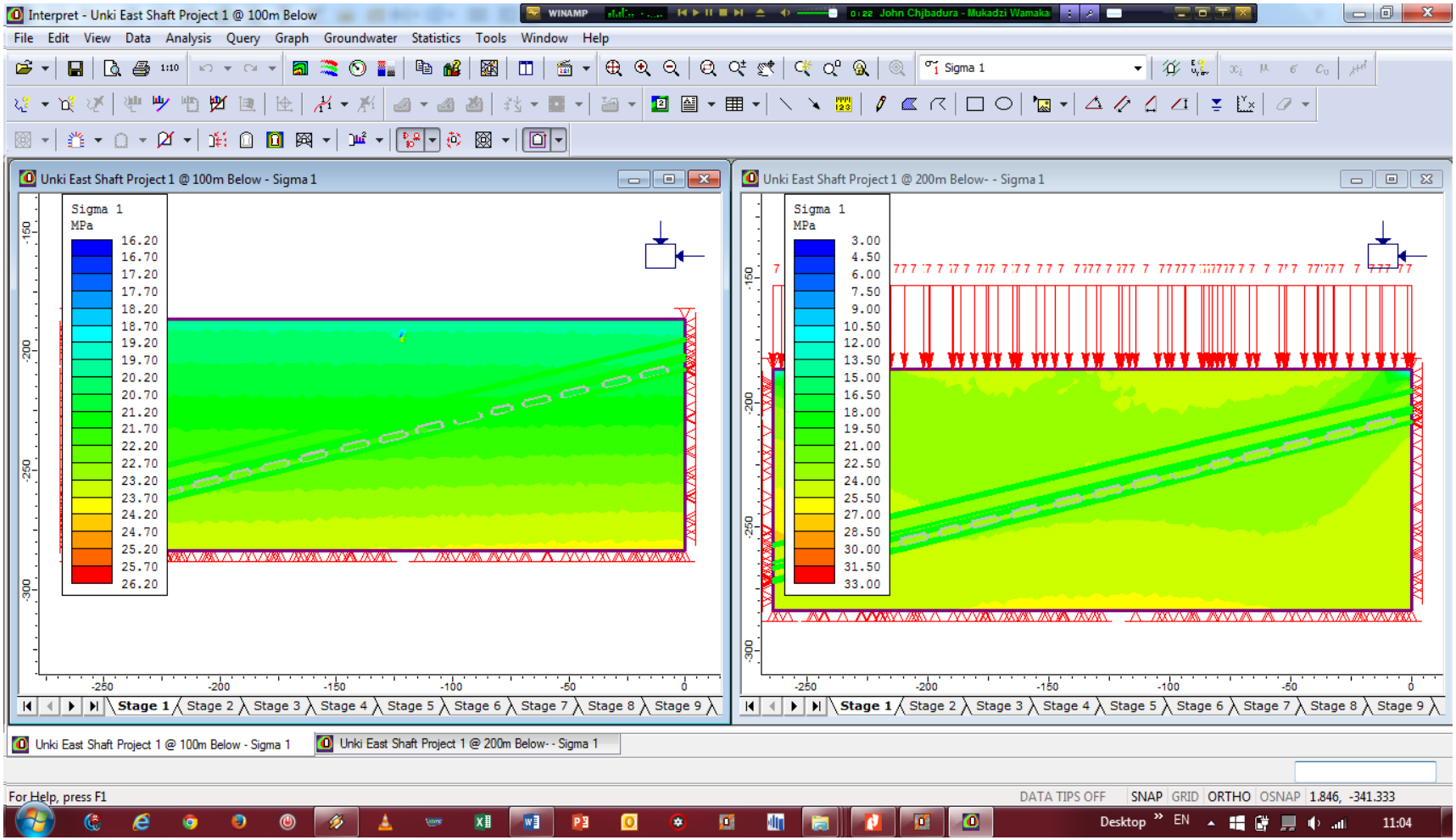

Figure C3. Interpret module in Phase[2]

Appendix D. Keyblock fall percentages

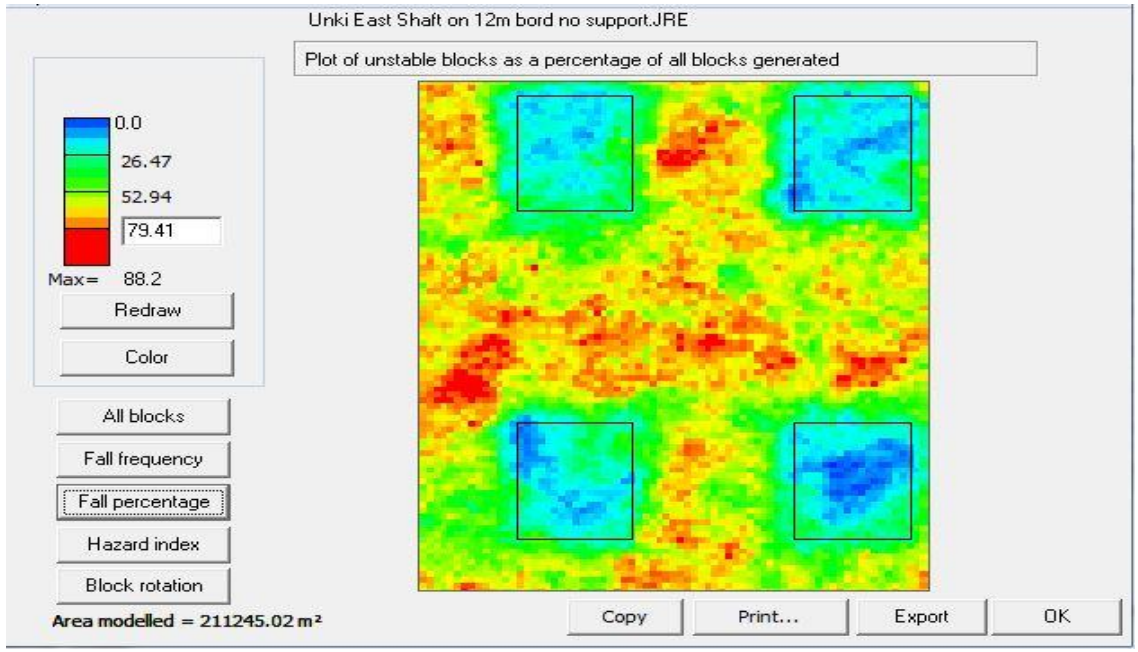

Figure D1. Scenario 1 Keyblock fall percentage

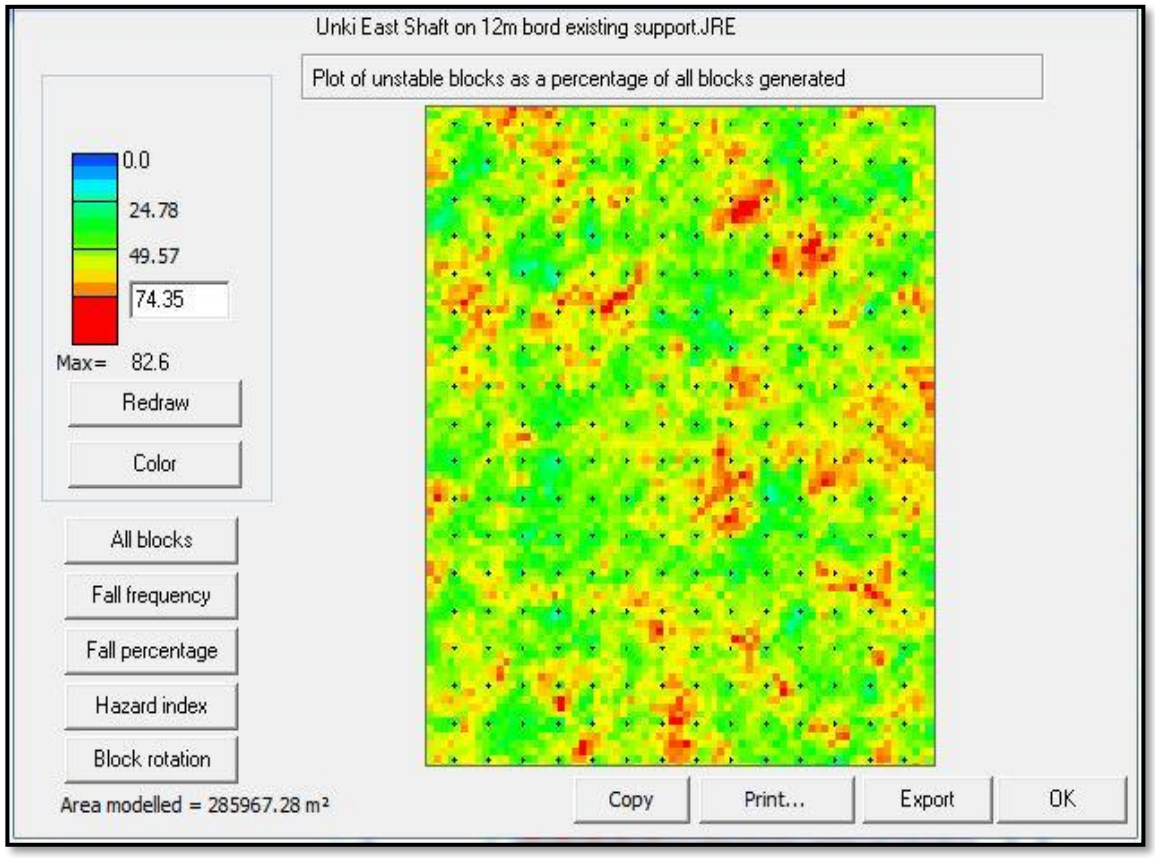

Figure D2. Scenario 2 Keyblock fall percentage

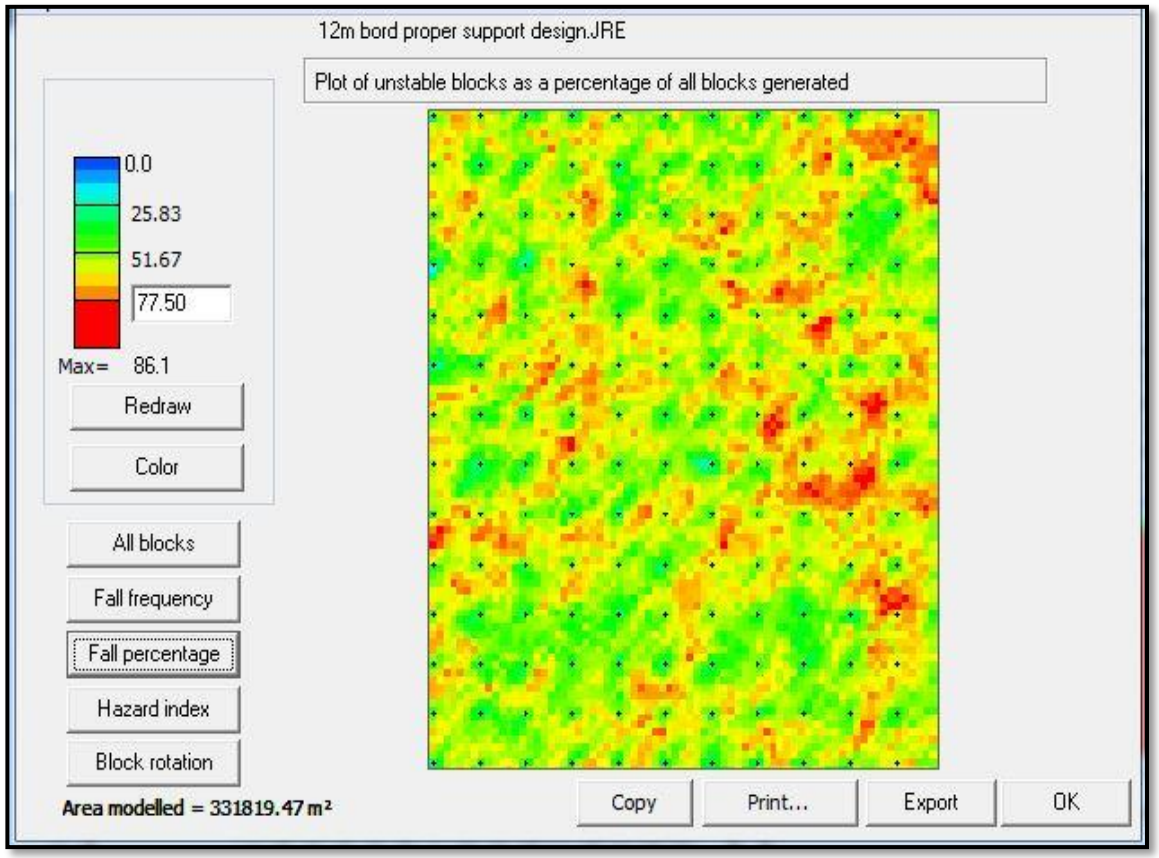

Figure D3. Scenario 3 Keyblock fall percentage

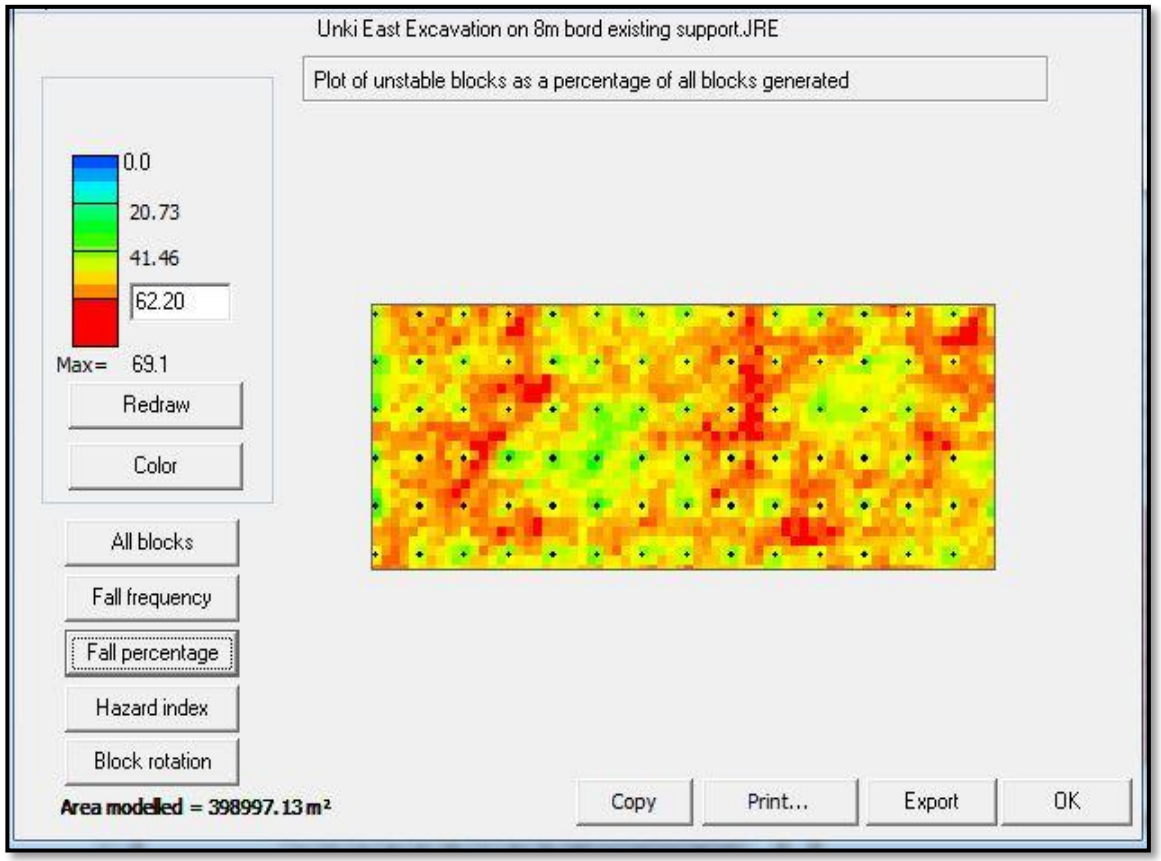

Figure D4. Scenario 4 Keyblock fall percentage

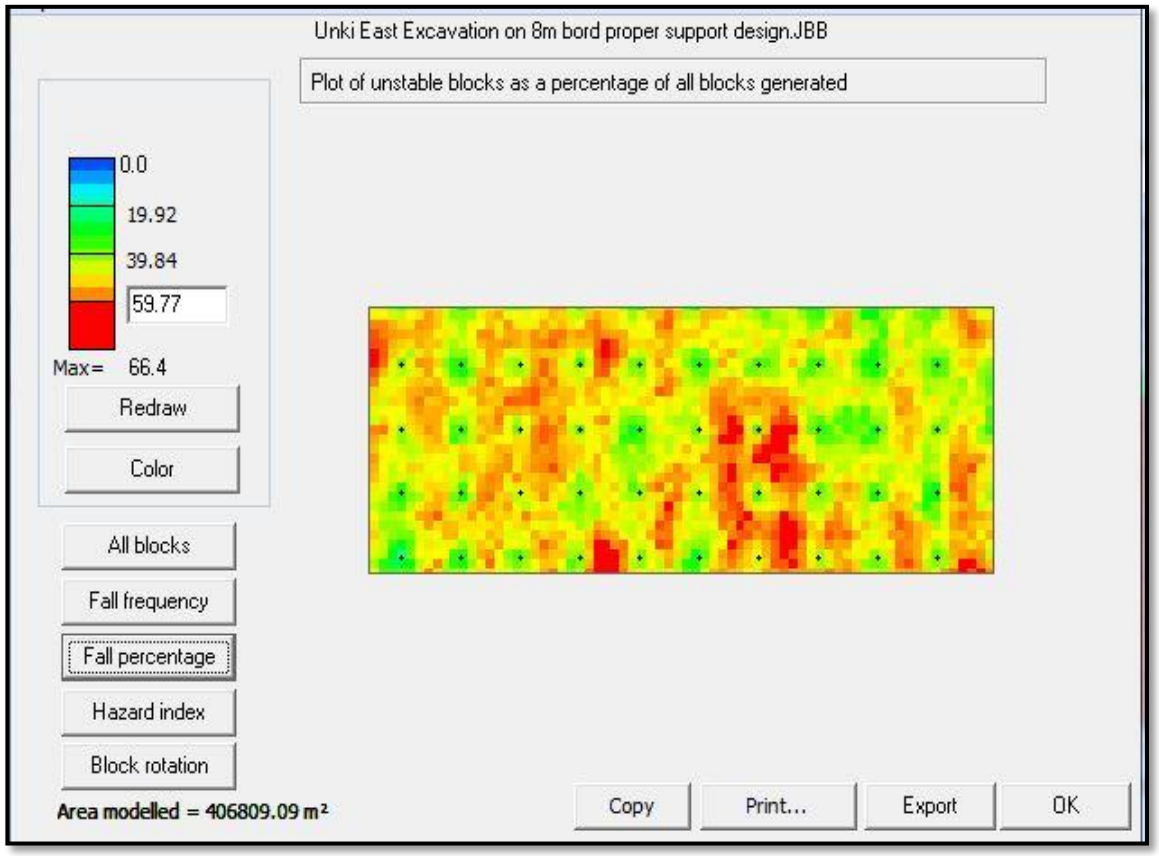

Figure D5. Scenario 5 Keyblock fall percentage

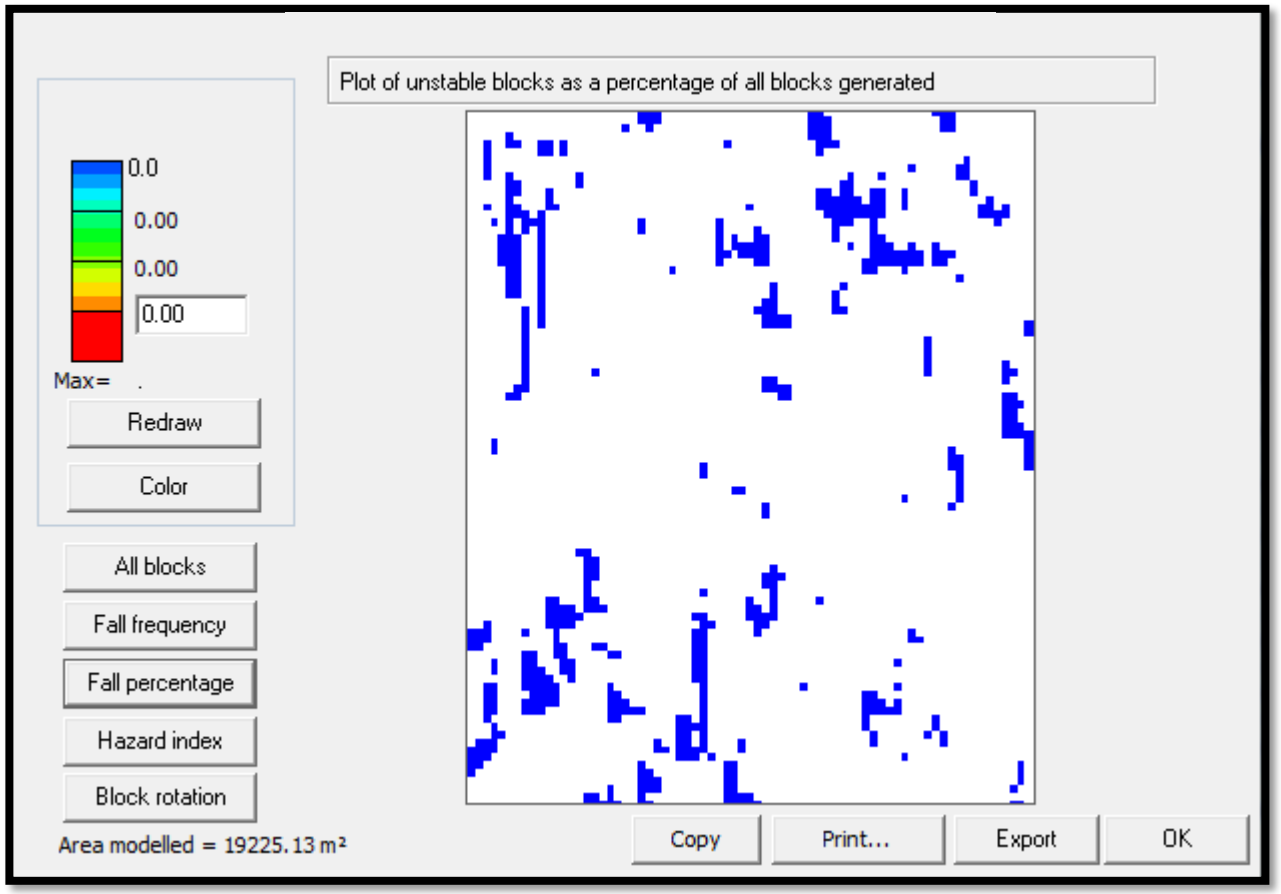

Figure D6. Additional Scenarios keyblock fall percentage